7000-25-T

A STUDY OF AN INHOMOGENEOUSLY SHEATHED SPHERICAL-DIPOLE ANTENNA IN A COMPRESSIBLE PLASMA

RONAL W. LARSON

September 1966

Radiation Laboratory for
Willow Run Laboratories
THE INSTITUTE OF SCIENCE AND TECHNOLOGY
THE UNIVERSITY OF MICHIGAN
Ann Arbor, Michigan

FOREWORD

The number of the project under which this report was written is 5042 and the Task number is 504206. The contractor for the project is The University of Michigan, Ann Arbor, Michigan. The Contract Number is AF 33(615)-1452 and the contractor's report number is 7000-25-T. This contract was monitored for the Air Force Avionics Laboratory by H. E. Yoder, AVNT. The research reported was initiated under a preceding Contract AF 33(616)-8365 and was performed between November 1963 and August 1965. This report contains no information extracted from classified documents.

This report was submitted in August 1965 as a dissertation in partial fulfillment of the requirements for the degree of Doctor of Philosophy at The University of Michigan.

ACKNOWLEDGMENTS

The author wishes to thank the members of his doctoral committee, Professors Gunnar Hok and Andrejs Olte, Co-chairmen; Ziya Akcasu; Chen To Tai; and Herschel Weil for their helpful suggestions and criticisms. He is especially grateful to Professors Olte and Hok for numerous helpful discussions and for respectively suggesting the dipole problem and the emphasis on compressible plasmas. The author also wishes to express his appreciation to the Head of the Radiation Laboratory, Mr. Ralph E. Hiatt, for arranging support for this investigation and for his continued interest.

Finally, he gratefully acknowledges the help of his colleagues Mr. W. E. Zimmerman, for assistance in early experimental measurements and computations, Mr. V. M. Powers, for early assistance in programming and for numerous discussions, and Mr. D. C. Laurin, for assistance in preparing the figures and checking the manuscript.

ABSTRACT

This study investigated the terminating admittance and spatial field variations of a symmetrically excited spherical dipole in an inhomogeneous, compressible plasma using the macroscopic approach. Four coupled, first order, ordinary differential equations were obtained for each mode by employing modal decomposition. Numerical integration was performed on a digital computer with a sheath model in which the static electron density varied as the distance from the outer sheath edge.

Admittance plots are presented as a function of the sheath potential distribution, plasma frequency, electron temperature, radiator size, and for several alternative radiator boundary conditions: elastic electron reflection, zero perturbed electron density, and a bilinear admittance relation. The main effect of plasma compressibility was found to be an additional resonance caused by cancellation of reactive electromagnetic and electroacoustic energies. This manifests itself in a Smith Chart presentation as a loop or multiple loops when the plasma frequency, operating frequency, or electron thermal velocity are varied. The sheath was found to diminish the effects found with a homogeneous plasma and caused the susceptance to be increased significantly; each of the alternative boundary conditions gave similar results.

It is concluded that the sheath has been unjustifiably neglected in previous analyses and that the plasma compressibility has therefore been overemphasized. It is suggested that future experimental evidence of excitation of an electroacoustic wave be obtained with a moveable radial surface probe as well as by measurements of the admittance.

CONTENTS

FIGURES

TABLES

SYMBOLS

STANDARD MATHEMATICAL SYMBOLS

$\frac{d}{dx}$	Total differential operator with respect to the variable x
$h_n(x)$	Spherical Hankel function of order n and argument x
i	Imaginary coefficient ($\sqrt{-1}$)
$j_n(x)$	Spherical Hankel function of order n and argument x
$n_n(x)$	Spherical Hankel function of order n and argument x
$P_n(x)$, $P_n^1(x)$	Legendre and associated Legendre functions of degree n and argument x
$Q_n(x)$, $Q_n^1(x)$	Same as $P_n(x)$ and $P_n^1(x)$, second kind
$\hat{r}$	Radial unit vector (fig. 1)
$\hat{\theta}$	Angular unit vector (fig. 1)
$\hat{\phi}$	Angular unit vector (fig. 1)
∇	Gradient operator
$\nabla\times$	Curl Operator
$\nabla\cdot$	Divergence operator
$\frac{\partial}{\partial x}$	Partial differential operator with respect to the variable x

STANDARD ELECTROMAGNETIC SYMBOLS

c	Velocity of light
E	Electric field
e	Charge of an electron, absolute value
H	Magnetic field
m	Mass of electron
t	Time
TE	Transverse electric
TEM	Transverse electromagnetic
TM	Transverse magnetic
v	Velocity
ϵ	Dielectric permittivity
ϵ_r	Relative dielectric permittivity
μ	Permeability
ν	Collision frequency
ρ	Charge density
ω	Radian frequency
ω_p	Plasma radian frequency $=\sqrt{-e\rho_0/m\epsilon_0}$

NONSTANDARD SYMBOLS

a	Cylindrical dipole radius
$A_{1n} \ldots A_{4n}$	Arbitrary constants for "analytical" solutions
$A_{5n} \ldots A_{8n}$	Arbitrary constants (using Hankel functions) for solutions with homogeneous media
B_n	Modal susceptance, imaginary part of Y_n
B_{0n}	Modal free space susceptance
B_t	Terminating susceptance, imaginary part of Y_t
C_n	Modal constants defining $E_\theta(r_1)$
C_t	Input capacitance at low frequencies
C_{jk}	Combinations of boundary functions, $q_{jn}(y_2)$
D_{jk}	Matrix for reduced fundamental differential equations
f	Particle density
$f(n, \psi)$	Gap angle reduction factor
$f_2 \ldots f_5$	Functions of d-c electric field and electron velocity
f_p	Plasma frequency
F_j	Force in j direction
F_0	Normalized d-c electric field
F_1	Normalized plasma frequency
F_2	Normalized d-c electric field
F_{1m}, F_{2m}	Factors in "analytical" modal solutions
G_n	Modal conductance, real part of Y_n
G_t	Terminating conductance, real part of Y_t
$\vec{G}$	Inhomogeneity parameter $\frac{1}{k^2}\nabla k^2$
$H_{2n}(z)$	Combination of Bessel functions $\frac{z\frac{d}{dz}h_n(z)}{h_n(z)}$
I	Current
I_Q	Collision integral
j_0	Integration parameter used in section 3
J_e	Electron random current density
$\vec{J}^s$	Source current density
k	Boltzmann constant
k	EM propagation constant in plasma
k_0	EM propagation constant in free space
k_p	EA propagation constant
K	$\frac{\sqrt{\mu_0/\epsilon_0}}{\pi} \ell n \cot \frac{\psi}{2}$

L	$n(n + 1)$
n	Mode number
n_{1Q}	Modified perturbed number density
n_0	D-C electron number density
$\hat{n}$	Unit normal surface vector
N_{max}, N_m	Maximum calculated value of modal number (n)
N_n	Legendre function normalization constant
p	Pressure
Q	Fluid flux source
$Q(\vec{v})$	Arbitrary function of velocity
$q_{jn}(y_2)$	Boundary functions
r_1, r_2	Radiator (r_1) and sheath edge (r_2) radii
r_0	D-C plasma parameter
r_a, r_b	Permittivity parameters
$R_1(r), R_2(r)$	Total radial portions of solutions to wave equations, related respectively to magnetic field and perturbed electron density
R_q	Bilinear admittance circle radius
$S_1, \ldots, S_6$	Normalized total variables related respectively to the TM mode components: Tangential magnetic field Perturbed electron density Tangential electric field Radial electron velocity Tangential electron velocity Radial electric field
$S'_1, \ldots, S'_6$	Modified forms of above, $S'_1 = \frac{1}{120} S_1$, etc.
T_e	Electron temperature
$T_1, \ldots, T_6$ $T_{1n}, \ldots, T_{6n}$	Normalized radial variables (related respectively to same fields as $S_1, \ldots, S_6$)
u_0	Electron drift velocity
u_0^+	Ion drift velocity
U	Normalized electron drift velocity, u_0/c
v	Electron velocity
v_0	Electron rms velocity
V	v_0/c; normalized thermal velocity
V'	Gap voltage
w	Transformed complex plane coordinates
$\vec{w}$	Random velocity
w_q	Bilinear admittance circle center

W_{1n}, W_{2n}	Modified radial solutions for "analytical" model
x_1	$k_0 r_1$; normalized radiator radius
x	$k_0 r$; normalized radial distance
y	Natural logarithm of normalized radius, $\ell n \frac{k_0 r}{k_0 r_1}$
y_a, y_b, Y_A, Y_B	Bilinear admittance parameters
Y_n	Modal admittance defined by equation 169
Y_n^+	Modal wave admittance defined by equation 157
Y_t	Terminating admittance
z_1	$\frac{\omega}{c} r_2 \sqrt{1 - (\omega_p/\omega)^2}$ normalized EM sheath edge distance
z_2	$\frac{\omega}{v_0} r_2 \sqrt{1 - (\omega_p/\omega)^2}$ normalized EA sheath edge distance
Z_n	Modal impedances
γ	Adiabatic constant
γ_1, γ_2	Normalized "propagation constants"
$\Delta\theta$	Spherical dipole gap angle
ϵ_r	Relative dielectric constant $\left(1 - (\omega_p/\omega)^2\right)$
ζ	Drift velocity factor, $\left(1 - \frac{u^2}{v^2}\right)^{-1}$
η	Normalized sheath potential, $\frac{e\phi_0}{kT}$
η_w	Normalized wall potential
$\Theta_1(\theta)$, $\Theta_2(\theta)$	Total angular portions of solutions to wave equations related respectively to magnetic field and perturbed electron density
κ_m	"Propagation constants" for "analytical" model
λ_D	Debye length, $\sqrt{\epsilon_0 kT_e/n_0 e^2}$
ξ	Perturbed electron position
ρ	Electron charge density
ρ^s	Source charge density
ρ_Q^s	Modified source charge density
σ	Surface charge density
Φ_e	Voltage equivalent of electron temperature
Φ_0	D-C plasma potential relative to the potential in the uniform region
ψ	Stress tensor
ψ	Gap edge angle $\psi = \pi/2 - \Delta\theta/2$
$\sum_n'$	Summation over odd integers

SUBSCRIPTS

j, k, ℓ, m, β	Matrix element subscripts, taking on values from 1-6 (j also denotes spatial components in appendix II)
n	Spherical "mode" number (odd integers only)
0	D-C quantities with the exception dictated by convention $v_0 \triangleq$ thermal velocity for perturbed electrons
r, θ, ϕ	Directions in a right-handed spherical coordinate system
T	Total quantities, i.e. $E_T = E_0 + E$
1, 2, 3, 4, 5, 6	Used for combinations of parameters to simplify algebraic manipulations, i.e., $T_3 = i\omega\epsilon_0 E_\theta$

Symbols with no subscripts denote first order (perturbed) quantities.

SUPERSCRIPTS

s	Source quantities (as opposed to surface quantities)
0	Field solutions normalized so that $T_{3n}^{(0)}(r_1) = 1$
1	$P_n^1(x)$ denotes associated Legendre Function
(1), (2)	Denotes first and second kind of spherical Hankel Functions, usually suppressed; i.e., $h_n^{(1)}(x) = h_n(x)$
+	Denotes ion quantities

A STUDY OF AN INHOMOGENEOUSLY SHEATHED SPHERICAL-DIPOLE ANTENNA IN A COMPRESSIBLE PLASMA

1
INTRODUCTION

1.1. STATEMENT OF PROBLEM

The basic problem discussed in this study is:

> What is the influence of a finite electron temperature on the terminating admittance of a plasma-imbedded spherical dipole?

It will be shown that previous analyses have oversimplified the problem and predicted influences much larger than those obtained with the more realistic model used in this study. A more specific statement of the problem considered is therefore:

> What is the influence of boundary conditions, realistic density inhomogeneities and d-c electric fields on the terminating admittance of a spherical dipole in a "warm" plasma?

A schematic illustration of the spherical dipole and typical plasma parameters that are considered is shown in figure 1. Previous analyses are modified in the light of the results obtained, and comparisons made where possible to the cylindrical dipole.

1.2. SURVEY OF PREVIOUS PLASMA-IMBEDDED DIPOLE ANALYSES

The term "dipole" is used to denote those antennas consisting of two separate conductors. The term is usually associated with thin cylindrical shapes with a pair of input terminals separating equal halves. Although this shape is most common for reasons of simplicity, the definition also includes conical, spheroidal and spherical shapes, not necessarily with symmetrical excitation, all of which have the virtue of being amenable to exact analysis, while the cylindrical dipole is not.

The theory of dipoles in homogeneous, isotropic, non-dissipative media is well established, with excellent agreement between theory and experiment. The theory for the cylindrical dipole antenna has been largely brought to its present state by King [1] based on the early work of Hallén who first analyzed the cylindrical dipole using an integral equation now bearing his name. The theory of conical dipoles was developed by Schelkunoff [2], that for spheroidal and spherical

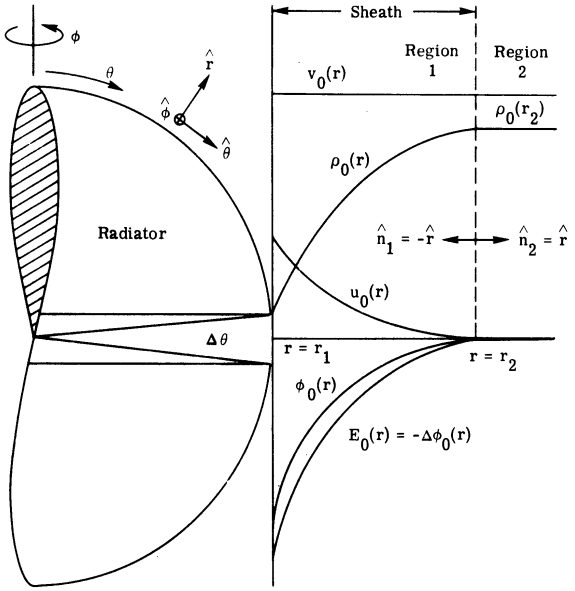

FIGURE 1. GEOMETRY AND NOMENCLATURE

dipoles by Chu and Stratton [3] (discussed also by Schelkunoff [2]). All but the first were developed by "modal" analysis—a method in which the wave equation is solved as a sum of "modes"; this method is described at length in the following sections.

When these dipoles are imbedded in a collisionless plasma and the plasma is considered as a dielectric, minor modifications appear in the various theories. These methods cannot be used as successfully with dissipative media (the simplest model of a plasma including collisions describes it as a dissipative medium) because of the lack of tabulations of the necessary functions for complex variables, although in principle the techniques remain the same. The problem is especially complicated for the cylindrical dipole, although King has successfully analyzed short and half-wave cylindrical dipoles with the Hallén integral equation approach [4, 5, 6]. It has also been shown by Deschamps [7] that the input impedance of dipoles in homogeneous dissipative media can be obtained from the non-dissipative medium results by analytic continuation into the complex frequency plane. The technique is not particularly convenient, since an accurate specification of the behavior in a dissipationless medium is needed first, but for complicated shapes on which experimental data is available, Deschamp's method would have an application. The present status of work on dipoles in homogeneous lossy media (which includes plasmas with finite collision frequency) has been given by Tai and Wait in recent survey articles [8, 9]. Experimental results in conducting fluids and plasmas seem to be in good qualitative agreement with the available theory [10, 11].

Subsequent to the King theoretical studies of plasma-imbedded cylindrical dipoles, Naval Research Laboratory reports were issued on the results of ionospheric probing using dipole impedance measurements [12, 13]. These discussed a sheath effect; but, more interestingly,

they attributed several of their results to the influence of the "electroacoustic" wave discussed in the next section. Shortly afterward, an analysis by Cohen [14] appeared on the excitation of these electroacoustic waves using a modification of the Poynting vector method (assumed current distribution). Similar Poynting vector method analyses have since been published by Chen [15], Wait [16], and Balmain [10]. These theories all predict a large effect.

A different type of analysis was performed by Hessel and Shmoys [17] for the spherical dipole. They also used an assumed current, but the ideas of modal analysis were inherent in their work. This has been extended by Wait [18] who included a complete modal analysis. However, Wait obtained only the input resistance by evaluating the Poynting vector in the far field rather than evaluating the surface fields as in the modal analyses of Chu and Stratton.

Another interesting aspect of previous electroacoustic wave investigations is that of propagation in an inhomogeneous plasma. The earliest inhomogeneous "warm" plasma study was that of Field [19], who obtained two coupled wave equations describing the behavior of waves propagating in an electric fieldfree, inhomogeneous warm plasma. Since then, similar equations have been given in the book by Ginzburg [20]. Because of the complexity, neither of these analyses were carried through for a particular inhomogeneity. Fortunately, a modal solution is possible for spherical inhomogeneities, even with the inclusion of the electroacoustic wave; several methods of solution are discussed in the next chapter.

There have been numerous other studies of electroacoustic wave influence on the radiation characteristics of slot as well as dipole antennas, but always in homogeneous compressible plasmas. Without exception these have predicted large effects; modifications of these analyses will be discussed in appendix V.

1.3. BRIEF DESCRIPTION OF A COMPRESSIBLE PLASMA

The earliest studies of plasmas largely ignored the influence of electron thermal motion on electromagnetic wave propagation. It is only recently that the influence of the electron kinetic energy has been included in predictions of electromagnetic wave phenomena. In these analyses, the terms "compressible," "thermal," and "warm" are used interchangeably to signify the inclusion of the effects of an electron velocity distribution. As for a non-ionized gas, it is found that a pressure or acoustic (longitudinal) wave can be transmitted with corresponding density variations.

There is no standard designation for these longitudinal waves. It is proposed that throughout this discussion, the longitudinal wave shall be termed the "electroacoustic" wave, shortened to "EA" wave in accordance with common usage in shortening electromagnetic to EM. The term "electroacoustic" is both descriptive and historical. The same waves are often termed plasma waves and even space charge waves; the term EA shall identify those waves whose essential

feature is propagation through an electron density gradient. It is an especially appropriate name since there is no magnetic field and the propagation is in some respects similar to that of sound waves. A term which may be valuable in denoting these waves, and also including those in media with zero temperature (but non-zero perturbed density), was suggested by Hok [21]: it is "electrokinetic" or "EK," which signifies energy propagation involving only electric and kinetic, but not magnetic, energy. These terms are still nonstandard, but since "electroacoustic" is the most widely used term in radiation analyses, it seems preferable to retain this terminology. A description of the differences between sound waves and EA waves has been given by Denisse and Delcroix [22] who refer to EA waves as "plasma waves."

There are two approaches that have been used in studying the EA wave: the kinetic, or microscopic, and hydrodynamic, or macroscopic. The former is most general and would probably be used exclusively were it not for its complexity in all but the simplest problems. Thus virtually all analyses have employed the hydrodynamic approach. The equivalence between the methods for propagation in infinite homogeneous media has been shown by Oster [23].

The basic equations in the hydrodynamic approach are the Maxwell (curl) equations, the equation for charge continuity, and the equation for force on an electron. The latter two can be derived as moment equations of the Boltzmann equation, which is the fundamental equation of the kinetic approach. Higher order moments are dropped by arbitrarily setting the heat flux tensor equal to zero. Since these moment equations are not the matter of prime interest, the derivation and further discussion of the nature of the EA wave is given in appendix II.

A few further general remarks are necessary, however. In the equations which follow in the next section, the perturbed electron charge density rather than pressure perturbation is used as the fundamental parameter. Thus, it follows from the adiabatic change-of-state relation, that

$$-ep = \gamma k T_e \rho \tag{1}$$

where p is the pressure, T_e the electron temperature, ρ the perturbed electron charge density and γ is the ratio of specific heats. The rms thermal velocity is obtained from the equipartition law

$$v_0^2 = 3k\frac{T_e}{m} \tag{2}$$

where k is the Boltzmann constant. A further discussion of these relations is contained in appendix II and section 3, where the use of $\gamma = 3$ is justified. Consequently, we can write

$$-ep = mv_0^2\rho \tag{3}$$

The conditions which must be imposed on the plasma to allow a description in this form are fairly severe [22]. First, "the wavelength must be considerably larger than the interparticle distance, $n_0^{-1/3}$." Second, "the speed of the particle must be so low that the mean distances between most of the interacting particles do not change appreciably during the period of oscillations." Further characteristics and assumptions are best discussed in the context of the Boltzmann equation given in appendix II.

1.4. JUSTIFICATION AND DESCRIPTION OF THE PROPOSED METHOD OF ANALYSIS

Experimental cylindrical dipole results in an early phase of this study never indicated any evidence of an EA wave, in contradiction with the large results predicted by Cohen [14] and others. Moreover, a comparison of the NRL results [12, 13] with the King material [4, 6] indicated that the NRL experimental results could be caused by collision frequency rather than by EA wave effects. Because of the possibility of mode conversion between EM and EA waves in an inhomogeneous medium, it was obviously important to retain the influence of the physical "sheath" region that surrounds objects in a plasma, which had not been previously discussed. For these reasons, it became evident that there was a definite need to critically examine the excitation of electroacoustic waves. Because of its simplicity and prior experimental work, the dipole was chosen for this study.

Various methods of analysis have been used in the past to analyze dipole antennas. An account of the different types of analyses is given by Krause [24], it is only necessary here to relate these methods to the problem of dipoles in inhomogeneous and compressible plasmas. The methods as listed by Krause for the electric dipole are:

(1) The boundary-value problem approach
(2) The transmission-line method
(3) The Poynting vector method

The boundary-value problem approach is the most rigorous, but in its simplest form is limited in applicability to antenna shapes such as the sphere and spheroid. For the EA wave there is the complication of additional boundary conditions. Practical electric dipoles are nearly always cylindrical and analyzed by using the Hallén integral equation. The extension of this integral equation approach to include compressible plasmas may be possible, but its use does not seem justified at this point in the developing theory of EA wave excitation. Its use is not possible for inhomogeneous media, due to the nonavailability of Green's functions. Surprisingly, the use of any of these techniques when the compressible plasma is assumed homogeneous is not necessary, with certain plausible boundary conditions. This is discussed in appendix VI.

The transmission-line method "lends itself most appropriately to the biconical antenna . . . It may also be called a boundary-value method . . . [24]." This method is not discussed herein

because the wave equation cannot be separated in spherical coordinates with the angular inhomogeneity necessary to approximate a sheath surrounding a biconical antenna. For that reason the method is not of interest in this discussion.

The general approach of the third method, the Poynting vector method, "is to integrate the Poynting vector over a surface enclosing the antenna or to perform an equivalent calculation. Two limiting cases of this method have been discussed: (1) where the surface of integration coincides with the surface of the antenna and (2) where the surface of integration is a sphere at a large distance from the antenna [24]." This method has been applied to the compressible plasma by numerous authors and is discussed in detail in appendix VI. Its use is questionable even for EM waves since a current must be assumed; the method is mainly justified by its success. With EA waves an assumption of the form of the current is even less tenable since there is no prior experience to justify a choice. The study of sheath influence cannot be handled in this way without prior knowledge of the influence of the sheath on the current distribution. In appendix VI the validity of this method is questioned both in terms of the reasonableness of the results and of the basic equations.

It is now obvious that in order to accurately model the complicated region surrounding a plasma-imbedded radiator only the first method is suitable. Because most practical dipoles are cylindrical, it would be of definitely greater engineering importance to study the spheroid rather than the sphere. However, as for the biconical antenna, the wave equation expressed in spheroidal coordinates is not separable when the medium is inhomogeneous.

Having thus limited the study to a spherical configuration does not, however, mean that the results are of value only for the spherical dipole. Since the free-space characteristics of many different shapes of dipoles are similar, the present results should be of decided advantage in interpreting experimental results for less restricted shapes. Extensions will be made where possible.

The physical model which is to be studied is shown in figure 1. The antenna consists of two hemispheres separated by a narrow gap of width $\Delta\theta$. Internally there is presumed to exist a generator which supplies an antisymmetric excitation to the two hemispheres. This manifests itself as an applied electric field across the gap of magnitude $\frac{V'}{r_1\Delta\theta}$. This study will concern itself mainly with the evaluation of the terminating admittance seen at the gap. This is the ratio of current to voltage in the equivalent circuit for the TEM wave by itself. In using these admittance data for experimental verification, the gap angle, $\Delta\theta$, and the exact nature of the input region are of great importance. This aspect of the problem has been thoroughly explored by others [2], therefore the present study is restricted to calculation of the terminating admittance seen at the sphere edge.

Figure 1 indicates schematically two regions which lie external to the sphere: (1) a non-uniform plasma region known as the sheath and (2) a uniform region beyond radius r_2 known as the homogeneous region. The plasma is presumed to not exist in the biconical region (perhaps prevented by a thin dielectric). In the sheath region, the electrons experience a repulsive force from the indicated potential $\phi(r)$. A perturbing body, such as the spherical dipole, must have zero random current arrival—that is, equal numbers of incoming electrons and ions. The lighter mass electrons therefore accumulate on the perturbing body (the sphere) until the static potential is sufficiently negative to equate the incoming electron and ion currents. Although each electron experiences a repulsive force, there are a sufficient number of high energy electrons to give a net drift velocity inward and thereby balance the accelerated ion flow. This electron drift velocity has been ignored in previous analyses but is initially retained here in order to demonstrate the problems involved in including it in the analysis and to allow for its development in future work. The influence of the gap on the d-c drift velocity is assumed to be small (i.e., $\vec{u}_0 = u_0(r)\hat{r}$). In the external homogeneous region the d-c drift velocity, potential, and electric field are assumed to be zero.

Further discussion of the sheath parameters and justifications for the models used in the numerical analysis are presented in section 3 where it is shown that the assumed electron density and potential profiles are reasonable approximations to more complete theoretical results.

1.5. OUTLINE OF THE ANALYSIS

The approach to be followed in the remainder of this study is:

(1) Presentation and simplification of the most basic equations
(2) Solutions, as possible, for successively simpler physical models
(3) Specification of the parameters
(4) Discussion of the boundary conditions
(5) Discussion of the method of solution and modifications to the usual mode theory of spherical dipoles
(6) Presentation of numerical results for terminating admittance
(7) Spatial variations
(8) Discussion of results

The first two topics comprise the second section; the remaining topics are contained in the sections with corresponding numbers.

Some of the important material has been placed in separate appendixes because its inclusion in the main body would slow down the reader who is already familiar with this field. Appendix I covers mathematical relations; appendix II, hydrodynamic equations; appendix III, boundary

conditions; appendix IV, limiting value of input susceptance; appendix V, influence of collision frequency; and appendix VI, modification of previous EA wave excitation analyses.

2
MATHEMATICAL FORMULATION

2.1. SIMPLIFICATION OF THE MOST GENERAL BASIC EQUATIONS

As described in the first section, compressible plasma studies fall into two categories: the kinetic (microscopic) and hydrodynamic (macroscopic). The derivation of the hydrodynamic equations from the kinetic formulation has been given many times, but is repeated in appendix II in a form that includes inhomogeneities and explains the assumptions necessary in this application. The hydrodynamic equations given below do not include source terms which are, however, used in the Poynting vector method described in appendix VI.

In this free electron description, Maxwell's equations and the electron moment equations (continuity and force) are

$$\nabla \times \vec{H}_T - \rho_T \vec{v}_T + \rho_T^+ \vec{v}_T^+ - \epsilon_0 \frac{\partial \vec{E}_T}{\partial t} = 0 \tag{4}$$

$$\nabla \times \vec{E}_T + \mu_0 \frac{\partial \vec{H}_T}{\partial t} = 0 \tag{5}$$

$$\nabla \cdot \rho_T \vec{v}_T + \frac{\partial \rho_T}{\partial t} = 0 \tag{6}$$

$$\rho_T \left[m\left(\frac{\partial \vec{v}_T}{\partial t} + (\vec{v}_T \cdot \nabla)\vec{v}_T \right) + e\vec{E}_T \right] - e\nabla p_T = 0 \tag{7}$$

The field variables are defined in (8); the symbolism is fairly standard. It is also summarized in the list of symbols. Similar moment equations could be given for the ions, but their influence is ignored in this analysis.

The basic equations above may be simplified by assuming that separation into d-c (subzero) and RF (no subscript) quantities is permissible:

$$\begin{aligned}
&\text{magnetic field: } \vec{H}_T = 0 + \vec{H}\, e^{-i\omega t} \\
&\text{electric field: } \vec{E}_T = E_0(r)\hat{r} + \vec{E}\, e^{-i\omega t} \\
&\text{electron density: } \rho_T = \rho_0(r) + \rho\, e^{-i\omega t};\ \rho_0 = -en_0 \\
&\text{electron velocity: } \vec{v}_T = u_0(r)\hat{r} + \vec{v}\, e^{-i\omega t} \\
&\text{ion density: } \rho_T^+ = \rho_0^+(r) \\
&\text{ion velocity: } v_T^+ = u_0^+(r) \\
&\text{pressure: } -ep_T = \tfrac{1}{3} m v_0^2 \rho_0 + m v_0^2 \rho
\end{aligned} \tag{8}$$

where $e = |e|$, so ρ_0 is negative, ρ_0^+ is positive. This pressure definition and thermal velocity, v_0, are discussed in appendix II and section 3.

This technique allows the development of separate d-c and linear RF equations when products of RF quantities are ignored. With the help of vector identities and differentiations given in appendix I, the zeroth order (d-c) equations are

$$\begin{aligned} \rho_0 u_0 - \rho_0^+ u_0^+ &= 0 \\ \rho_0\left(u_0 m \frac{du_0}{dr} + eE_0\right) + \frac{mv_0^2}{3}\frac{d\rho_0}{dr} &= 0 \\ \frac{d}{dr}\left(\rho_0 u_0 + \rho_0^+ u_0^+\right) &= 0 \end{aligned} \tag{9}$$

The development of functions which satisfy these d-c relations is postponed to the next chapter in order to facilitate the development of the first order equations which are of immediate interest.

These first order equations are easily shown to be

$$\nabla \times \vec{H} = \rho_0 \vec{v} + u_0 \rho \hat{r} + \epsilon_0 \frac{\partial \vec{E}}{\partial t} \tag{10}$$

$$\nabla \times \vec{E} = -\mu_0 \frac{\partial \vec{H}}{\partial t} \tag{11}$$

$$\nabla \cdot (\rho_0 \vec{v} + u_0 \rho \hat{r}) + \frac{\partial \rho}{\partial t} = 0 \tag{12}$$

$$\begin{aligned} m\rho_0\left[\frac{\partial \vec{v}}{\partial t} + u_0 \nabla v_r + v_r \nabla u_0\right] + m\rho u_0 \nabla u_0 - m\rho_0 u_0 \hat{r} \times (\nabla \times \vec{v}) \\ + \rho_0 e\vec{E} + \rho e E_0 \hat{r} + mv_0^2 \nabla \rho = 0 \end{aligned} \tag{13}$$

These four equations give ten linear relations between the ten variables: $\vec{H}$, $\vec{E}$, $\vec{v}$, $\vec{\rho}$. Four of the relations involve only four variables if the assumption is made that all variables are independent of $\phi\left(\text{i.e., } \frac{\partial}{\partial \phi} = 0\right)$. Using the relations of appendix I $\left(\text{when } \frac{\partial}{\partial t} \triangleq -i\omega\right)$ gives for these four relations comprising the transverse electric (TE) mode (variables: H_r, H_θ, E_ϕ, v_ϕ)

$$\begin{aligned} (\text{curl } E)_r \quad & \frac{1}{r \sin\theta}\frac{\partial}{\partial \theta}(\sin\theta E_\phi) - i\omega\mu_0 H_r = 0 \\ (\text{curl } E)_\theta \quad & -\frac{1}{r}\frac{\partial}{\partial r}(rE_\phi) - i\omega\mu_0 H_\theta = 0 \\ (\text{curl } H)_\phi \quad & \frac{1}{r}\frac{\partial}{\partial r}(rH_\theta) - \frac{1}{r}\frac{\partial H_r}{\partial \theta} - \rho_0 v_\phi + i\omega\epsilon_0 E_\phi = 0 \\ (\text{force})_\phi \quad & + i\omega m\rho_0 v_\phi - \frac{\rho_0 m u_0}{r}\frac{\partial}{\partial r}(rv_\phi) - e\rho_0 E_\phi = 0 \end{aligned} \tag{14}$$

The remaining six equations define the (TM) mode (variables: H_ϕ, E_r, E_θ, v_r, v_ϕ, ρ). The fact that equation (14) can be separated from the others is most important: there is no coupling between TE and TM modes due to the compressibility of the plasma if the mode fields do not depend on ϕ (and only if $\vec{u}_0$ is assumed to be independent of θ as herein). Since the boundary conditions (given in section 4) preclude the existence of E_ϕ at the radiator, the entire TE mode (given in (14)) will remain unexcited and can be dropped from further discussion.

The six relations defining the TM mode are presented in table I. The format used there is intended to illustrate the influence of the various parameters and models on the number and type of terms that must be included. For the free space radiation problem, only three variables and the top three equations of column I are necessary. A cold stationary plasma (column II) requires only the addition of simple equations although this is usually handled by defining $\epsilon_r = 1 + \frac{e\rho_0}{m\epsilon_0\omega^2} = 1 - \frac{\omega_p^2}{\omega^2}$. The inclusion of thermal velocities (column III) is seen to require another equation as well as added force terms. The inclusion of field-free inhomogeneities (column IV) only adds a single term in the continuity equation, while the inclusion of electric fields (column V) affects only the radial force equation. Finally, the inclusion of a (varying) drift velocity is seen to add seven terms in the last four equations, as shown in column VI.

This set of six scalar equations seems to be the only approach to solving the problem when the drift velocity is included; no other study is known which includes the drift velocity. The

TABLE I. BASIC EQUATIONS

Equation	I Free Space Terms	II Cold Plasma	III Warm Plasma	IV Inhomogeneities	V Electric Field	VI Drift Velocity	
$(\text{curl } E)_\phi$	$i\omega\mu_0 H_\phi - \frac{1}{r}\frac{\partial}{\partial r}(rE_\theta) + \frac{1}{r}\frac{\partial E_r}{\partial \theta}$						$= 0$
$(\text{curl } H)_\theta$	$-\frac{1}{r}\frac{\partial}{\partial r}(rH_\phi) + i\omega\epsilon_0 E_\theta$	$-\rho_0 v_\theta$					$= 0$
$(\text{curl } H)_r$	$-\frac{1}{r\sin\theta}\frac{\partial}{\partial\theta}(\sin\theta H_\phi) - i\omega\epsilon_0 E_r$	$+\rho_0 v_r$				$u_0\rho$	$= 0$
$(\text{force})_\theta$	$-e\rho_0 E_\theta$	$+i\omega m\rho_0 v_\theta$	$-mv_0^2\frac{1}{r}\frac{\partial\rho}{\partial\theta}$			$-\rho_0\frac{mu_0}{r}\frac{\partial}{\partial r}(rv_\theta)$	$= 0$
$(\text{force})_r$	$-e\rho_0 E_r$	$+i\omega m\rho_0 v_r$	$-mv_0^2\frac{\partial\rho}{\partial r}$		$-eE_0\rho$	$-\rho_0 mu_0\frac{\partial v_r}{\partial r}$ $-\rho_0 m\left(\frac{du_0}{dr}\right)v_r$ $-mu_0\left(\frac{du_0}{dr}\right)\rho$	$= 0$
(continuity)		$-\frac{\rho_0}{r\sin\theta}\frac{\partial}{\partial\theta}(\sin\theta v_\theta)$ $+\rho_0\frac{\partial v_r}{\partial r}$	$+i\omega\rho$	$-\frac{1}{r^2}\left[\frac{d}{dr}\left(r^2\rho_0\right)\right]v_r$		$-u_0\frac{\partial\rho}{\partial r}$ $-\frac{1}{r^2}\left[\frac{d}{dr}\left(r^2u_0\right)\right]\rho$	$= 0$

arbitrary exclusion of the drift velocity does, however, allow considerable simplification, which is presented in the next section. It should also be noted that the usual [14, 17] decomposition into separate electromagnetic and electroacoustic modes is neither necessary nor profitable, even with a homogeneous plasma. Such a decomposition is noted briefly in appendix VI. Thus, the difficulty of the basic equations is believed to preclude any other attack.

To proceed further with the six partial differential equations of table I requires the assumption that the fields have the same angular variation that they would have in a homogeneous plasma. This allows a separation of variables in order to obtain ordinary differential equations. The assumption can, of course, be correct only if the solutions satisfy all six equations. Completeness and uniqueness follow as for homogeneous media.

The solutions are therefore assumed to take the form

$$
\begin{aligned}
H_\phi &= \sum_n T_{1n}(r) P_n^1(\cos\theta) = S_1(r, \theta) \\
\frac{v_0^2}{i\omega}\rho &= \sum_n T_{2n}(r) P_n(\cos\theta) = S_2(r, \theta) \\
i\omega\epsilon_0 r E_\theta &= \sum_n T_{3n}(r) P_n^1(\cos\theta) = S_3(r, \theta) \\
\rho_0 r v_r &= \sum_n T_{4n}(r) P_n(\cos\theta) = S_4(r, \theta) \\
\rho_0 r v_\theta &= \sum_n T_{5n}(r) P_n^1(\cos\theta) = S_5(r, \theta) \\
i\omega\epsilon_0 r E_r &= \sum_n T_{6n}(r) P_n(\cos\theta) = S_6(r, \theta)
\end{aligned}
\tag{15}
$$

where $P_n(\cos\theta)$ and $P_n^1(\cos\theta)$ are respectively the Legendre function of degree n and associated Legendre function of degree n and order one. The normalization and ordering of the variables given above allows considerable simplification in the equations. In accordance with the discussion given in section 4, n is required to be an integer, and the Legendre functions of the second kind, $\left(Q_n(\cos\theta) \text{ and } Q_n^1(\cos\theta)\right)$, are excluded to maintain finiteness in the fields at $\theta = 0, \pi$. The summation convention is that $\sum_n = \sum_{n=-\infty}^{\infty}$.

In order to verify this choice of field representation, two identities involving Legendre functions are necessary:

$$\frac{d}{d\theta}(P_n(\cos\theta)) = -P_n^1(\cos\theta)$$
$$\frac{1}{\sin\theta}\frac{d}{d\theta}\left(\sin\theta\, P_n^1(\cos\theta)\right) = n(n+1)P_n(\cos\theta) \tag{16}$$

Application of these identities in the equations of table I shows that the first, third, and fourth rows involve only summations of $P_n^1(\cos\theta)$, while the second, fifth, and sixth involve only summations of $P_n(\cos\theta)$. Since both functions are orthogonal functions (that is, multiplication by $P_k^1(\cos\theta)$ or $P_k(\cos\theta)$ and integrations over $0 \leqq \theta \leqq \pi$ give a contribution only for n = k), the equations must be satisfied for each n separately, giving (note the change of order)

$$(\text{curl } H)_\theta: \quad \frac{1}{r}\frac{d}{dr}rT_1 = \frac{1}{r}(T_3 - T_5)$$

$$(\text{force})_r: \quad i\omega m\frac{dT_2}{dr} + \rho_0 mu_0\frac{d}{dr}\left(\frac{T_4}{\rho_0 r}\right) = \left(-eE_0 - mu_0\frac{du_0}{dr}\right)\frac{i\omega}{v_0^2}T_2$$
$$+\left(im\omega\rho_0 - m\rho_0\frac{du_0}{dr}\right)\frac{T_4}{\rho_0 r} - \frac{e\rho_0}{i\omega\epsilon_0 r}T_6$$

$$(\text{curl } E)_\phi: \quad \frac{1}{r}\frac{d}{dr}\left(\frac{T_3}{i\omega\epsilon_0}\right) = i\omega\mu_0 T_1 - \frac{1}{r^2}\frac{T_6}{i\omega\epsilon_0}$$

$$(\text{continuity}): \quad u_0\frac{i\omega}{v_0^2}\frac{dT_2}{dr} + \rho_0\frac{d}{dr}\left(\frac{T_4}{\rho_0 r}\right) = +\left(i\omega - \frac{1}{r^2}\frac{d}{dr}\left(r^2 u_0\right)\right)\frac{i\omega}{v_0^2}T_2 \tag{17}$$
$$-\frac{1}{r^2}\frac{d}{dr}\left(r^2\rho_0\right)\frac{T_4}{\rho_0 r} - \frac{n(n+1)}{r^2}T_5$$

$$(\text{force})_\theta: \quad \rho_0 mu_0\frac{1}{r}\frac{d}{dr}\left(\frac{T_5}{\rho_0}\right) = +i\omega m\frac{T_2}{r} + \frac{-e\rho_0}{i\omega\epsilon_0 r}T_3 + i\omega m\frac{T_5}{r}$$

$$(\text{curl } H)_r: \quad 0 = -\frac{n(n+1)}{r}T_1 + \frac{i\omega u_0}{v_0^2}T_2 + \frac{T_4}{r} - \frac{T_6}{r}$$

Note that the subscript "n" has been suppressed in these equations. These equations may be rewritten in a normalized form by defining

$$\frac{\omega^2}{c^2} = \omega^2 \mu_0 \epsilon_0 = k_0^2,\ k_0 r = x$$

$$\omega_p^2 = \frac{-e\rho_0}{m\epsilon_0}$$

$$L = n(n+1)$$

$$U = u_0/c$$

$$V = v_0/c \tag{18}$$

$$f_2 = \frac{1}{V^2}\left(r\frac{eE_0}{mc^2} + Ux\frac{dU}{dx}\right)$$

$$f_3 = \rho_0 x \frac{d}{dx}\left(\frac{U}{\rho_0 x}\right)$$

$$f_4 = 2xU + x^2\frac{dU}{dx}$$

$$f_5 = \frac{U}{\rho_0}\frac{d}{dx}\rho_0$$

This gives

$$x\frac{dT_1}{dx} = -T_1 + T_3 - T_5$$

$$x\frac{dT_2}{dx} - iU\frac{dT_4}{dx} = -f_2 T_2 + (1 + if_3)T_4 - \frac{\omega_p^2}{\omega^2}T_6$$

$$x\frac{dT_3}{dx} = -x^2 T_1 - T_6$$

$$i\frac{U}{V^2}x^2\frac{dT_2}{dx} + x\frac{dT_4}{dx} = -\frac{1}{V^2}\left(x^2 + if_4\right)T_2 - T_4 - LT_5 \tag{19}$$

$$iU\frac{dT_5}{dx} = -T_2 + \frac{\omega_p^2}{\omega^2}T_3 - (1 - if_5)T_5$$

$$0 = -LT_1 + \frac{iU}{V^2}xT_2 + T_4 - T_6$$

These equations are considerably simpler than the partial differential equations given in table I. It is apparent that T_6 can be easily eliminated since no derivatives of T_6 appear and thus the system reduces to five equations. It is also advantageous to manipulate the second and fourth equations of (19) so that the left-hand sides contain only one derivative; the resultant set can be put in the matrix form

$$x\frac{dT_j}{dx} = D_{jk}T_k (j,k = 1, \ldots, 5) \tag{20}$$

The elements of the D_{jk} matrix are given in table II. In this form the coupled equations are compactly presented, but nevertheless sufficiently complicated to preclude attempts at further analytical development.

TABLE II. MATRIX ELEMENTS D_{jk} where $\zeta = \left(1 - \frac{U^2}{V^2}\right)^{-1}$

	K				
J	1	2	3	4	5
1	-1	0	1	0	-1
2	$\zeta\frac{\omega_p^2}{\omega^2}L$	$-\zeta\frac{U}{V^2}\left(\frac{reE_0}{Umc^2} - 2U\right)$ $-i\zeta\frac{U}{V^2}\left(1 + \frac{\omega_p^2}{\omega^2}\right)x$	0	$\zeta\left(1 - \frac{\omega_p^2}{\omega^2}\right)$ $+i\zeta x^2\rho_0\frac{d}{dx}\left(\frac{U}{\rho_0 x^2}\right)$	$-i\zeta\frac{UL}{x}$
3	$L - x^2$	$-i\frac{U}{V^2}x$	0	-1	0
4	$-i\zeta\frac{U}{V^2}\frac{\omega_p^2}{\omega^2}Lx$	$-\zeta\frac{x^2}{V^2}\left(1 + \frac{U^2\omega_p^2}{V^2\omega^2}\right)$ $+i\frac{\zeta}{V^2}\left[\frac{U^2x}{V^2}\left(\frac{reE_0}{Umc^2} + x\frac{dU}{dx}\right) - \frac{d}{dx}(x^2U)\right]$	0	$\zeta\left[-1 + \frac{\rho_0 Ux^2}{V^2}\frac{d}{dx}\left(\frac{U}{\rho_0 x}\right)\right]$ $-i\left(1 - \frac{\omega_p^2}{\omega^2}\right)\zeta\frac{U}{V^2}x$	$-L\zeta$
5	0	$i\frac{1}{U}x$	$-i\frac{1}{U}\frac{\omega_p^2}{\omega^2}x$	0	$\frac{x}{\rho_0}\frac{d\rho_0}{dx}$ $+i\frac{1}{U}x$

Numerical integration of this set of equations is necessary because of the complicated nature of the d-c sheath parameters $E_0(r)$, $u_0(r)$ and $\rho_0(r)$. Further discussion of the solution to the set of equations in (20) must, however, be postponed until these parameters are specified (section 3) and the boundary conditions justified (section 4).

However, an appreciation of the influence of the sheath inhomogeneity can be obtained by dropping the d-c velocity terms in (20). A special case is then found to be amenable to analytic solution. The further development of the simplified defining equations is, therefore, presented below in section 2.2.

2.2. BASIC EQUATIONS IGNORING D-C VELOCITY

When the effect of the d-c velocity is ignored a priori (while retaining the d-c electric field term), the equations in (20) take on a much simpler form. After multiplication by u_0 and letting u_0 go to zero, the last of the equations in (20) takes on a much simpler form, allowing the variable T_5 to be eliminated from the equations through

$$T_5 = -T_2 + \frac{\omega_p^2}{\omega^2} T_3 \tag{21}$$

Substitution of (21) into (20) gives the set

$$x\frac{dT_1}{dx} = -T_1 + T_2 + \left(1 - \frac{\omega_p^2}{\omega^2}\right)T_3 \tag{22}$$

$$x\frac{dT_2}{dx} = L\left(\frac{\omega_p^2}{\omega^2}\right)T_1 - \frac{1}{V^2}\left(\frac{reE_0}{mc^2}\right)T_2 + \left(1 - \frac{\omega_p^2}{\omega^2}\right)T_4 \tag{23}$$

$$x\frac{dT_3}{dx} = (L - x^2)T_1 - T_4 \tag{24}$$

$$x\frac{dT_4}{dx} = \left(L - \frac{1}{V^2}x^2\right)T_2 - L\left(\frac{\omega_p^2}{\omega^2}\right)T_3 - T_4 \tag{25}$$

where, as before,

$$x = k_0 r$$

$$V = \frac{v_0}{c}$$

$$L = n(n + 1)$$

and T_1, T_2, T_3, T_4 denote the nth mode radial variations of variables related to H_ϕ, ρ, E_θ, and v_r respectively.

To effect a further simplification, it can be noted that the variables T_3 and T_4 may be eliminated from (24) and (25) by use of (22) and (23). If we introduce a change of variables

$$y = \ell n\left(\frac{x}{x_1}\right);\ x = x_1 e^y \tag{26}$$

where $x_1 = k_0 r_1$, so

$$\frac{d}{dy} = x\frac{d}{dx} \tag{27}$$

and further define

$$-F_2 = \frac{1}{V^2}\frac{reE_0}{mc^2} \tag{28}$$

$$\epsilon_r = 1 - \frac{\omega_p^2}{\omega^2} \tag{29}$$

and denote y derivatives by primed quantities, equations (24) and (25) can be put in a form suitable for numerical (especially analog) computations:

$$T_1'' + T_1'(1 - (\ell n\,\epsilon_r)') + T_1\left[\epsilon_r\left(-L + x_1^2 e^{2y}\right) - (\ell n\,\epsilon_r)' - \frac{\omega_p^2}{\omega^2}L\right] = T_2[F_2 - (\ell n\,\epsilon_r)'] \tag{30}$$

$$T_2'' + T_2'(-F_2 + 1 - (\ell n\,\epsilon_r)') + T_2\left[-(1 - (\ell n\,\epsilon_r)')F_2 - (F_2)' + \epsilon_r\left(-L + \frac{x_1^2}{V^2}e^{2y}\right) - L\frac{\omega_p^2}{\omega^2}\right] = -T_1 L(\ell n\,\epsilon_r)' \tag{31}$$

When the medium is homogeneous, these equations are satisfied by spherical Bessel functions. However, the effect of the inhomogeneous medium is to couple the two wave equations and thereby modify the propagation and character of both the electromagnetic (T_1) and electroacoustic (T_2) waves. The calculations which follow will illuminate the nature of this modification.

An alternative derivation of (30) and (31) is helpful in understanding the role of the density inhomogeneity. By manipulating the fundamental equations (10) and (13) when $u_0 = 0$

$$i\omega\epsilon_0\vec{E} = \frac{-1}{1 - (\omega_p/\omega)^2}\left\{\nabla\times H + \frac{iv_0^2}{\omega}\nabla\rho + \frac{ie\rho}{m\omega}E_0\hat{r}\right\} \tag{32}$$

$$\frac{m\epsilon_0\omega^2}{e}\vec{v} = \frac{1}{1-\left(\omega_p/\omega\right)^2}\left\{\nabla\times\vec{H} + \frac{i\omega v_0^2}{\omega_p^2}\nabla\rho + \frac{ie\omega\rho}{m\omega_p^2}E_0\hat{r}\right\} \tag{33}$$

(Separate equations for E and v are not obtainable when the d-c velocity is retained. Insertion of (32) and (33) into (11) and (12) gives

$$(\nabla^2 + k^2)\vec{H} + \vec{G}\times(\nabla\times\vec{H} = -i\frac{v_0^2}{\omega}(\vec{G} + \vec{F}_0)\times\nabla\rho \tag{34}$$

$$\left(\nabla^2 + k_p^2\right)\rho - (\vec{G} - \vec{F}_0)\cdot\nabla\rho + (\nabla\cdot\vec{F}_0 - \vec{G}\cdot\vec{F}_0)\rho = -\frac{i\omega}{v_0^2}\vec{G}\cdot(\nabla\times\vec{H}) \tag{35}$$

where

$$\vec{G} = \frac{1}{k^2}\nabla k^2 = \frac{1}{\epsilon_r}\nabla\epsilon_r \tag{36}$$

$$\vec{F}_0 = \frac{eE_0\hat{r}}{mv_0^2} = \frac{F_2}{r}\hat{r} \tag{37}$$

$$k^2 = \omega^2\mu_0\epsilon_0\epsilon_r \tag{38}$$

$$\epsilon_r = 1 - \frac{\omega_p^2}{\omega^2} \tag{39}$$

$$k_p^2 = k^2\frac{c^2}{v_0^2} \tag{40}$$

The first terms in each equation are those for homogeneous plasmas; they have been derived by numerous authors [14, 17], and are invariably obtained after an unnecessary separation of the fields into EM and EA components. A comparison of (34) and (35) with (30) and (31) is somewhat difficult, but can be accomplished. To prove the necessary agreement, it is most straightforward to drop the d-c electric field. This is undertaken not only to simplify the problem, but also to obtain a closed form solution which can be used as an independent measure of the accuracy of the numerical computations presented in later sections when F_0 is included. Although the coupling of the EM and EA waves can be studied, there does not seem to be any means of obtaining a closed form solution when F_0 is included.

2.3. PARTICULAR SOLUTION FOR DENSITY INHOMOGENEITY ONLY

As mentioned in the preceding section, an analytical solution to the four coupled first order equations (22) through (25) is not, in general, possible, even with the exclusion of the electric field, E_0. In fact, in this form it is not apparent even what special cases might simplify the problem. For this reason, and in order to appreciate the modifications in the usual wave equation analysis, the alternative approach begun in the last section (but now letting $F_0 = 0$) will now be developed further. Using the differential operators from appendix I, the coupled wave equations (34) and (35) take the form

$$\frac{1}{r^2}\frac{\partial}{\partial r}\left(r^2\frac{\partial H_\phi}{\partial r}\right) + \frac{1}{r^2\sin\theta}\frac{\partial}{\partial\theta}\left(\sin\theta\frac{\partial H_\phi}{\partial\theta}\right) - \frac{H_\phi}{r^2\sin^2\theta} + k^2 H_\phi - \frac{1}{r}G_r\frac{\partial}{\partial r}(rH_\phi) + \frac{1}{r}i\frac{v_0^2}{\omega}G_r\frac{\partial\rho}{\partial\theta} = 0 \quad (41)$$

and

$$\frac{1}{r^2}\frac{\partial}{\partial r}\left(r^2\frac{\partial\rho}{\partial r}\right) + \frac{1}{r^2\sin\theta}\frac{\partial}{\partial\theta}\left(\sin\theta\frac{\partial\rho}{\partial\theta}\right) + k_p^2\rho - G_r\frac{\partial\rho}{\partial r} + \frac{i\omega G_r}{v_0^2 r\sin\theta}\frac{\partial}{\partial\theta}(\sin\theta H_\phi) = 0 \quad (42)$$

Assume, as in section 2.1, that separation of variables is possible:

$$\begin{aligned} H_\phi(r,\theta) &= R_1(r)\Theta_1(\theta) \\ \rho(r,\theta) &= \rho(r,\theta) = \left(i\omega/v_0^2\right)(R_2(r)\Theta_2(\theta)) \end{aligned} \quad (43)$$

so that (41) and (42) become (after inserting (43) and dividing through by H_ϕ/r^2 and ρ/r^2 respectively)

$$\left[\frac{1}{R_1}\frac{d}{dr}\left(r^2\frac{dR_1}{dr}\right) + k^2r^2\right] + \left[\frac{1}{\Theta_1\sin\theta}\frac{d}{d\theta}\left(\sin\theta\frac{d\Theta_1}{d\theta}\right) - \frac{1}{\sin^2\theta}\right] - \left[\frac{G_r}{R_1}r\frac{d}{dr}(rR_1)\right] - \left[\frac{rR_2G_r}{R_1\Theta_1}\cdot\frac{d\Theta_2}{d\theta}\right] = 0 \quad (44)$$

$$\left[\frac{1}{R_2}\frac{d}{dr}\left(r^2\frac{dR_2}{dr}\right) + k_p^2r^2\right] + \left[\frac{1}{\Theta_2\sin\theta}\frac{d}{d\theta}\left(\sin\theta\frac{d\Theta_2}{d\theta}\right)\right] - \left[\frac{G_r}{R_2}\frac{r^2dR_2}{dr}\right] + \left[\frac{R_1r}{R_2\Theta_2}\frac{G_r}{\sin\theta}\frac{d}{d\theta}(\sin\theta\Theta_1)\right] = 0 \quad (45)$$

The assumption of separation of variables for a single wave equation is usually followed by noting that specific combinations of the terms are functions of only one variable and, therefore, must be constants. In the present example, for homogeneous media, $G_r = 0$, the last two

bracketed terms of (44) and (45) are zero. Then setting each second term equal to -n(n + 1) gives spherical Bessel's equation for the radial variation and Legendre's equation for the angular variation, with well-known solutions (see appendix I for details).

When $G_r \neq 0$, the last bracketed term of (44) and (45) is apparently a function of both r and θ. However, the combination of θ terms is such that if the second term in each equation is still considered as a constant the θ variations in the last bracketed term vanish. Thus, the second term of (44) is set equal to $-n_1(n_1 + 1)$ and the second term of (45) is set equal to $-n_2(n_2 + 1)$. In order to maintain finiteness at $\theta = 0$ and π for both H_ϕ and ρ, it is necessary that both n_1 and n_2 be integers and, therefore, $n_1 = n_2 = n$. The following solutions are, therefore, obtained (see appendix I for details) for the angular variations:

$$\begin{aligned} \Theta_1(\theta) &= P_n^1(\cos\theta) \\ \Theta_2(\theta) &= P_n(\cos\theta) \end{aligned} \tag{46}$$

In the last bracketed terms of (44) and (45), use of the identities

$$-\frac{dP_n(\cos\theta)}{d\theta} = P_n^1(\cos\theta)$$

and

$$\frac{d}{d\theta}\left(\sin\theta\, P_n^1(\cos\theta)\right) = n(n+1)\sin\theta P_n(\cos\theta) \tag{47}$$

gives

$$\frac{1}{r^2}\frac{d}{dr}\left(r^2\frac{dR_1}{dr}\right) + \left(k^2 - \frac{n(n+1)}{r^2}\right)R_1 - \frac{G}{r}\frac{d}{dr}(rR_1) = -\frac{G}{r}R_2 \tag{48}$$

$$\frac{1}{r^2}\frac{d}{dr}\left(r^2\frac{dR_2}{dr}\right) + \left(k_p^2 - \frac{n(n+1)}{r^2}\right)R_2 - G\frac{dR_2}{dr} = -\frac{G}{r}n(n+1)R_1 \tag{49}$$

By letting

$$\begin{aligned} H_\phi &= R_1(r)\Theta_1(\theta) = \sum_n T_{1n}(r)P_n^1(\theta) \\ \frac{v_0^2}{i\omega}\rho &= R_2(r)\Theta_2(\theta) = \sum_n T_{2n}(r)P_n(\theta) \end{aligned} \tag{50}$$

as before, it is apparent that the nth component of T_{1n} and T_{2n} must satisfy (48) and (49). The total field is determined from that combination of the components which satisfies the boundary conditions; the subscript "n" will be suppressed whenever possible.

In an attempt to obtain an analytic solution for "exact" numerical computations, many variations of k^2 and G(r) have been studied. One (and perhaps there is only one) variation has proven fruitful:

$$k^2 = k_0^2 \frac{r_0^2}{r^2} \tag{51}$$

from which

$$\rho_0(r) = \frac{m\epsilon_0\omega^2}{-e}\left(1 - r_0^2/r^2\right) \tag{52}$$

and

$$G = \frac{\frac{d}{dr}k^2}{k^2} = -\frac{2}{r} \tag{53}$$

Although equations (30) and (31) are not of quite the same form as (48) and (49), equivalence is exact since

$$(\ell n\ \epsilon_r)' = \frac{x\frac{d}{dx}(\epsilon_r)}{\epsilon_r} = \frac{r\frac{d}{dr}(k^2)}{k^2} = rG = -2 \tag{54}$$

With the substitutions

$$y = \ell n \frac{x}{x_1} = \ell n\left(\frac{k_0 r}{k_0 r_1}\right)$$

$$W_{1n} = (k_0 r)^{3/2} T_{1n} \tag{55}$$

$$W_{2n} = (k_0 r)^{3/2} T_{2n}$$

the two representations of the coupled wave equations become

$$\frac{d^2 W_{1n}}{dy^2} - \gamma_1^2 W_{1n} = 2W_{2n} \tag{56}$$

$$\frac{d^2 W_{2n}}{dy^2} + \gamma_2^2 W_{2n} = 2n(n+1)W_{1n} \tag{57}$$

where

$$\gamma_1^2 = \left(n + \frac{1}{2}\right)^2 - k_0^2 r_0^2$$

$$\gamma_2^2 = \frac{c^2}{v_0^2} k_0^2 r_0^2 - \left(n + \frac{1}{2}\right)^2 - 2 \tag{58}$$

The advantage of assuming the density variation above is now obvious—constant coefficients are obtained. A single fourth-order equation is possible, and the solution can be seen to be

$$W_{1n} = \sum_{m=1}^{4} A_{mn} e^{\kappa_m y} \tag{59}$$

$$W_{2n} = \sum_{m=1}^{4} \frac{A_{mn}}{2}\left(\kappa_m^2 - \gamma_1^2\right) e^{\kappa_m y} \tag{60}$$

where

$$\kappa_m = \pm\sqrt{-\frac{1}{2}\left(\gamma_2^2 - \gamma_1^2\right) \pm \sqrt{\left(\gamma_2^2 + \gamma_1^2\right)^2 + 16n(n+1)}}$$

and m = 1, 2, 3, 4 signify the signs chosen in the order ++, -+, +-, --.

In summary, for the special case when ρ_0 varies so as to make $k^2 r^2$ constant, it has been found that the fields are given by

$$H_\phi = \sum_{n=1}^{\infty} \sum_{m=1}^{4} A_{mn} \frac{e^{\kappa_m \ell n\,(k_0 r)}}{(k_0 r)^{3/2}} P_n^1(\cos\theta) \tag{61}$$

$$\rho = \frac{i\omega}{v_0^2} \sum_{n=1}^{\infty} \sum_{m=1}^{4} A_{mn} \left(\frac{\kappa_m^2 - \gamma_1^2}{2}\right) \frac{e^{\kappa_m \ell n\,(k_0 r)}}{(k_0 r)^{3/2}} P_n(\cos\theta) \tag{62}$$

The remaining field variables are obtained from equations (32) and (33). In particular

$$i\omega\epsilon_0 r E_\theta = \frac{1}{\epsilon_r} \sum_{n=1}^{\infty} \sum_{m=1}^{4} A_{mn}(F_{2m} - F_{1m}) \frac{e^{\kappa_m \ell n\,(k_0 r)}}{(k_0 r)^{3/2}} P_n^1(\cos\theta) \tag{63}$$

$$\rho_0 r v_r = \frac{1}{\epsilon_r} \sum_{n=1}^{\infty} \sum_{m=1}^{4} A_{mn}\left[-n(n+1)\frac{\omega_p^2}{\omega^2} + F_{1m}(F_{2m} - 1)\right] \frac{e^{\kappa_m \ell n\,(k_0 r)}}{(k_0 r)^{3/2}} P_n(\cos\theta) \tag{64}$$

where

$$F_{1m} = \frac{\kappa_m^2 - \gamma_1^2}{2}$$
$$F_{2m} = \kappa_m - \frac{1}{2} \tag{65}$$

Extensive study of this solution will be postponed until after discussion of the d-c parameters, boundary conditions, and method of solution in the next three sections. However, it can be seen that the four exponential solutions do not possess a wave character; in fact, only two have an imaginary part. Furthermore, in this solution, the "propagation constants" (κ_m) are dimensionless; wavelengths, phase and group velocities, etc., are unobtainable. Nevertheless, as in coupled oscillator problems, the propagation constants remain close to the uncoupled values. For electromagnetic wave propagation, in an incompressible plasma with this same assumed density variation, the magnetic field has been given by Tai [25](correcting an obvious error in the definition of γ), or can be seen from (56) to be given by

$$H_\phi = \sum_n \frac{1}{(k_0 r)^{3/2}} \left(A_{1n} e^{\gamma_1 \ell n k_0 r} + A_{2n} e^{-\gamma_1 \ell n k_0 r} \right) P_n^1(\cos\theta) \tag{66}$$

where γ_1^2 is given by (58). The lack of wave character is obvious when $k_0 r < n + \frac{1}{2}$.

Two of the propagation constants in the present problem generally remain close to the value $\pm\gamma_1$. The influence of the various components, however, is dependent on the boundary conditions and can only be determined by calculation. This will be further developed in sections 5 and 6.

2.4. HOMOGENEOUS PLASMAS

The field variables for homogeneous plasmas are easily obtained from equations (44) and (45) when $G_r = 0$. Using the material in appendix I, general solutions are

$$H_\phi = \sum_{n=0}^{\infty} \left[A_{5n} h_n^{(1)}(kr) + A_{7n} h_n^{(2)}(kr) \right] P_n^1(\cos\theta) \tag{67}$$

$$\frac{v_0^2}{i\omega}\rho = \sum_{n=0}^{\infty} \left[A_{6n} h_n^{(1)}(k_p r) + A_{8n} h_n^{(2)}(k_p r) \right] P_n(\cos\theta) \tag{68}$$

The constants are labeled $A_{5n}, \ldots, A_{8n}$ in order to avoid confusion with the constant A_{mn}, $m \leq 4$, used in the previous section. The propagation constants k and k_p are defined in equations (38) and (40). For radiation in an infinite homogeneous medium, the radiation condi-

tion precludes the existence of the Hankel function of the second kind. Hereafter, the constants A_{7n} and A_{8n} will, therefore, be set equal to zero, and the superscript on $h_n^{(1)}$ deleted whenever possible.

From the basic equations (32) and (33), it is a straightforward matter to show

$$i\omega\epsilon_0 rE_\theta = \frac{1}{\epsilon_r}\sum_{n=0}^{\infty}\left[A_{5n}\frac{d}{dr}(rh_n(kr)) - A_{6n}h_n(k_p r)\right]P_n^1(\cos\theta) \tag{69}$$

$$\rho_0 rv_r = -\frac{1}{\epsilon_r}\sum_{n=0}^{\infty}\left[A_{5n}(n)(n+1)\frac{\omega_p^2}{\omega^2}h_n(kr) - A_{6n}r\frac{d}{dr}(h_n(k_p r))\right]P_n(\cos\theta) \tag{70}$$

$$\rho_0 rv_\theta = \frac{1}{\epsilon_r}\sum_{n=0}^{\infty}\left[A_{5n}\frac{\omega_p^2}{\omega^2}\frac{d}{dr}(rh_n(kr)) - A_{6n}h_n(k_p r)\right]P_n^1(\cos\theta) \tag{71}$$

$$i\omega\epsilon_0 rE_r = \frac{-1}{\epsilon_r}\sum_{n=0}^{\infty}\left[A_{5n}n(n+1)h_n(kr) - A_{6n}r\frac{d}{dr}(h_n(k_p r))\right]P_n(\cos\theta) \tag{72}$$

Some readers might wish now to transfer to section 6 where the numerical integration of equations (22) through (25) is discussed. This integration is performed for a model which is discussed in the next section and which can be visualized in figure 2. The method of solution used to satisfy the boundary conditions is covered in section 4. Section 5 discusses the definition and problems associated with calculating the terminating admittance. The material in each of these sections is summarized in section 6 and the reader familiar with this material may wish to omit some of it.

3
SPECIFICATION OF PARAMETERS

3.1. INTRODUCTION

This section is concerned with the specification of the steady-state parameters to be used in the differential equations given in the preceding section. These parameters are:

(1) electron density, $\rho_0(r)$

(2) electron rms thermal velocity, v_0

(3) electric field, $E_0(r)$

(4) drift velocity, $u_0(r)$

A brief description of these variables was given in section 1.4; figure 1 indicated their general character. It now remains to justify the variations used in the numerical computations which are given in the sixth and seventh sections.

The specification of the steady-state parameters is itself a major undertaking and an exact specification is beyond the scope of this study. The objective of this study is to obtain a substantive appreciation of the influence of the sheath on the input admittance through the numerical values for this approximate sheath description. The difficulty in this radiation analysis is that the radiated fields must at some radius be matched to the fields which propagate in the uniform region exterior to the sheath. For an actual sheath region the d-c fields disappear rapidly away from the perturbing body; however, an approximation which makes this region finite must be made to make the computations feasible.

The next section discusses the steady-state parameters $\rho_0(r_2)$ and v_0, which are the only variables needed to describe the steady-state characteristics of the homogeneous region outside the radius r_2. The model used in the sheath is then discussed in section 3.3; this is compared in section 6.3.1 with the model analyzed in section 2.3 which permitted an analytical solution.

3.2. UNIFORM PLASMA REGION

A laboratory plasma is never uniform because the production of the plasma necessitates methods of both containment and generation, with consequent d-c flow of both ions and electrons. Even for ionospheric plasmas, homogeneity is unlikely. For analytical purposes, however, these other nonuniformities will be assumed to be negligible and the plasma will be assumed to be homogeneous beyond some distance from the dipole. In this uniform region the plasma is assumed to be electrically neutral with no steady-state forces on either electrons or ions. The electron density n_0 and electron temperature T_e are therefore the only two parameters needed to specify this region. In the equations of section 2, these appear as charge rather than number density and as thermal velocity (of the perturbed electrons) rather than temperature:

$$\rho_0 = -en_0 \tag{73}$$

$$\frac{1}{2}mv_0^2 = \frac{3}{2}kT_e \text{ (Equipartition law)} \tag{74}$$

These are further modified to give

$$\frac{\omega_p^2}{\omega^2} = \frac{-e\rho_0}{m\epsilon_0\omega^2} \tag{75}$$

$$V^2 = \frac{v_0^2}{c^2} = \frac{3kT_e}{mc^2} \tag{76}$$

Numerical values can be obtained by using

$$k = 1.38047 \times 10^{-23} \frac{\text{watt sec}}{^{o}K}$$

$$e = 1.602 \times 10^{-19} \text{ coulombs}$$

$$m = 9.1066 \times 10^{-31} \text{ kg}$$

$$\epsilon_0 = 8.854 \times 10^{-12} \frac{F}{m}$$

$$c = 2.998 \times 10^{8} \frac{m}{sec}$$

Thus it is possible to show that

$$f_p = \frac{\omega_p}{2\pi} = 8980 \sqrt{n_0 \text{ cps}} \tag{77}$$

(when n_0 is expressed in cm^{-3})

and

$$V = \frac{v_0}{c} = 2.25 \times 10^{-5} \sqrt{T_e} \tag{78}$$

Since electron densities in laboratory plasmas are typically less than $10^{12}/cm^3$, and the electron temperature is in the range from 10^3 to 10^6 degrees Kelvin, then f_p is less than 10^{10} cps, and V is in the range from 10^{-3} to 3×10^{-2}.

Since the electron temperature is also often expressed as ϕ_e (in electron volts), it is convenient to note that

$$\phi_e = \frac{k}{e} T_e = \frac{T_e}{11{,}600^{o}/ev}$$

Another parameter for a homogeneous plasma which is often used is the shielding, or Debye, length λ_D (often denoted by h_e or $1/k_D$) which is given by

$$\lambda_D = \sqrt{\frac{\epsilon_0 k T_e}{n_0 e^2}} = \frac{v_0}{\omega_p} \frac{1}{\sqrt{3}} \tag{79}$$

The size of the spherical dipole can be stated in Debye lengths, giving

$$\frac{r_1}{\lambda_D} = \frac{k_0 r_1}{k_0 \lambda_D} = \frac{k_0 r_1}{\sqrt{3}} \frac{\omega_p/\omega}{v_0 c} \tag{80}$$

Typical values for this ratio in the laboratory and ionosphere are in the range of 1.0 to 10^4. The extent of the inhomogeneous region surrounding the spherical dipole is contained in Section 3.3.

3.3. SHEATH REGION

The word "sheath" refers to the electron-deficient plasma boundary region. The formation of a sheath is necessary to balance electron and ion currents. The lighter weight electrons have much larger thermal velocity than the ions; consequently, electron accumulation on the boundary surface creates a "wall" potential. This attracts ions and repels electrons in amounts sufficient to balance their currents.

A complete description of the potential profile surrounding a perturbing sphere does not seem to have been given. This is partially because of the complexity of the problem, but also because the profile need not be known in order to calculate current collection as the probe potential is externally varied (e.g. Langmuir [26, 27]). From such "Langmuir probe" diagnostics, both the temperature and electron density in the homogeneous region can be obtained.

The technique for obtaining a complete potential profile is necessarily numerical, and has been carried out with certain geometries and assumptions. The basic equation to be solved is the Poisson equation

$$\nabla^2 \phi_0 = \frac{1}{\epsilon_0}\left(\rho_0 - \rho_0^+\right) \tag{81}$$

The assumption is made that

$$\rho_0(r) = \rho_0(r = \infty)\, e^{\eta(r)} \tag{82}$$

where

$$\eta(r) = \frac{e\phi_0(r)}{kT} \tag{83}$$

that is, that the distribution is Maxwellian. The ion density, ρ_0^+, is usually related to the potential through an orbit analysis. For large potentials, the electron density can be ignored and a sheath solution obtained. Similarly, in the region where the potential is not rapidly varying, the plasma solution is obtained by making the so-called quasi-neutral approximation (dropping the left-hand side of (81). In analytical studies, these solutions can be fitted together at the "sheath edge." The potential in this analysis is taken as zero at $r = \infty$.

In his work, Langmuir [26, 27] discussed solutions in spherical coordinates for various assumptions about the right hand side of equation 81, such as zero space charge density, constant density, and constant current density $\left(\text{so } \rho^+ = J/u_0\right)$ with one or two kinds of carriers, but neglected the generation of ions in the sheath. Bohm [28] also analyzed the spherical collector in greater detail using the Langmuir approach (two carriers, constant current density), but in-

cluded the effects of field penetration into the plasma region as well as ion temperature. Somewhat later, Allen, Boyd and Reynolds [29] analyzed the spherical collector in the manner of Bohm, but studied the sheath potential profile which Bohm had not done. Their work contains a description of the literature prior to 1957. Bernstein and Rabinowitz [30] also considered this same problem using an entirely numerical integration of (81). Laframboise [31] has apparently used a similar numerical integration but retained a Boltzmann distribution for the ions. Bernstein and Rabinowitz have assumed monoenergetic ions in order to make the problem more tractable. Lam [32] has discussed these various analyses (excluding Laframboise); however, since he preferred to avoid numerical integration, no numerical potential profile data is available from his work.

In addition to these studies of the spherical collector, there is a large body of literature for planar and cylindrical Langmuir probes. In particular, Self [33, 34] and Caruso and Cavaliere [35] show potential profile data for planar geometries obtained in much the same way. Collisions are neglected in most of these analyses, although Self does discuss ion generation in the sheath. Self's analysis has been used by Parker [36] and Nickel [37, 38], in their plasma (EA) wave analyses in nonuniform plasma columns. Their work is somewhat similar to the present study, but they dropped the magnetic field and therefore the EM wave in the interior plasma region. Consequently, mode coupling in the sheath region and the metallic radiator problem are not contained in their work.

The problem in utilizing the material described above is that all of the work was performed for relatively "small" collectors; a typical parameter is r_1/λ_D equal to ten. Much of the data presented in the sixth and seventh sections are for somewhat larger values of r_1/λ_D. Consequently the desired sheath potential profile was extrapolated from each of the published curves; a typical comparison is shown in figure 2 as case A (Allen, Boyd, and Reynolds) extrapolated from data for $r_1/\lambda_D = 14.7$ when $\eta = -3.5$; case B (Bernstein and Rabinowitz) extrapolated from data for $r_1/\lambda_D = 13.0$ when $\eta = -3.5$ and $T_1/T_e = 0.1$; and case L (Laframboise) extrapolated from data for $r_1/\lambda_D = 10$ when $\eta = -3.5$.

In addition, case C, which is shown, is an example of the computational model used in sections 6 and 7 which is described below. In each case, the curves have been plotted to correspond to a normalized wall potential of $\eta_w = -3.5$ when $r_1/\lambda_D = 19.6$. This value of normalized sphere size is obtained from equation 80 with parameters of $\omega_p/\omega = 0.707$, $v_0/c = 1/32$ and $k_0 r = 0.5$.

There are obvious similarities between each of the cases shown in figure 2. The differences are a result of the assumptions employed and the method of computation as well as the problems involved in extrapolating data from published graphs. In some parts of the computation, thinner sheaths are considered in deference to the statement by Spitzer [39] that sheath thicknesses of one Debye length are to be expected. Actually, it can be seen that most of the potential rise does

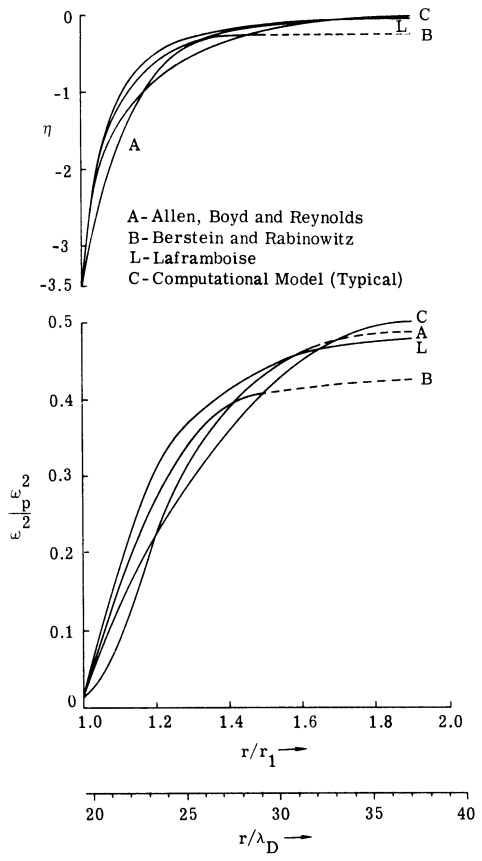

FIGURE 2. COMPARISON OF SHEATH POTENTIAL AND DENSITY PROFILES

occur within several Debye lengths although the density profile rises less sharply than the potential profile.

Before describing the sheath representation that has been chosen for study, some comment is appropriate on the magnitude of the drift velocity since the inclusion of a drift velocity will affect the model. It was originally intended that the drift velocity would be included in this analysis. However, the difficulty of establishing the added boundary condition (see sec. 4), the much more involved (if even possible) numerical computations, the complexity of the analysis even without u_0, and the absence of definite experimental evidence of the detectability of the EA wave by any plasma-imbedded dipole lead to the exclusion of the drift velocity from this study. It has been retained in the previous section in order to demonstrate that its influence should not be large. Thus, it is now pertinent to determine the magnitude of the drift velocity.

Although a large majority of the electrons are reflected in the sheath, the average velocity of those that continue on must necessarily increase. The maximum value can be obtained from a calculation of the random current at the dipole (given by Lam [32] or Self [33]).

$$J_e = \rho_0(r_1)u_0(r_1) = \rho_0\, e^{\eta_w\left(\frac{kT_e}{2\pi m}\right)^{1/2}} \tag{84}$$

Since

$$v_0 \triangleq \sqrt{\frac{3kT_e}{m}} \tag{85}$$

then

$$u_0(r_1) = \frac{1}{\sqrt{6\pi}} v_0 \cong 0.23 v_0 \tag{86}$$

The drift velocity decreases to zero at the sheath edge; the actual variation is determined by the details of ion generation. However, even with the maximum value at the radiator, it can be seen that many of the terms in table I involving u_0 are of small magnitude As an example, the term $i\omega m\rho_0 v_\theta$ is never less than $\frac{c}{v_0} x_1$ times as large as the neglected term $\rho_0 \frac{mu_0}{r} v_\theta$ in the component of the force equation. However, because of the complexity of the equations it is not possible to show that all of the terms will always have negligible influence. In fact, because many of the added terms are imaginary, even small terms might be influential in affecting the admittance. Nevertheless, even though all terms containing u_0 are not demonstrably of small order, they must be dropped for the reasons given previously.

With the exclusion of the drift velocity the d-c static equation which must be satisfied becomes quite simple. From equation 9

$$\rho_0 eE_0 + kT_e \frac{d\rho_0}{dr} = 0, \tag{87}$$

since $E_0 = -d\phi_0/dr$, then

$$\frac{d}{dr}\left(\frac{e\phi_0(r)}{kT_e}\right) = \frac{1}{\rho_0}\frac{d}{dr}\rho_0 = \frac{d}{dr}\,\ell n\,\rho_0 \tag{88}$$

and so (since it is assumed that $\phi_0 = 0$ at $r = r_2$)

$$\rho_0(r) = \rho_0(r_2)\, \exp\,(e\phi_0(r_2)/kT_e) \tag{89}$$

or

$$\eta(r) = \frac{e\phi_0(r)}{kTe} = \ell n \frac{\rho_0(r)}{\rho_0(r_2)} \tag{90}$$

In the defining differential equations (22-25), the term reE_0/mv_0^2 appears, which can therefore be replaced, using (74)

$$-\frac{reE_0}{mv_0^2} = +\frac{1}{3}\frac{x}{\rho_0}\frac{d\rho_0}{dx} = F_2 \tag{91}$$

Since only the d-c potential (or electric field) and d-c electron density appear as static variables in the simplified defining differential equations (22-25) a specification of either quantity and use of either (89) or (90) completely defines the static variables. The only restriction is that the electron density gradient (and therefore the potential) be zero at the outer sheath edge. This condition is necessary in order to simplify the boundary conditions; of course, a potential discontinuity would not be physically meaningful anyway. A number of choices were attempted and compared to the sheath models shown in figure 2. The most satisfactory alternative was to approximate the d-c electron density as

$$\frac{n_0(r_2) - n_0(r)}{n_0(r_2) - n_0(r_1)} = \left(\frac{r_2 - r}{r_2 - r_1}\right)^2 \tag{92}$$

or in terms of the variable $y = \ell n\ r/r_1$ used hereafter

$$\frac{\omega_p^2(y)}{\omega^2} = \frac{\omega_p^2(y_2)}{\omega^2} - \left(\frac{\omega_p^2(y_2)}{\omega^2} - \frac{\omega_p^2(y_1)}{\omega^2}\right)\frac{\left(e^{y_2} - e^{y}\right)^2}{\left(e^{y_2} - 1\right)^2} \tag{93}$$

where the three parameters r_2/r_1 (or $y_2 = \ell n\ r_2/r_1$), $\omega_p^2(y_2)/\omega^2$, and $\omega_p^2(y_1)/\omega^2$ must be independently specified. The d-c electric field is related to this specified d-c electron density through (91). With this model and using the normalized distance y this gives

$$F_2 = \frac{1}{3}\frac{1}{\rho_0}\frac{d\rho_0}{dy} = \frac{\dfrac{\omega_p^2(y_2)}{\omega^2} - \dfrac{\omega_p^2(y_1)}{\omega^2}}{3\left(e^{y_2} - 1\right)^2} - \frac{2\left(e^{y_2}\, e^{y} - e^{2y}\right)}{\dfrac{\omega_p^2(y)}{\omega^2}} \tag{94}$$

with $0 \leqq y \leqq \ell n\ r_2/r_1$.

The only remaining parameter to be discussed is the d-c radiator potential. In Langmuir probe studies and hereafter this is termed the wall potential. This quantity is actually used to specify the parameter $\omega_p^2(r_1)/\omega^2$ through (89). Langmuir [26, 27] was the first to give an analysis of this quantity, showing that the wall potential can be obtained if the electron current given by (84) is equated to the ion current

$$J_i = \left(\frac{2kT}{M}\right)^{1/2} n_0 e I(\eta) \tag{95}$$

where $I(\eta) = \int_0^{\eta} \exp(-\gamma\eta')\left(\frac{ds}{d\eta'}\right) d\eta'$ (96)

In this equation γ is a parameter describing ion generation in the sheath ($\gamma = 0$ for uniform generation, $\gamma = 1$ for generation proportional to electron density) and $s = \alpha r$ where r is the actual distance from the center of symmetry and α is a characteristic inverse distance scale.

With the "plasma approximation" these integrations can be performed in terms of an integration parameter, j_0, giving

$$I(\eta) = I_p(\eta) = \left(\frac{2kT_e}{m_p}\right)^{1/2} n_0 e j_0 \tag{97}$$

so that

$$\eta_w = \ell n \left[\left(\frac{m_p}{m_e}\right)^{1/2} \frac{1}{2\sqrt{\pi}} \frac{1}{j_0}\right] \tag{98}$$

and for hydrogen

$$\eta_w = \ell n \left[12.1 \frac{1}{j_0}\right] \tag{99}$$

Langmuir discussed numerous geometries and cases, but did not obtain wall potentials for the spherical collector. However, Bohm [28] showed that j_0 was a function of ion temperature and obtained values from 0.38 to 0.50 depending on the assumptions involved. For the planar case, Self [33, 34] obtained $j_0 = 0.3444$. These values give normalized wall potentials from -3.18 to -3.63 for hydrogen; values for mercury would be near -6. In most of the numerical computations, a value of $\eta_w = -3.5$ was arbitrarily chosen, which gives an electron density at the wall that is three percent as large as in the homogeneous region (using (82)). However, normalized wall potential variations from -2 to -10.0 are discussed in sections 6.3.3 and 6.3.4.

In conclusion, this section has presented data to show that the sheath model offers a reasonable approximation to what is now known about the sheath region surrounding a spherical collector. The relatively small influence of the model on the calculations justifies the use of this approximate form.

4
BOUNDARY CONDITIONS

4.1. INTRODUCTION

In the second section, a system of four ordinary differential equations was obtained from a set of ten partial differential equations. These equations interrelated the ten variables required to specify the field radiated from a spherical dipole in a compressible, drifting, inhomogeneous plasma medium. One restriction that was necessary in the simplification of the equations was the assumption of no angular variation around the spherical axis of symmetry for both d-c and perturbed variables. The solutions in each case were obtained by what is known as "modal analysis." Separation of variables was shown to be possible, and the complete solution was found as a summation over an infinity of "modes," as in equations 15 ff., i.e.,

$$H_\phi = \sum_{n=0}^{\infty} T_{1n}(r) P_n^1(\cos\theta)$$

When the medium is homogeneous and stationary, each field variable can be obtained explicitly as given in section 2.4, i.e., equation 67

$$T_{1n} = A_{5n} h_n^{(1)}(kr) + A_{7n} h_n^{(2)}(kr)$$

When a particular inhomogeneity was retained, but d-c electric fields and drift velocities ignored, the solution was given in section 2.3, i.e., equation 61

$$T_{1n} = \sum_{m=1}^{4} A_{mn} \frac{e^{\kappa_m \ell n k_0 r}}{(k_0 r)^{3/2}}$$

In the more general inhomogeneous medium cases it is necessary to resort to numerical solutions, but a complete solution can be obtained from a set of arbitrary solutions when the differential equations are linear, as in this problem.

From the above discussion it can be seen that the solution is not complete until the constants are specified. In the first spherical dipole analysis by Chu and Stratton [3] the determination of the constants was accomplished by specifying one condition at the radiator and one at infinity. The condition at infinity is known as the radiation condition; it requires that all fields behave as outgoing spherical waves. The condition at the radiator is that the tangential electric field be zero except at the gap, where a driving voltage exists. For a homogeneous dielectric these two conditions then allow the complete determination of all fields and the terminating admittance. The conditions at these two boundaries will be described at greater length in the following sections.

In an extension of this type of analysis to a nonuniform medium, two possible methods of representation exist: (1) the medium gradually becomes uniform as the distance from the sphere approaches infinity and (2) a jump discontinuity in the representation of the nonuniform medium or its gradient exists beyond which the medium is homogeneous. In both cases, the radiation and radiator tangential electric field conditions still apply. For the first case, numerical solutions can be obtained such that beyond some radius the solution is arbitrarily close to that in a uniform medium. In the second case, separate solutions are obtained in the two regions. Two new constants are involved which can be readily calculated since the tangential electric and magnetic fields must be continuous across the discontinuity. A discussion and derivation of these conditions is given in appendix III. The first type of representation is not often used because of the sparsity of analytical solutions. The only two spherical radiator problems using the first method of which the author is aware are by Fikioris [40], who studied the case $\epsilon(r) = \epsilon_\infty \frac{r + r_a}{r + r_b}$ for various combinations of r_a and r_b, and C. T. Tai [41], who gave solutions for this and several other stratifications.

It can be seen that in principle there is no major problem in studying the propagation of electromagnetic waves alone in a homogeneous medium. This is not true in the present analysis, in which electroacoustic waves are also presumed to exist. It is the purpose of the following sections to justify the conditions used in this study. This will be done for the second approach described above. However, as shown in appendix IV, in order to match all of the fields to the usual Hankel function representation it is necessary that the density gradient (and therefore the static electric field and electron drift velocity) be zero at the outer sheath edge. With this approach, it is well known that the radiation condition is satisfied by excluding the second kind of Hankel function (if $e^{-j\omega t}$ time convention is used) in the external homogeneous region.

Mode conversion with an inhomogeneous sheath is inherent in the differential equations used in the sheath region. However, because the present improved sheath model is still a far from perfect approximation of the microscopic physical processes that occur at the radiator, it does not indicate a single set of criteria for a choice of continuity relations at the radiator boundary. A number of such relations although imperfect may be considered equally acceptable for approximate solutions.

The boundary conditions at the outer sheath edge are discussed in section 4.2; those at the radiator in section 4.3. The general solution obtained from these boundary conditions is given in section 4.4 and several special solutions are in section 4.5. A major conclusion of this study is that previous analyses have predicted an excessively large EA mode contribution. Therefore, the set of boundary conditions used in these analyses is critically reviewed in appendix V and an alternative set is presented. Figure 1 indicates the nomenclature being used in the following discussion.

4.2. OUTER SHEATH EDGE CONDITIONS

In this section, boundary conditions will be obtained from the various field components when the sheath edge is as nearly perfect as possible, possessing neither density discontinuities nor density gradient discontinuities. The expected result is that there is no mode conversion, so that all field components are continuous. Only four need be specified and the usual set of nonredundant conditions is

$$\hat{n} \times (\vec{H}_1 - \vec{H}_2) = 0 \tag{100}$$

$$\rho_1 - \rho_2 = 0 \tag{101}$$

$$\hat{n} \times (\vec{E}_1 - \vec{E}_2) = 0 \tag{102}$$

$$\hat{n} \cdot (\vec{v}_1 - \vec{v}_2) = 0 \tag{103}$$

The derivation of these conditions is presented in appendix III in the belief that most readers will find them intuitively acceptable, because the derivations are so lengthy and because all that is being varied at this boundary is the representation of the medium, not the medium itself. For numerical computations, however, it is desirable to reformulate these boundary relations so that neither the field solutions nor the arbitrary constants in the homogeneous medium need be calculated explicitly.

This will be done by eliminating the arbitrary constants of the homogeneous medium which are implied in equations 100-103. First, it can be noted that these boundary relations are satisfied for each order n separately (this is both necessary and sufficient because of the orthogonality of the Legendre functions). Then, using the definitions of (15), (100-103) can be written in the simpler form

$$T_{jn}^{\text{interior}}(r_2) = T_{jn}^{\text{exterior}}(r_2) \tag{104}$$

The fields in both the sheath and homogeneous plasma regions can be expressed in terms of "known" solutions and arbitrary constants. In order to emphasize the two regions, the interior (sheath) fields will be written in terms of the independent variable, $y = \ell n\, k_0 r / k_0 r_1$, while the exterior fields will be written in terms of $kr = \frac{\omega}{c}\sqrt{1 - (\omega_p/\omega)^2}\, r$ and $k_p r = \frac{\omega}{v_0}\sqrt{1 - (\omega_p/\omega)^2}\, r$, which at the sheath edge will be termed z_1 and z_2.

In this approach, it is known that the sheath fields at any position, y, can be written in terms of independent solutions, i.e.

$$
\begin{aligned}
T_{1n}(y) &= A_{1n}t_{1n}^{(1)}(y) + A_{2n}t_{1n}^{(2)}(y) + A_{3n}t_{1n}^{(3)}(y) + A_{4n}t_{1n}^{(4)}(y) \\
T_{2n}(y) &= A_{1n}t_{2n}^{(1)}(y) + A_{2n}t_{2n}^{(2)}(y) + A_{3n}t_{2n}^{(3)}(y) + A_{4n}t_{2n}^{(4)}(y) \\
T_{3n}(y) &= A_{1n}t_{3n}^{(1)}(y) + A_{2n}t_{3n}^{(2)}(y) + A_{3n}t_{3n}^{(3)}(y) + A_{4n}t_{3n}^{(4)}(y) \\
T_{4n}(y) &= A_{1n}t_{4n}^{(1)}(y) + A_{2n}t_{4n}^{(2)}(y) + A_{3n}t_{4n}^{(3)}(y) + A_{4n}t_{4n}^{(4)}(y)
\end{aligned}
\tag{105}
$$

or, more concisely, as

$$
T_{jn}(y) = \sum_{k=1}^{4} A_{kn}t_{jn}^{(k)}(y) \qquad j = 1, 2, 3, 4 \tag{106}
$$

The functions $t_{jn}^{(k)}(y)$ can be any set of four independent solutions, but for clarity lower case "t" is used to denote "preliminary" values obtained when only one of the four independent variables has a value of unity at the radiator and the others have the value zero. For example, $t_{1n}^{(2)}(y)$ is the variable $T_{1n}(y)$ obtained when $T_{2n}(y_1) = 1.0$ and $T_{1n}(y_1) = T_{3n}(y_1) = T_{4n}(y_1) = 0$. In the external homogeneous region, the solution is specified as

$$
T_{1n}(r) = A_{5n}h_n^{(1)}(kr) + A_{7n}h_n^{(2)}(kr) \tag{107}
$$

$$
T_{2n}(r) = A_{6n}h_n^{(1)}(k_p r) + A_{8n}h_n^{(2)}(k_p r) \tag{108}
$$

The eight (for each n) arbitrary constants $A_{1n}, \ldots, A_{8n}$ must be obtained by satisfying eight boundary conditions. In addition to the four relations given by (100-103), two relations are specified at the radiator (discussed in section 4.3) and two more are obtained from the radiation conditions. These last two are satisfied by setting $A_{7n} = A_{8n} = 0$ as discussed in section 4.1. The four boundary relations of equation 104 which involve the six constants $A_{1n}, \ldots, A_{6n}$ can thus be written

$$
\begin{aligned}
&t_{1n}^{(1)}(y_2)A_{1n} + t_{1n}^{(2)}(y_2)A_{2n} + t_{1n}^{(3)}(y_2)A_{3n} + t_{1n}^{(4)}(y_2)A_{4n} - h_n(z_1)A_{5n} = 0 \\
&t_{2n}^{(1)}(y_2)A_{1n} + t_{2n}^{(2)}(y_2)A_{2n} + t_{2n}^{(3)}(y_2)A_{3n} + t_{2n}^{(4)}(y_2)A_{4n} - h_n(z_2)A_{6n} = 0 \\
&t_{3n}^{(1)}(y_2)A_{1n} + t_{3n}^{(2)}(y_2)A_{2n} + t_{3n}^{(3)}(y_2)A_{3n} + t_{3n}^{(4)}(y_2)A_{4n}
\end{aligned}
\tag{109}
$$

(equation continued)

$$-\frac{1}{\epsilon_r}\frac{d}{dz_1}[(z_1 h_n(z_1))]A_{5n} + \frac{1}{\epsilon_r}h_n(z_2)A_{6n} = 0$$

$$t_{4n}^{(1)}(y_2)A_{1n} + t_{4n}^{(2)}(y_2)A_{2n} + t_{4n}^{(3)}(y_2)A_{3n} + t_{4n}^{(4)}(y_2)A_{4n}$$

$$+\frac{1}{\epsilon_r}n(n+1)\frac{\omega_p^2}{\omega^2}h_n(z_1)A_{5n} - \frac{1}{\epsilon_r}z_2\frac{d}{dz_2}h_n(z_2)A_{6n} = 0$$

As stated earlier, it is advantageous to eliminate the arbitrary constants of the homogeneous region to obtain two relations involving only the four arbitrary constants of the sheath region. By solving the first two of the set in equation 109 for A_{5n} and A_{6n} respectively and inserting them into the last two equations of (109), one obtains

$$\begin{aligned} q_{1n}^{(1)}(y_2)A_{1n} + q_{1n}^{(2)}(y_2)A_{2n} + q_{1n}^{(3)}(y_2)A_{3n} + q_{1n}^{(4)}(y_2)A_{4n} &= 0 \\ q_{2n}^{(1)}(y_2)A_{1n} + q_{2n}^{(2)}(y_2)A_{2n} + q_{1n}^{(3)}(y_2)A_{3n} + q_{2n}^{(4)}(y_2)A_{4n} &= 0 \end{aligned} \tag{110}$$

where

$$q_{1n}^{(m)}(y_2) = -t_{1n}^{(m)}(y_2) + t_{2n}^{(m)}(y_2) + \left(1 - \omega_p^2(y_2)/\omega^2\right)t_{3n}^{(m)}(y_2) - \left(\frac{z_1\frac{d}{dz}h_n(z_1)}{h_n(z_1)}\right)t_{1n}^{(m)}(y_2)$$

and (111)

$$q_{2n}^{(m)}(y_2) = n(n+1)\left(\omega_p^2(y_2)/\omega^2\right)t_{1n}^{(m)}(y_2) + \left(1 - \omega_p^2(y_2)/\omega^2\right)t_{4n}^{(m)}(y_2) - \left(\frac{z_2\frac{d}{dz_2}h_n(z_2)}{h_n(z_2)}\right)t_{2n}^{(m)}(y_2)$$

By comparison with equations 22 and 23 and using the fact that the d-c electric field is zero at the sheath edge, it can be seen that these can be put into the form

$$q_j^{(m)}(y_2) = \left[t_j^{(m)}(y_2)\right]' - H_2(z_j)t_j^{(m)}(y_2) \tag{112}$$

where

$$H_2(z) = \frac{z\frac{d}{dz}h_n(z)}{h_n(z)} \tag{113}$$

It is thus seen that, after application of the radiation conditions and elimination of the arbitrary constants of the exterior homogeneous region, two simple relations can be obtained

involving only the constants of the sheath region

$$\sum_{m=1}^{4} q_{jn}^{(m)}(y_2)A_{mn} = 0 \qquad j = 1, 2 \tag{114}$$

with $q_{jn}^{(m)}(y_2)$ defined by (112).

4.3. RADIATOR CONDITIONS

In the next section arguments will be presented to justify the approximate radiator condition

$$\begin{aligned} E_\theta(r_1) &= \frac{V'}{r_1 \Delta\theta}, \qquad \left|\theta - \frac{\pi}{2}\right| \leqq \frac{\Delta\theta}{2} \\ &= 0, \qquad \frac{\pi}{2} \geqq \left|\theta - \frac{\pi}{2}\right| \geqq \frac{\Delta\theta}{2} \end{aligned} \tag{115}$$

Chu and Stratton [3] gave a derivation of this condition that ignored the problem of applying a generator to the gap. The Schelkunoff derivation [2], which assumes a biconical transmission line feeding the gap, is modified in the next chapter to include the effects of the inhomogeneous, compressible plasma. For the purposes of this section it is only necessary to note that because (115) is a function only of angular position θ, $E_\theta(r_1)$ can be expressed as a series containing the associated Legendre functions

$$\begin{aligned} i\omega\epsilon_0 E_\theta(r_1) &= \sum T_{3n}(r_1)P_n^1(\cos\theta) \\ &= \sum C_n P_n^1(\cos\theta) \end{aligned} \tag{116}$$

The C_n's will be defined in section 5. Because certain of the results resemble Schelkunoff's when C_n is taken as unity, the boundary condition that will be employed is

$$T_{3n}^{(0)}(r_1) = A_{3n} = 1$$

The superscript (0) is used to signify these normalized solutions. The actual sheath fields are then simply modified by the C_n's, i.e.

$$T_{jn}(r) = C_n T_{jn}^{(0)}(r)$$

At this point in the solution of the original set of equations, seven boundary conditions have been proposed and only one more need be found to completely specify the fields in both regions.

These seven conditions consist of two at a large radius (radiation conditions), four at the outer sheath edge (sec. 4.2), and the above condition on the tangential electric field. Unfortunately, there is no unequivocal, proven boundary condition that can be employed to complete the set of eight conditions. This is so largely because of the assumptions that had to be made in order to make the problem tractable. Therefore it is necessary to study the results obtained with several conditions. The ones used in the remainder of this study are

$$v_r(r_1) = 0 \tag{117}$$

or

$$\rho(r_1) = 0 \tag{118}$$

or

$$\hat{n}\cdot\vec{v} = y_a \hat{n}\cdot\vec{E} + y_b\left(\frac{\rho}{-e}\right) \tag{119}$$

where the geometry and nomenclature is that shown in figure 1. The reader should be warned that condition in (118) is one that does not seem to have been employed in any previous analysis. The condition in (119) is Cohen's [14] bilinear admittance relation; it is discussed below.

In past radiation analyses only equation 117 has been used; it is known as the elastic reflection condition and guarantees that there shall be no perturbed motion of particles at the radiator. It will be termed the "hard" boundary condition in accordance with terminology in acoustics. It usually is used without justification and without derivation. One justification that has been offered is that this boundary condition prevents separation of the medium from the boundary [42], although the ideas concerning a surface charge given in appendix V also satisfy this criterion. It is a boundary condition that cannot be imposed for a cold plasma, since all fields would then be zero if condition (115) were also employed (the problem would be overspecified).

Equation 118 likewise cannot be rigorously derived, but it also has some merits; it will be termed the "soft" boundary condition. If used with the homogeneous plasma, only the electroacoustic fields are zero so that it is consistent with the cold plasma model. It can be simply justified heuristically by observing that the electroacoustic wave effects (the perturbed charge density) should disappear as the d-c electron density which supports these EA waves disappears.

In the following numerical studies, the results obtained with the use of condition in (117) will be compared with those derived from the condition in (118). It will be shown that when the d-c density at the radiator is small the difference in results is not marked. The condition in (118) is discussed further in appendix VI.

Equation 119 can be studied in accordance with the suggestion of Cohen [14] that the velocity at a metal surface might be expressed as a "bilinear admittance" relation. In the present nomen-

clature, this becomes an expression relating T_{4n} to T_{1n} and T_{2n} through normalized admittance parameters Y_A and Y_B which are defined further below:

$$T_{4n} = Y_A T_{1n} + Y_B T_{2n} \tag{120}$$

It is an incomplete specification since there is no known basis for choosing the parameters Y_A and Y_B. However, the following brief treatment gives an indication of their form. If equations 22 and 23 are solved for T_{3n} and T_{4n}, respectively, which are then inserted into (25), an equation is obtained relating $\frac{dT_{4n}}{dy}$ to only T_{1n}, $\frac{dT_{1n}}{dy}$, $T_{2n}(y)$, and $\frac{dT_{2n}}{dy}$:

$$\frac{dT_{4n}}{dy} + \frac{L\omega_p^2/\omega^2}{1 - (\omega_p/\omega)^2}\frac{dT_{1n}}{dy} + \frac{1}{1 - (\omega_p/\omega)^2}\frac{dT_{2n}}{dy} = \left[\frac{L - F_{2n}}{1 - (\omega_p/\omega)^2} - \frac{x^2}{V^2}\right]T_{2n} \tag{121}$$

or

$$\frac{dT_{4n}}{dy} + \frac{d}{dy}\left[\frac{L\omega_p^2/\omega^2}{1 - (\omega_p/\omega)^2}T_{1n}\right] + \frac{d}{dy}\left[\frac{T_{2n}}{1 - (\omega_p/\omega)^2}\right] = \left[\frac{d}{dy}\left(\frac{L\omega_p^2/\omega^2}{1 - (\omega_p/\omega)^2}\right)\right]T_{1n}$$
$$+ \left[\frac{L - F_2}{1 - (\omega_p/\omega)^2} - \frac{x^2}{V^2} + \frac{d}{dy}\left(\frac{1}{1 - (\omega_p/\omega)^2}\right)\right]T_{2n} \tag{122}$$

Performing an integration of this equation across the radiator boundary gives

$$\left[T_{4n} + \frac{L\omega_p^2/\omega^2}{1 - (\omega_p/\omega)^2}T_{1n} + \frac{1}{1 - (\omega_p/\omega)^2}T_{2n}\right]\Bigg|_{-\Delta/2}^{+\Delta/2} = \lim_{\Delta \to 0}$$
$$\left[T_{1n}\frac{d}{dy}\left(\frac{L\omega_p^2/\omega^2}{1 - (\omega_p/\omega)^2}\right) + \left(\frac{L - F_2}{1 - (\omega_p/\omega)^2} - \frac{x^2}{V^2} + \frac{d}{dy}\left(\frac{1}{1 - (\omega_p/\omega)^2}\right)\right)T_{2n}\right]\Delta \tag{123}$$

Dropping the right hand side (for the moment) and assuming all interior fields are zero, gives

$$T_{4n} = -\frac{L\omega_p^2/\omega^2}{1 - (\omega_p/\omega)^2}T_{1n} - \frac{1}{1 - (\omega_p/\omega)^2}T_{2n} = Y_A T_{1n} + Y_B T_{2n} \tag{124}$$

It can be noted here that if T_{2n} is zero, the result

$$T_{4n} = \frac{-L\omega_p^2/\omega^2}{1 - (\omega_p/\omega)^2} T_{1n}, \tag{125}$$

is in accord with usual EM Theory for a homogeneous plasma. (A 90^o phase difference actually exists but is hidden because of the normalization given by (15).)

Returning to the question of contributions from the right hand side of (123), it must be remembered that this is an ordinary integration rather than surface or volumetric, so that limiting values of surface charge or current cannot be obtained. Thus, although the right hand side is probably not zero, it seems most probable that only a small contribution will be forthcoming, and then only from terms containing T_{2n}, which, as previously discussed, should be small. The use of this bilinear admittance condition is discussed in section 5 and results are presented in section 6.5.

Cohen states [14] in his formulation that his admittance parameters y_a and y_b (not the normalized parameters Y_A and Y_B) should be negative real numbers, but fails to make it clear whether he is restricting that fact to zero frequency. This statement can be investigated by combining the last equation of (17) (with $u_0 = 0$),

$$n(n + 1)T_{1n} = T_{4n} - T_{6n} \tag{126}$$

with equation 124, obtaining

$$T_{4n}(r_1) = \frac{\omega_p^2}{\omega^2} T_{6n}(r_1) - T_{2n}(r_1) \tag{127}$$

By reintroducing the Legendre functions, the definitions from (15) and summing over n, one obtains

$$v_r(r_1) = \frac{-ieE_r(r_1)}{m\omega} + \frac{iv_0^2}{\rho_0 r_1 \omega} \rho(r_1) = y_a \hat{n}\cdot\vec{E} + y_b \rho \tag{128}$$

It is obvious from (128) that Cohen's y_a and y_b should be imaginary rather than the negative real numbers for non-zero frequencies which he implied. This correction of Cohen's implication is emphasized because of its importance in the numerical computations given in section 6.

The Cohen condition above will be retained in section 4.4, because the hard and soft conditions can be obtained directly. By setting both Y_A and Y_B equal to zero, the hard condition ($v_r(r_1) = 0$) can be obtained from (120). Similarly, the soft condition ($\rho(r_1) = 0$) can be obtained with $Y_A = 0$ and $Y_B = \infty$.

In conclusion, this section has discussed the various radiator boundary conditions that can be employed. These can be summarized (using the relations (105)) as

$$T_{3n}^{(0)}(r_1) = A_{3n} = 1$$

$$T_{4n}^{(0)}(r_1) = A_{4n} = Y_A A_{1n} + Y_B A_{2n} \tag{129}$$

In section 4.4, these are combined with the results of the previous section to obtain the arbitrary constants explicitly.

4.4. SOLUTIONS FOR ARBITRARY CONSTANTS

Equations 114 and 129 can be combined to solve for the four arbitrary constants of the sheath region, since the two constants of the exterior region have already been eliminated. The boundary relations are thus

$$A_{3n} = 1$$

$$Y_A A_{1n} + Y_B A_{2n} - A_{4n} = 0$$

$$q_{1n}^{(1)}(y_2)A_{1n} + q_{1n}^{(2)}(y_2)A_{2n} + q_{1n}^{(3)}(y_2)A_{3n} + q_{1n}^{(4)}(y_2)A_{4n} = 0 \tag{130}$$

$$q_{2n}^{(1)}(y_2)A_{1n} + q_{2n}^{(2)}(y_2)A_{2n} + q_{2n}^{(3)}(y_2)A_{3n} + q_{2n}^{(4)}(y_2)A_{4n} = 0$$

By using the first two equations to eliminate A_{3n} and A_{4n} from the last two equations, the solutions for A_{1n} and A_{2n} can be readily obtained:

$$A_{1n} = -\frac{C_{32} + Y_B C_{34}}{C_{12} + Y_B C_{14} + Y_A C_{42}} \tag{131}$$

$$A_{2n} = -\frac{C_{13} + Y_A C_{43}}{C_{12} + Y_B C_{14} + Y_A C_{42}} \tag{132}$$

where

$$C_{jk} = q_{1n}^{(j)}(y_2)q_{2n}^{(k)}(y_2) - q_{2n}^{(j)}(y_2)q_{1n}^{(k)}(y_2) \tag{133}$$

with $q_{1n}^{(m)}(y_2)$ and $q_{1n}^{(m)}(y_2)$ defined by (112). Because of the definition of the preliminary solutions that was given by (105) the fields at the radiator assume the simple form

$$T_{1n}^{(0)}(y_1) = A_{1n} \tag{134}$$

$$T_{2n}^{(0)}(y_1) = A_{2n} \qquad \text{(equation continued)}$$

$$T_{3n}^{(0)}(y_1) = A_{3n} = 1$$

$$T_{4n}^{(0)}(y_1) = A_{4n} = Y_A A_{1n} + Y_B A_{2n}$$

The general sheath solutions $T_{jn}^{(0)}(y)$ could be obtained from these A_{mn} and the previously calculated preliminary solutions, $t_{jn}^{(m)}(y)$. Thus the quantities $A_{1n}, \ldots, A_{4n}$ can be considered as factors that modify the preliminary solutions. However, it is more practical to reintegrate the defining equations for those few cases (in section 7) where the radial variation is desired.

4.5. SPECIAL SIMPLE CASES

The values of the radiator fields defined by equations 131-134 are in a simple form for numerical computations. However, when the plasma is assumed to be homogeneous, general solutions can be given explicitly as in section 2.4. It is then more straightforward to obtain the arbitrary constants directly.

The conditions at the boundary between two homogeneous regions are discussed in appendix VI and are not necessarily the same as those discussed in section 4.2. Because these conditions are not well defined, this section will concern itself only with the no-sheath model for which the conditions of section 4.3 can be used:

$$\begin{aligned} T_{3n}^{(0)}(r_1) &= 1 \\ T_{4n}^{(0)}(r_1) &= Y_A T_{1n}(r_1) + Y_B T_{2n}(r_1) \end{aligned} \tag{135}$$

Using the radiation condition, the results of section 2.4 take the form

$$T_{1n}^{(0)}(r_1) = A_{5n} h_n(z_1)$$

$$T_{2n}^{(0)}(r_1) = A_{6n} h_n(z_1)$$

$$T_{3n}(r_1) = A_{5n}\left[\frac{1}{\epsilon_r(r_1)} \frac{d}{dz_1}(z_1 h_n(z_1))\right] - A_{6n}\left[\frac{1}{\epsilon_r(r_1)} h_n(z_2)\right] \tag{136}$$

$$T_{4n}(r_1) = A_{5n}\left[\frac{n(n+1)}{\epsilon_r(r_1)} \frac{\omega_p^2(r_1)}{\omega^2} h_n(z_1)\right] - A_{6n}\left[\frac{z_2}{\epsilon_r(r_1)} \frac{d}{dz_2} h_n(z_2)\right]$$

The solutions to (135) using (136) are then

$$A_{5n} = \epsilon_r \frac{H_{2n}(z_2) + Y_B}{D_n h_n(z_1)}$$

$$A_{6n} = \epsilon_r \frac{n(n+1)\omega_p^2/\omega^2 - Y_A}{D_n h_n(z_2)} \tag{137}$$

where

$$D_n = [1 + H_{2n}(z_1)][H_{2n}(z_2) + Y_B] - \left[n(n+1)\frac{\omega_p^2}{\omega^2} - Y_A\right] \tag{138}$$

The only solutions considered in section 6 are for what have been termed the soft and hard boundary conditions. In these cases, the results simplify to

(1) Soft Boundary ($Y_A = 0$, $Y_B = \infty$):

$$A_{5n} = \frac{\epsilon_r}{h_n(z_1)[1 + H_{2n}(z_1)]}$$

$$A_{6n} = 0 \tag{139}$$

(2) Hard Boundary ($Y_A = 0$, $Y_B = 0$):

$$A_{5n} = \frac{\epsilon_r n(n+1)\omega_p^2/\omega^2}{h_n(z_1)\left[1 + H_{2n}(z_1) - \dfrac{n(n+1)\omega_p^2/\omega^2}{H_{2n}(z_2)}\right]}$$

$$A_{6n} = \frac{\epsilon_r n(n+1)\omega_p^2/\omega^2}{h_n(z_2)H_{2n}(z_2)\left[1 + H_{2n}(z_2) - \dfrac{n(n+1)\omega_p^2/\omega^2}{H_{2n}(z_2)}\right]} \tag{140}$$

The results for the soft boundary case can also be used directly for the free space case by letting $\epsilon_r = 1$, since the soft boundary condition precludes the existence of the EA wave (with this model). In conclusion, in the following sections, the main interest for this model is on the value

$$T_{1n}^{(0)}(r_1) = A_{5n} h_n(z_1) \tag{141}$$

with A_{5n} given by (139) or (140).

5
METHOD OF COMPUTING INPUT ADMITTANCES

5.1. BASIC SPECIFICATION OF TERMINATING ADMITTANCE

The preceding sections have laid the groundwork for the calculation of the terminating admittance of a spherical dipole in an inhomogeneous compressible plasma. In this section, these results are combined to show how the terminating admittance can be calculated for those cases when numerical methods are necessary. The numerical methods themselves are considered in the following section.

The basic "modal" method of calculating the terminating admittance of the spherical dipole was apparently first discussed by Chu and Stratton [3]. The method presented here will begin, however, with the more complete derivation of Schelkunoff [2]. The Schelkunoff method and nomenclature will be modified in this section to include the effects of inhomogeneities, the EA wave, and the numerical methods of calculating the fields. In order to obtain results that are in agreement with Schelkunoff's results and standard engineering practice it is necessary to adopt the usual circuit theory time convention of $e^{+j\omega t}$. This is accomplished simply by letting -i be replaced by +j in the results of previous chapters. The $e^{-i\omega t}$ convention was employed because virtually all previous electroacoustic wave analyses have used it.

Schelkunoff's derivation of the terminating admittance of the spherical dipole is based on limiting values of his results for a biconical antenna of wide angle (or small gap width). His analysis begins by defining the fields in the interior biconical region in terms of the dominant TEM mode as well as higher order modes; the magnetic field at all angular positions θ at the sphere radius r_1 can be expressed in terms of these interior fields as

$$H_\phi(r_1, \theta) = \frac{I_0(r_1)}{2\pi r_1 \sin\theta} + \frac{1}{2\pi r_1}\sum_{n_0} \frac{a_{n_0}}{n_0(n_0+1)} \frac{d}{d\theta} M_{n_0}(\cos\theta) \tag{142}$$

and one then replaces $I_0(r_1)$ by $Y_t V'(r_1)$ where Y_t is defined as the terminating admittance seen by the TEM wave at the output boundary, $V'(r_1)$ is the voltage difference across the gap, the constants a_{n_0} are to be determined from the boundary conditions, the quantity $M_{n_0}(\cos\theta)$ is an odd Legendre function

$$M_{n_0}(\cos\theta) = \frac{1}{2}\left[P_{n_0}(\cos\theta) - P_{n_0}(-\cos\theta)\right] \tag{143}$$

and the summation is over all the zeros, n_0, of $M_{n_0}(\cos\psi)$, where ψ is the biconical angle $\frac{\pi}{2} - \frac{\Delta\theta}{2}$. The derivation of this form is not repeated here since it is given by Schelkunoff.

In the exterior region (and also on the sphere) the fields are similarly expressed as an infinite series. Using the nomenclature of section 2, which replaces Schelkunoff's series involving Hankel functions, this series is

$$H_{\phi}(r_1, \theta) = \sum_n T_{1n}(r_1) P_n^1(\cos \theta) \tag{144}$$

By equating the interior and exterior region representations (142) and (144) and integrating from $\theta = \psi$ to $\pi - \psi$, all the terms on the right of (142) disappear except the first, so that

$$Y_t = \frac{2r_1\sqrt{\mu_0/\epsilon_0}}{KV'(r_1)} \sum_n T_{1n}(r_1) P_n(\cos \psi) \tag{145}$$

where

$$K = \frac{\sqrt{\mu_0/\epsilon_0}}{2\pi} \int_{\psi}^{\pi-\psi} \frac{d\theta}{\sin \theta} = \frac{\sqrt{\mu_0/\epsilon_0}}{\pi} \ln \cot \frac{\psi}{2} \tag{146}$$

and

$$\frac{1}{2} \int_{\psi}^{\pi-\psi} P_n^1(\cos \theta)\, d\theta = P_n(\cos \psi) \tag{147}$$

Although the higher order mode constants, a_{n_0}, in (142) will always disappear with this integration, in general they will affect the calculation of the fields in the external region. This is because the electric field in the interior biconical region and on the boundary,

$$E_{\theta} = \frac{V'(r_1)\sqrt{\mu_0/\epsilon_0}}{2\pi r_1 K \sin \theta} + \frac{j\sqrt{\mu_0/\epsilon_0}}{2\pi r_1} \sum_{n_0} \frac{a_{n_0} Z_{n_0}^-}{n_0(n_0+1)} \frac{d}{d\theta} M_{n_0}(\cos \theta) \tag{148}$$

must be matched to that valid in the external region and on the boundary,

$$E_{\theta}(r_1 \theta) = \sum_n \frac{T_{3n}(r_1)}{j\omega\epsilon_0 r_1} P_n^1(\cos \theta) \tag{149}$$

Following Schelkunoff's equations 73 and 74, multiplication of (149) by $\sin \theta\, P_k^1(\cos \theta)$ and integration from 0 to π gives, because of orthogonality,

$$T_{3k}(r_1) = \frac{+j\omega\epsilon_0 r_1}{N_k} \int_{\psi}^{\pi-\psi} E_{\theta}(r_1, \theta) \sin \theta \frac{d}{d\theta} P_k(\cos \theta)\, d\theta \tag{150}$$

where N_k is defined as

$$N_k = \int_0^{\pi} \left[P_k^1(\cos\theta)\right]^2 \sin\theta \, d\theta = \int_{-1}^{+1} \left[P_k^1(x)\right]^2 dx = \frac{2k(k+1)}{2k+1} \tag{151}$$

Inserting (148) into (150) gives

$$T_{3k}(r_1) = \frac{-j\omega\epsilon_0\sqrt{\mu_0/\epsilon_0}V'(r_1)}{KN_1} P_k(\cos\psi) + \sum_{n_0} a_{n_0} Z_{n_0}^{-} v_{kn_0} = C_k \tag{152}$$

where a definition similar to Schelkunoff's equation 74 defines the quantities v_{kn_0} as functions of k, n, and ψ, and k is an odd integer for which $P_k(\cos\psi) = -P_k(-\cos\psi)$, since for even degree $P_k(\cos\psi) = P_k(-\cos\psi)$. Hereafter summation over the odd integers will be denoted by $\sum_n''$.

Schelkunoff shows in his equations 78-83 [2, pp. 50, 51] that the zeros of $M_{n_0}(\cos\theta)$ occur at approximately $n_0 = \frac{2\pi}{\Delta\theta}m(m = 1, 2, 3, \ldots)$. He concludes that the last term in (152) can be ignored for all practical purposes so long as the gap is small. This reasoning involves only the parameters of the interior, biconical region which is assumed to be plasma-free, perhaps implemented by a thin dielectric whose influence is otherwise ignored. Therefore, Schelkunoff's analysis also applies in the present problem and need not be repeated here.

It was noted in section 4 that it was convenient to always perform the numerical integrations of equations 22-25 with $T_{3n}(r_1) = 1.0$. The corresponding $T_{jn}(r_1)$ were denoted with a superscript zero, i.e. $T_{1n}^{(0)}(r_1)$. Because of the linearity of the defining equations, then

$$T_{1n}(r_1) = T_{1n}^{(0)}(r_1)C_n \tag{153}$$

Substituting the simplified form of (152) into (153) gives

$$T_{1n}(r_1) = \frac{-j\omega\epsilon_0\sqrt{\mu_0/\epsilon_0}V'(r_1)}{KN_n} P_n(\cos\psi)T_{1n}^{(0)}(r_1) \tag{154}$$

so that (145) gives

$$Y_t = \frac{2\sqrt{\mu_0/\epsilon_0}}{K^2}\sum_n'' \frac{Y_n^+}{N_n}\left[P_n(\cos\psi)\right]^2 \tag{155}$$

where

$$Y_n^+ = -j\omega\epsilon_0 r_1 T_{1n}^{(0)}(r_1) \tag{156}$$

This form is chosen to emphasize the similarity to Schelkunoff's equation 77, where by definition

$$Y_n^+ = \frac{H_{\phi,n}(r_1,\ \theta)}{E_{\theta,n}(r_1,\ \theta)} = \frac{T_{1n}(r_1)P_n^1(\cos\ \theta)}{\frac{1}{-j\omega\epsilon_0 r_1}T_{3n}(r_1)P_n^1(\cos\ \theta)} = -j\omega\epsilon_0 r_1 T_{1n}^{(0)}(r_1) \tag{157}$$

This last form is the main justification for introducing the normalized solutions $T_{jn}^{(0)}(r_1)$.

5.2. MODIFICATIONS TO ACHIEVE RAPID CONVERGENCE

Unfortunately, (155) is a slowly convergent series (approximately as 1/n) as will be discussed in sections 6 and 7. Schelkunoff was able to overcome this problem in the free space case, by transforming to a different series which converged much more rapidly. This series is obtained by observing that in the limit of $x \to 0$ or $n \to \infty$ (as discussed in appendix I)

$$\lim H_{2n}(x_1) = -(n + 1) \tag{158}$$

Then from (139) and (141), when $\epsilon_r = 1$,

$$\lim T_{1n}^{(0)}(r_1) = \lim \frac{1}{1 + H_{2n}(x_1)} = -\frac{1}{n} \tag{159}$$

Putting this into (156) gives

$$\lim Y_n^+ = \frac{j\omega\epsilon_0 r_1}{n} \tag{160}$$

so that the terminating admittance approaches the admittance of the capacitor formed by the hemispheres

$$Y_t(\omega \to 0) = j\omega C_t \tag{161}$$

where

$$C_t = \frac{2\epsilon_0 r_1 \mu_0/\epsilon_0}{\pi K^2} \sum_n{}' \frac{[P_n(\cos\ \psi]^2}{nN_n} \tag{162}$$

Schelkunoff goes on to show how this simpler quantity may be evaluated for various values of ψ (his equations 85-98, pp. 51-53). A modification of this technique (suggested following his (98)) is given in appendix IV which improves the accuracy of his result considerably. This shows that a good approximation is

$$C_t = 2\epsilon_0 r_1(-\ell n\ \Delta\theta + 2.0) \tag{163}$$

By adding and subtracting $j\omega C_t$ from the series given in (155) a difference series is obtained in the free space case that converges approximately as $1/n^4$ (as shown in section 6) which is much more rapidly than the original series. Schelkunoff's next step is to note that further simplification for the difference series is possible as $\Delta\theta$ approaches zero. This results, because for small gap angles

$$P_k(\cos\psi) = P_k\left[\cos\left(\frac{\pi}{2} - \frac{\Delta\theta}{2}\right)\right] \cong P_k\left(\cos\frac{\pi}{2}\right) - \frac{\Delta\theta}{2}\frac{d}{d\psi}P_k(\cos\psi)\Big|_{\psi=\pi/2} \tag{164}$$

and

$$K = \frac{\sqrt{\mu_0/\epsilon_0}}{\pi}\ln\cot\frac{\psi}{2} \cong \frac{\sqrt{\mu_0/\epsilon_0}}{\pi}\ln\frac{1+\frac{\Delta\theta}{4}}{1-\frac{\Delta\theta}{4}} \simeq \frac{\sqrt{\mu_0/\epsilon_0}}{\pi}\frac{\Delta\theta}{2} \tag{165}$$

Since

$$P_k\left(\cos\frac{\pi}{2}\right) = 0, \text{ and } P_k^1(\cos\theta) = -\frac{d}{d\theta}P_k(\cos\theta)$$

then

$$\left[\frac{P_k(\cos\psi)}{K}\right]^2 \cong \frac{\pi^2\epsilon_0}{\mu_0}\left[P_k^1(0)\right]^2 \tag{166}$$

This simplification allows the variation in admittance due to the gap width to be included only in the term $j\omega C_t$. Thus, Schelkunoff obtains his equation 101, [2, p. 54] which in the present nomenclature could be written

$$Y_t = j\omega C_t + \sum_{n=1}^{\infty}(\Delta B)_n \tag{167}$$

where

$$(\Delta B)_n = Y_n - B_{0n} \tag{168}$$

$$Y_n = -j\frac{2\pi\omega\epsilon_0 r_1}{N_n}\left[P_n^1(0)\right]^2 T_{1n}^{(0)}(r_1) \tag{169}$$

$$B_{0n} = j\frac{2\pi\omega\epsilon_0 r_1}{N_n}\left[P_n^1(0)\right]^2\frac{1}{n} \tag{170}$$

The term Y_n is introduced to emphasize the similarity between the Schelkunoff and Chu-Stratton formulations. Chu and Stratton calculated the Y_n's; Schelkunoff calculated $\sqrt{\frac{\mu_0}{\epsilon_0}}Y_n^+$,

which is equivalent to $jx_1 T_{1n}^{(0)}(y_1)$ as seen in (156). Hereafter, Y_n will be termed a modal admittance.

The Schelkunoff method is directly applicable in this study only for the soft boundary condition with the homogeneous plasma model. Because of the boundary condition, $\rho(r_1) = 0$, the perturbed electron density is then zero everywhere, and the result is therefore identical to that obtained for the cold plasma. With this model of the plasma, the only change in the equation above is that ϵ_0 is replaced by $\epsilon_0\epsilon_r = \epsilon_0\left(1 - \omega_p^2/\omega^2\right)$ in the definition of C_t and B_{0n} and (139) is used in defining $T_{1n}^{(0)}(r_1)$ in the definition of Y_n:

$$T_{1n}^{(0)}(r_1) = \frac{\epsilon_r}{1 + H_{2n}(z_1)} \tag{171}$$

For the hard boundary and the homogeneous compressible plasma model, the Schelkunoff method must be further modified. This is because the definition of $T_{1n}^{(0)}(r_1)$ obtained from (140) is now

$$T_{1n}^{(0)}(r_1) = \frac{\epsilon_r}{1 + H_{2n}(z_1) - \dfrac{n(n+1)(\omega_p/\omega)^2}{H_{2n}(z_2)}} \tag{172}$$

Using equation 158, it is found that as $n \to \infty$

$$\lim_{n\to\infty} T_{1n}^{(0)}(r_1) = \frac{1 - \omega_p^2/\omega^2}{1 - (n+1) - \dfrac{n(n+1)(\omega_p/\omega)^2}{-(n+1)}} = -\frac{1}{n} \tag{173}$$

exactly as is found in the free space case given by (159). It is shown in the next section that the rate of convergence of the same difference series as used in the free-space case is again approximately as $1/n^4$ for

$$n > z_2 = k_p r_2 = \frac{\omega}{v_0}\sqrt{1 - (\omega_p/\omega)^2}\, r_2$$

For the sheath model, these accurate representations were not possible. However, surprisingly, it was found that with the hard boundary conditions, the rate of convergence was still approximately $1/n^4$ when the free space B_{0n} were used. With the soft boundary condition, the rate of convergence was sometimes this large but was often much less, being only slightly greater than $1/n$. Because no better method seemed available for this soft boundary case, the final answer was obtained by using the smaller rate of convergence for terms through $n = 50$ and a rate of convergence of $1/n^4$ for larger values of n. Reduced accuracy is indicated in the tables with an asterisk, but as is shown in the figures, the general trends of the Y_t results are still readily discernible.

It should be emphasized that the answers could be made somewhat more accurate by using a finite gap angle when calculating low order series terms ($n < z_2$) while still employing the Schelkunoff subtraction techniques for the higher order calculations ($n > z_2$). The reason for this modification may be seen in figure 3, which gives the ratio

$$f(n, \psi) = \left[\frac{1}{\ell n \cot \frac{\psi}{2}} \frac{P_n(\cos \psi)}{P_n^1(\cos \psi)} \right]^2 \tag{174}$$

for n = 1, 3, . . . , 31 and for $\psi = 88.5^o$, 89.0^o and 89.5^o ($\Delta\theta = 3^o, 2^o, 1^o$). This is the ratio of the terms in the sum defined by (155) and those defined by (169) as a function of n and ψ. It is seen that, for these low orders and small gap angles, the ratio of the terms diminishes rather slowly, but will definitely affect the accuracy of the calculations. However, the accuracy of the final answers is not determined by this ratio alone. Only the difference series (consisting of small terms in general) should be multiplied by this factor above and for most of the cases considered, the effect would be barely noticeable in a graphical form. Of course, the error in this study is greater than for Schelkunoff's free space spherical dipole study since convergence now starts only for $n > z_2$ which in this study was near n = 15.

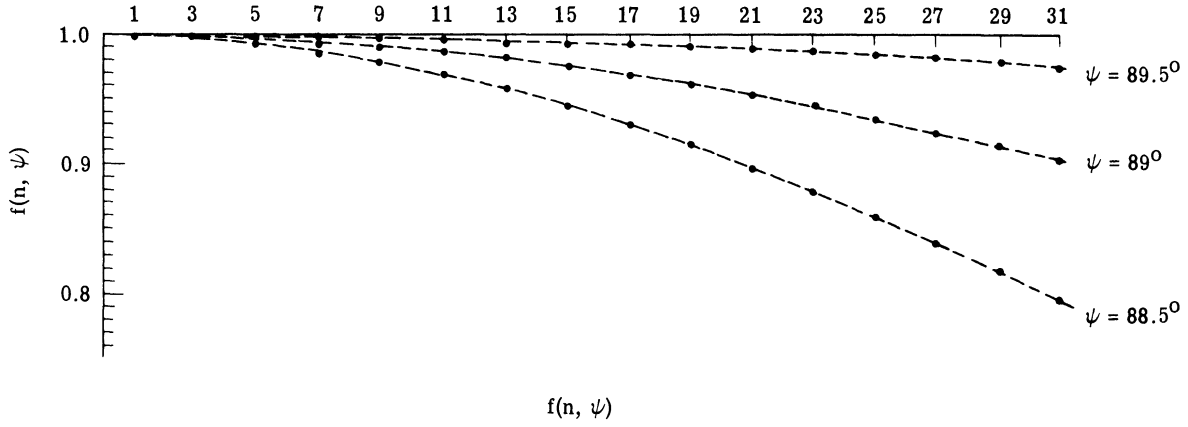

ψ = n = 1	3	5	7	9	11	13	15	17	19	21	23	25	27	29	31
89.5° 0.9999	0.9997	0.9992	0.9986	0.9977	0.9967	0.9954	0.9939	0.9923	0.9904	0.9883	0.9861	0.9836	0.9810	0.9781	0.9751
89.0° 0.9998	0.9988	0.9970	0.9944	0.9909	0.9867	0.9817	0.9759	0.9693	0.9620	0.9540	0.9452	0.9357	0.9256	0.9147	0.9032
88.5° 0.9996	0.9973	0.9932	0.9872	0.9796	0.9702	0.9591	0.9464	0.9320	0.9162	0.8988	0.8801	0.8600	0.8388	0.8164	0.7929

FIGURE 3. EFFECT OF FINITE GAP ANGLE, PLOT OF f(n, ψ) DEFINED BY EQUATION 174

For those interested in a particular gap angle this computation can be performed quite readily with the aid of the data in figure 3 (calculated on a computer). However, in order to present the data in a form that is independent of gap angle, the somewhat less accurate form given by equations 167-170 will be retained. This simplification can be further justified by recalling that the sheath profiles have been approximated, that several complicating features (drift velocity and pressure tensor) have been ignored and that a well justified boundary condition is simply not available. Thus, this method, which allows direct comparison with both the Chu and Stratton [3] and Schelkunoff [2] results, is deemed to be sufficiently accurate.

6
NUMERICAL RESULTS

6.1. INTRODUCTION

The purpose of this section is to present numerical results for the modal and terminating admittances of a spherical dipole in an inhomogeneous, compressible plasma. These admittances are obviously a function of the electrical size of the radiator, the unperturbed electron density and the thermal velocity. In addition, they are a function of three other parameters of the model: the assumed form for the density (or potential) profile, the sheath thickness, and the wall potential. Finally, it is necessary to study the effect of several different boundary conditions.

To study the influence of these parameters on the modal and terminating admittances, each of the above seven parameters will be varied separately. In order to illustrate fully the method of solution, one set of these parameters will be considered in detail. Where pertinent, the homogeneous plasma model will be discussed concurrently. Not only is each homogeneous medium case calculated much more rapidly and exactly, but the influence of some of the parameters are more clearly indicated.

6.2. DETAILS OF NUMERICAL SOLUTION

Many modifications have been made in the numerical techniques since the first results were obtained. The solution presented below has been chosen because it was the most intensively studied when these techniques were being perfected and it contains parameters suitable for comparison with the special model discussed in section 2.3. This "typical" case is characterized by

$$\omega_p^2(r) = \omega_p^2(r_2) - \left(\omega_p^2(r_2) - \omega_p^2(r_1)\right)\left(\frac{r_2}{r_1} - \frac{r}{r_1}\right)^2 \tag{175}$$

with the parameters given in table III. The homogeneous medium model, which is considered briefly, is defined by the right hand set of parameters (with $r_2/r_1 = 1.0$). A graphical presen-

tation of the static electron density and potential profiles in the sheath for these parameters is given in figure 9a as a curve labeled "Standard Model, equation 175."

TABLE III. PARAMETERS FOR EXAMPLE SHOWN IN FIGURES 4-8

$$\frac{r_2}{r_1} = 1.3784 \qquad \omega_p^2(r_2)/\omega^2 = 0.50$$

$$v_0/c = 1/32$$

$$\eta_w = -2.3\left(e^{\eta_w} = 0.1\right) \qquad k_0 r_1 = 0.5$$

$$\omega_p^2(r_1)/\omega^2 = 0.05$$

It was found that computational problems arose in obtaining accurate preliminary solutions (defined by equation 107), maintaining sufficient accuracy in the evaluation of the sheath edge quantities $q_j^{(m)}(y_2)$ defined by equation 112, and obtaining a convergent summation of the individual modal contributions. This section will illustrate the solutions to these problems. Estimates of overall accuracy are best discussed in the context of the special model considered in the next section, which was investigated using both numerical and analytical techniques.

It was shown in section 4 that the solution to a set of differential equations which must satisfy complicated boundary conditions at two different values of the independent variable can be obtained from the proper combination of preliminary solutions. These preliminary solutions could be any complete set of independent solutions, but in the usual set, which is used here, one dependent variable has an initial value of unity and the remaining dependent variables have initial values of zero. The nomenclature used for these preliminary results is described in section 4. Lower case $t_j^k(y)$ denotes the variable $T_j(y)$ when the variable $T_k(y)$ has an initial value of unity and all others are zero. In the present problem with the four differential equations (22-25), any of the sets of boundary conditions discussed in section 4 can be satisfied with no more than four (and possibly three) sets of solutions. A portion of these four sets is shown in figure 4 where only two (n = 1 and n = 21) of the modes needed to satisfy the boundary conditions are displayed.

The data in figure 4 are presented in the form used to compute the results: equal increments of the normalized radial distance $\left(y = \ell n \frac{r}{r}\right)$. This form was used since it greatly simplifies the computations by transforming the equations to the standard first order form discussed in section 2, equation 20. The important thing to note from these figures is that the logarithm of each dependent variable rapidly becomes proportional to y and that the slope of this proportionality increases with the order, n. This exponential growth is similar to that found

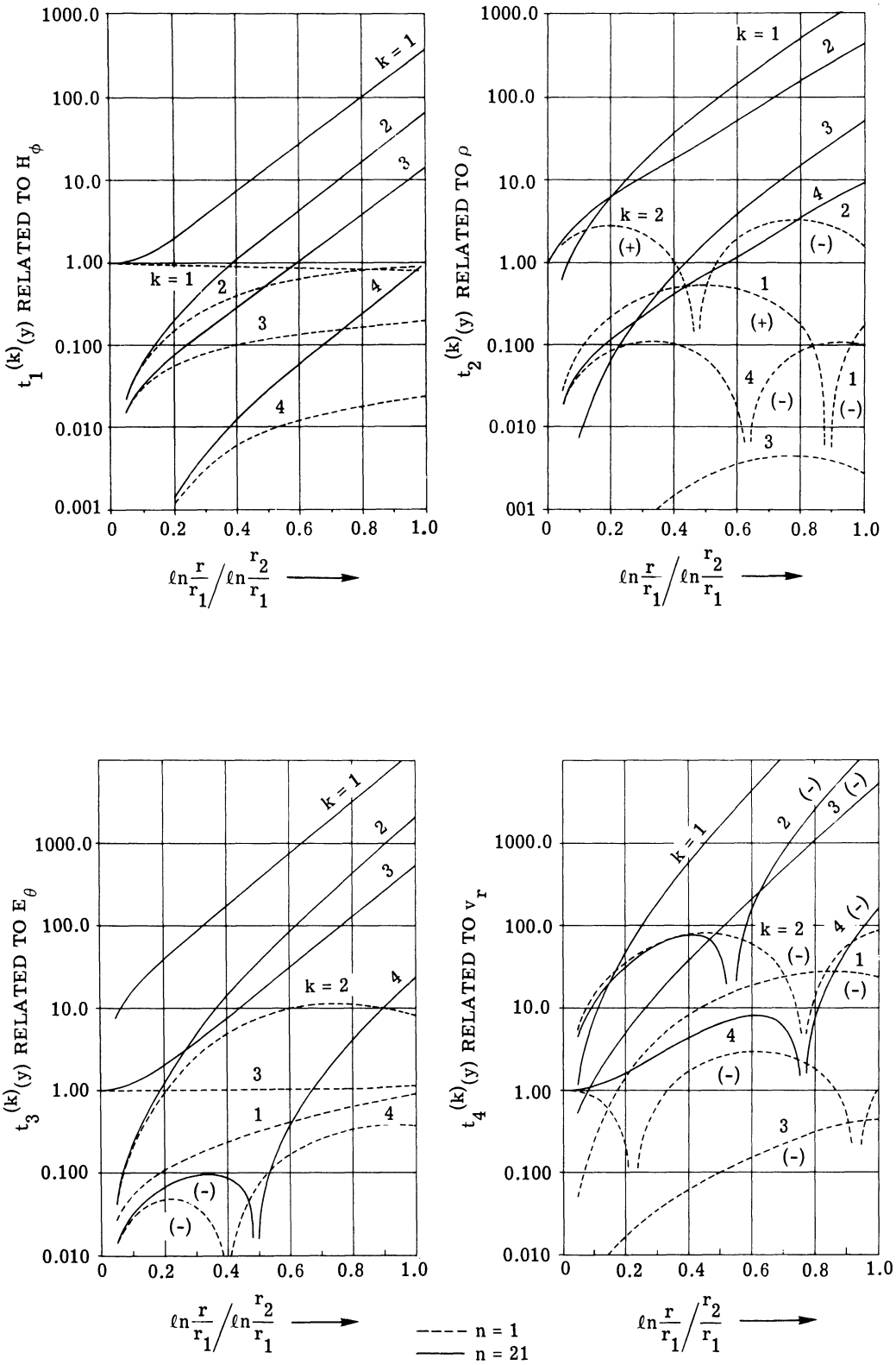

FIGURE 4. VARIATIONS OF PRELIMINARY SOLUTIONS WITH RADIUS. (Preliminary solutions defined by equation 107). Sheath, plasma, and sphere parameters are given in table III.

in the "special" solution (given in sec. 2.3) which will be further discussed in the next section.. It is important to emphasize again that the normalization employed transformed the differential equations into real (rather than complex) equations, thereby allowing a decided simplification in the numerical integration of the equations, but also eliminating evidence of wave character. Obviously, no wave character is seen in these preliminary solutions; one function of the boundary conditions is to introduce the proper wave behavior.

The technique used to obtain these solutions is important since early trials showed that extreme care was needed in starting the solution. The technique finally employed was to obtain the first point by using the first four terms in the MacLaurin series expansion of the four dependent variables around the origin $y = y_1 = 0$. That is

$$T_j(\delta y) \approx T_j(0) + (\delta y)T_j'(0) + 1/2(\delta y)^2 T_j''(0) + 1/6(\delta y)^3 T_j'''(0)$$

In most of the calculations to be presented, this point was at a distance $\delta y = y_2/20$, although in some cases it was found necessary to use a smaller δy such as $y_2/100$. The next four equally spaced sets of values were calculated using a Runge-Kutta integration subroutine. These values were used to start a more accurate Milne error correcting subroutine, which was used in the remainder of the integration. The importance of the first four terms in the MacLaurin series arises because, for certain of the preliminary solutions, not only is the value of the dependent variable zero, but the first and second derivatives are also zero. As an example it can be seen from equations 22-25 that when $T_4(y_1) = 1$ and $T_1(y_1) = T_2(y_1) = T_3(y_1) = 0$, then

$$\frac{dt_1^{(4)}(y)}{dy} = -t_1^{(4)}(y) + t_2^{(4)}(y) + \left(1 - \frac{\omega_p^2}{\omega^2}\right)t_3^{(4)}(y) = 0$$

$$\frac{d^2t_1^{(4)}(y)}{dy^2} = -\frac{dt_1^{(4)}(y)}{dy} + \frac{dt_2^{(4)}(y)}{dy} + \left(1 - \frac{\omega_p^2}{\omega^2}\right)\frac{dt_3^{(4)}(y)}{dy}$$

$$- t_3^{(4)}(y)\frac{d}{dy}\left(\frac{\omega_p^2}{\omega^2}\right) = \left(1 - \frac{\omega_p^2}{\omega^2}\right) - \left(1 - \frac{\omega_p^2}{\omega^2}\right) = 0$$

but

$$\frac{d^3t_1^{(4)}}{dy^3} = F_2\left(1 - \frac{\omega_p^2}{\omega^2}\right) + \frac{d}{dy}\left(\frac{\omega_p^2}{\omega^2}\right)$$

Hence,

$$t_1^{(4)}(\delta y) \cong \frac{1}{6}(\delta y)^3\left[F_2\left(1 - \frac{\omega_p^2}{\omega^2}\right) + \frac{d}{dy}\left(\frac{\omega_p^2}{\omega^2}\right)\right]_{y=0}$$

in this case. Thus, it was found that integration schemes that began with less than the first three derivatives gave final answers in appreciable error. The composite method of integration gave excellent accuracy as will be described in the next section.

The true initial conditions can now be obtained by using only the outer sheath edge value and slope of the variables $t_1^{(k)}(y_2)$ and $t_2^{(k)}(y_2)$. Numerical values for this typical case are given in table IV for the preliminary solutions. The results are shown only for $n \leqq 21$, though in most cases a few more orders were included. It can be seen that a definite pattern exists for each quantity with most quantities being positive and increasing with n; for $n \geqq 15$ all quantities are positive. It is important to note from figure 4 that the variation in each variable through the sheath is an important function of the assumed initial conditions as well as the differential equations. For example, for $n = 15, t_1^{(1)}(y_2) = 54.6$, but $t_1^{(4)}(y_2) = 0.221$ in this case.

TABLE IV. TERMINAL VALUES AND SLOPES AS A FUNCTION OF N

Variable	n = 1	3	5	7	9	11	13	15	17	19	21
$t_1^{(1)}(y_2)$	0.794	1.217	2.17	4.08	7.78	14.89	28.5	54.6	104.3	199.5	381.0
$t_1^{(2)}(y_2)$	88.1	1.050	1.401	2.03	3.10	4.93	8.05	13.40	22.7	38.8	66.9
$t_1^{(3)}(y_2)$	0.1844	0.220	0.293	0.424	0.651	1.038	1.702	2.85	4.84	8.32	14.45
$t_1^{(4)}(y_2)$	0.0222	0.0254	0.0319	0.0431	0.0615	0.0917	0.1408	0.221	0.355	0.577	0.950
$dt_1^{(1)}(y_2)/dy_2$	-0.358	2.17	9.16	26.4	67.0	159.2	363.0	807.0	1755.0	3757.0	7946.0
$dt_1^{(2)}(y_2)/dy_2$	1.483	2.98	6.40	13.31	26.8	52.9	103.0	199.0	383.0	733.0	1401.0
$dt_1^{(3)}(y_2)/dy_2$	0.371	0.679	1.384	2.18	5.62	11.09	21.7	42.0	81.3	156.6	301.0
$dt_1^{(4)}(y_2)/dy_2$	0.0608	0.0935	0.1646	0.300	0.549	1.002	1.823	3.32	6.03	10.98	19.98
$t_2^{(1)}(y_2)$	-0.01740	-0.0597	0.1111	1.207	5.12	16.53	46.6	121.1	298.0	703.0	1613.0
$t_2^{(2)}(y_2)$	-1.578	-1.791	-2.07	-2.11	-1.209	2.26	11.88	35.3	88.5	204.0	449.0
$t_2^{(3)}(y_2)$	0.00282	0.0206	0.0703	0.1935	0.481	1.122	2.51	5.45	11.58	24.2	49.8
$t_2^{(4)}(y_2)$	-0.1013	-0.1036	-0.1040	-0.0935	-0.0532	0.0564	0.315	0.879	2.06	4.55	9.19
$dt_2^{(1)}(y_2)/dy_2$	-0.460	-3.18	-9.49	-19.75	-26.4	+7.05	204.0	924.0	3133.0	9289.0	25400
$dt_2^{(2)}(y_2)/dy_2$	44.1	40.1	31.8	18.44	1.935	-6.12	33.1	227.0	846.0	2535.0	6774.0
$dt_2^{(3)}(y_2)/dy_2$	-0.0449	-0.265	-0.619	-0.900	-0.408	2.87	14.19	46.4	129.4	332.0	805.0
$dt_2^{(4)}(y_2)/dy_2$	0.553	0.374	0.0418	-0.436	-0.964	-1.202	-0.203	4.39	18.05	52.9	135.4

With the results presented in table IV, the quantities $q_j^{(k)}(y_2)$ were obtained from equation 112:

$$q_j^{(k)}(y_2) = \frac{d}{dy} t_j^{(k)}(y_2) - H_{2n}(z_j) t_j^{(k)}(y_2)$$

for j = 1, 2 and k = 1, 2, 3, 4. These are complex because $H_{2n}(z_j)$ is complex. The calculated values of $H_{2n}(z_j)$ are given in appendix I for this typical case. The next step is to obtain the complex initial values $T_{jn}^{(0)}(y_1)$ which satisfy the specified boundary conditions by using equations 131-134.

Having found these proper initial conditions, it is not necessary to re-enter the integration routine but this was usually done for n = 1 and $n = N_{max}$ as a check on the results. This can be done separately for the real and imaginary parts because the differential equations are themselves entirely real with the normalization employed. A sample plot of the quantity $T_{21}^{(0)}(y)$ is shown in figure 5 for two assumed conditions: the hard and soft boundaries.

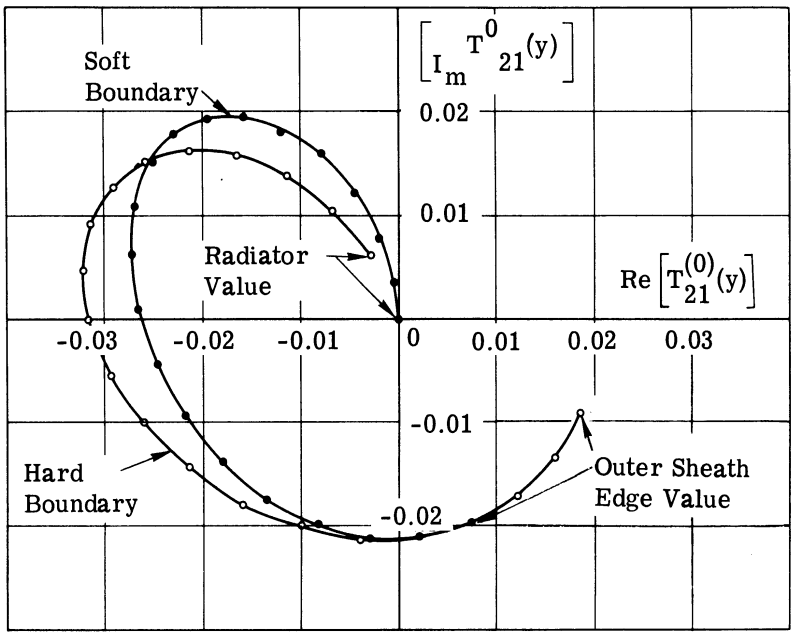

FIGURE 5. POLAR REPRESENTATION OF $T_{21}^{(0)}(y)$ VARIATION THROUGH SHEATH. Sheath, plasma, and sphere parameters are given in table III.

It is also possible to check the accuracy of the integration techniques by calculating the quantities

$$\frac{dT_{1n}^{(0)}(y_2)}{dy_2} \Big/ T_{1n}^{(0)}(y_2) \quad \text{and} \quad \frac{dT_{2n}^{(0)}(y_2)}{dy_2} \Big/ T_{2n}^{(0)}(y_2)$$

to ensure that the boundary conditions are satisfied. From figure 5

$$\frac{dT_{21}^{(0)}(y_2)}{dy_2} \Big/ T_{21}(y_2) = (0.1225 + i0.2979) \Big/ (0.01859 + i0.009087)$$

$$= -1.004 + i15.53$$

This calculated value is in excellent agreement with the value of $H_{21}(z_2)$ given in appendix I. A corresponding agreement was found in all cases tested, indicating the success of the integration technique. The phase variation through the sheath was about the same for the variable $T_{4n}^{(0)}(y)$ but was very small for $T_{1n}^{(0)}(y)$ and $T_{3n}^{(0)}(y)$ which remained essentially real, as did $T_{2n}^{(0)}(y)$ and $T_{4n}^{(0)}(y)$ for large orders. The total field variations through the sheath are discussed in section 7.

However, the main interest in this study is in the calculations of the input admittance, rather than just the field variation through the sheath. The formulas relating input admittance to the surface fields were developed in section 5, showing that one needs only to modify slightly the calculated variables $T_{1n}^{(0)}(y_1)$ to obtain the modal admittances Y_n through equation 169. All of the calculated variables $T_{1n}^{(0)}$, and consequently the modal admittances, are strongly influenced by the assumed boundary conditions. These Y_n values for the hard and soft boundary assumptions are given in table V and then plotted in figure 6b. A discussion of these values of Y_n will be postponed in order to demonstrate more fully the influence of the EA wave. This demonstration can be accomplished by first giving a brief description of results obtained for

TABLE V. MODAL ADMITTANCES FOR FIVE CASES
Sheath, plasma and sphere parameters are given in table III.

Order n	Limiting Free Space B_{0n}	Homogeneous Plasma Model				Sheath Model			
		Soft Boundary		Hard Boundary		Soft Boundary		Hard Boundary	
		G_n	B_n	G_n	B_n	G_n	B_n	G_n	B_n
1	6.250	0.1551	3.509	0.5034	3.474	0.2997	4.107	0.2901	4.020
3	1.823	---	0.919	0.1707	0.904	0.0551	1.249	0.0782	1.197
5	1.074	---	0.539	0.1577	0.509	0.0458	0.802	0.0841	0.755
7	0.763	---	0.382	0.1628	0.332	0.0392	0.607	0.0921	0.564
9	0.592	---	0.296	0.1835	0.208	0.0327	0.494	0.1011	0.459
11	0.484	---	0.242	0.2497	0.054	0.0265	0.419	0.1096	0.397
13	0.409	---	0.204	1.0540	-0.414	0.0231	0.369	0.1341	0.344
15	0.354	---	0.177	0.0235	0.795	0.0026	0.329	0.0636	0.524
17	0.312	---	0.156	2.1(-4)	0.475	3.1(-5)	0.285	2.5(-4)	0.356
19	0.280	---	0.140	1.8(-6)	0.369	3.1(-7)	0.255	1.8(-6)	0.300
21	0.253	---	0.126	1.1(-8)	0.310	2.2(-9)	0.213	1.0(-8)	0.265

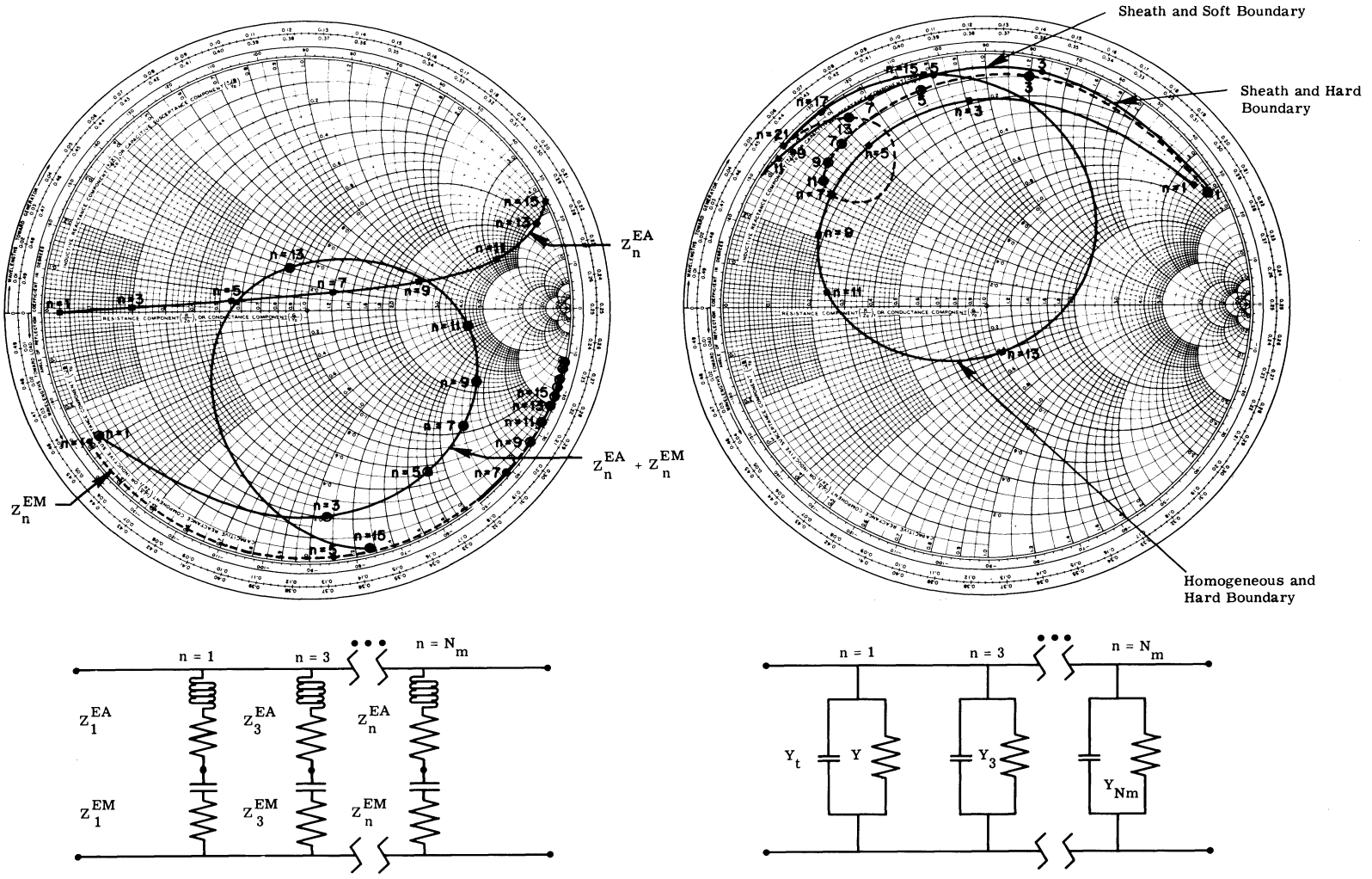

(a) Modal impedances (only for homogeneous medium and hard boundary)

(b) Modal admittances

FIGURE 6. MODAL IMPEDANCES AND ADMITTANCES FOR THREE CASES GIVEN IN TABLE V. Sheath, plasma, and sphere parameters are given in table III.

a much simpler case. This case assumes that the plasma is everywhere homogeneous and that the proper boundary condition is one of elastic reflection (the hard boundary). The field variations for this case were given in section 2.4, the arbitrary constants in section 4.5 and the value of $T_{1n}^{(0)}(y_1)$ (to find Y_n using (169)) in (172).

Thus it is found that Y_n is given explicitly by

$$Y_n = j \frac{2\pi\omega\epsilon_0 r_1}{N_n}\left[P_n^1(0)\right]^2 \frac{1 - \omega_p^2/\omega^2}{\left[1 + H_{2n}(z_1)\right] - \left[\frac{n(n+1)\omega_p^2/\omega^2}{H_{2n}(z_2)}\right]} \tag{176}$$

The advantage of this homogeneous medium model is that the contributions of the EM and EA components can be readily separated by first looking at modal impedances $\left(Z_n = \frac{1}{Y_n}\right)$ as seen in figure 6a. Two separate impedance components are obtained from the two parts of the denominator of (176). The interesting feature is that although both $j_n(z)$ and $n_n(z)$ are oscillating functions, the real part of $H_{2n}(z)$ is always negative and the imaginary part is positive or negative according to the assumed time convention, leading to the equivalent circuits shown in figure 6a. The line connecting the modal admittance plots are intended to assist in a visualization of the results; only the discrete odd-integer values have physical significance. On these Smith Chart graphs, the proper scales are indicated by the superimposed factors, in this case 10^3 and 10^{-3} respectively.

In this Smith Chart impedance plot, it is seen that for each mode the EM component is essentially capacitive at the chosen frequency with the dominant resistive component coming from the first mode. Each EA component is largely resistive for mode numbers less than the normalized EA size of the sphere; for higher orders each component is essentially inductive. The sum of these two impedance components for each mode is also shown in figure 6a, where it can be seen that the fifteenth mode is inductive and that, surprisingly, for high orders the results approach free space values. The mathematics of this last result were given in (173).

An inversion of the modal impedances ($Y_n = 1/Z_n$) gives the modal admittances as shown by the large loop in figure 6a. The admittance form is necessary of course to obtain the total input admittance by summation. Wait [18] has used the same set of equations, boundary conditions, and range of variables, but calculated only the radiation resistance for each of these components. His technique is the familiar Poynting vector method which, although somewhat simpler, cannot give the reactive component as found above. However, a comparison of results gives excellent agreement for the real part of the admittance in those cases that can be compared. This brief description of the homogeneous model will be supplemented in section 6.4 with modal and terminating admittance data as the plasma frequency and thermal velocity are varied.

The admittance results for the homogeneous medium model can now be compared with results obtained for the more realistic inhomogeneous sheath model, which is the major interest of this study. Separation into EM and EA components is not possible but the form of the modal admittance plots for the sheath model are, nevertheless, surprisingly similar to the results for the homogeneous medium model, as seen in figure 6a. The main difference between all these cases is the size of the loop. In the context of the impedance plot of figure 6b, it is readily seen that the size of the loop is a measure of the magnitude of the EA resistance component. The soft boundary condition predicts an appreciably smaller loop than the hard boundary condition for the inhomogeneous medium model, and both loops are in turn smaller than the loop for the homogeneous medium model. The smaller result obtained for the soft boundary condition is to be expected because that condition precludes any EA wave excitation at all with the homogeneous medium model. The large results for the homogeneous medium model are attributed directly to the hard boundary condition; the smaller results of the inhomogeneous medium models are due to the decreased electron density at the radiator. Perhaps the most surprising feature is that such a large influence is seen for the soft boundary condition with the inhomogeneous medium model. This shows that the EA wave excitation with this model is largely due to the inhomogeneous medium and the associated static electric field. In section 6.3, these various parameters will be examined in more detail.

The final topic in this discussion of a typical solution is that of obtaining a total terminating susceptance. The problem (discussed in section 5.2) is that with a gap of narrow width it is well known [2, 3] that the series solution converges only slightly faster than $\frac{1}{n}$. Rather than restrict this study to a single finite gap width and thereby obtain a convergent solution with the use of many terms, use was made of the fact, noted in section 5.2, that the modal admittances approach free space values for orders greater than $k_p r_2$.

A convergent solution for the total input susceptance was obtained by subtracting each calculated modal value from the low-frequency free-space value using equation 168. The difference terms for the typical cases under consideration are shown in figure 7. These difference values can be obtained directly from table V by subtracting each value of B_n from the listed value of B_{0n}. Also shown are the difference terms for the soft boundary case which were obtained by subtracting B_n from $\epsilon_r B_{0n}$ as in the sentences preceding (171). These values were then combined with a free-space total susceptance of 13×10^{-3} mhos using equation 167. The derivation of this quantity (and the correction term needed to include the contribution of terms from $n = N_{max}$ to ∞) is given in appendix IV. The final total admittance values for these four cases are then shown in the table and Smith Chart plot of figure 8. Also shown is the calculated point for the spherical dipole in free space.

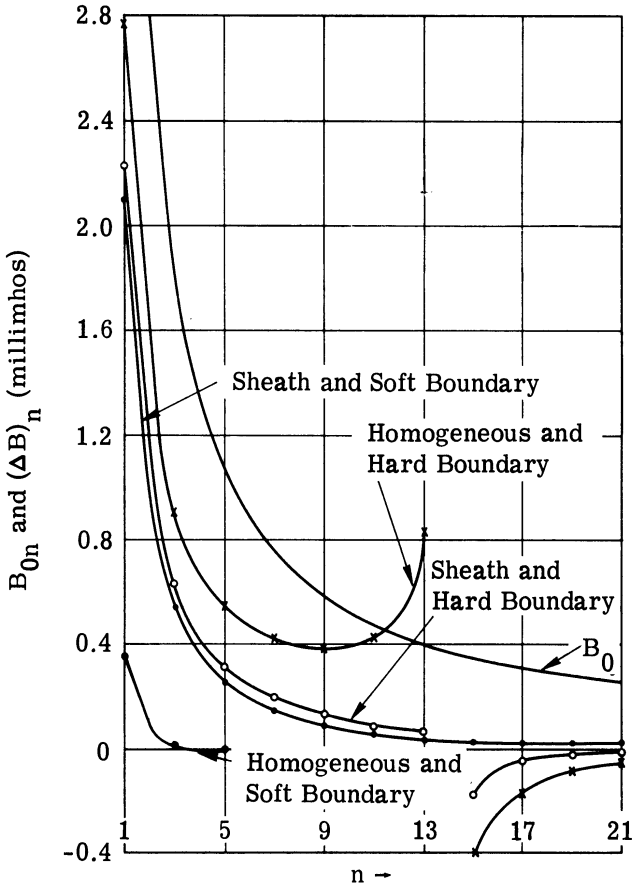

FIGURE 7. $(\Delta B)_n$ FOR FOUR MODELS AND B_{0n}. Sheath, plasma, and sphere parameters are given in table III.

From the Smith Chart plot of terminating admittance, two major conclusions can be drawn that will apply in most of the cases to be discussed in the remainder of this section. First, the total conductances for the inhomogeneous medium model fall between the extremes obtained with the homogeneous medium model; the hard boundary condition in each case leads to a larger conductance than does the soft. Secondly, the susceptances for the two boundary conditions in the inhomogeneous medium model are surprisingly similar. The susceptances with the homogeneous medium model are somewhat dissimilar; the hard boundary condition predicts a larger susceptance than does the soft boundary condition due of course to the EA wave. The large susceptance difference between the sheath and homogeneous plasma models shown in figure 8 should not be attributed to the EA wave, since it is largely due to the influence of the sheath on the EM wave. This explanation of the susceptance difference can be appreciated by noting that a dipole in a plasma looks electromagnetically smaller than when in free space. The sheath reduces this effect; the apparent EM propagation constant, the apparent EM electric size, and therefore the susceptance are thus caused to increase because of the presence of the sheath.

The EA wave similarly contributes to the susceptance but the influence is much less. Apparently because of the large difference in electrical size (a factor of $c/v_0 = 32$), the modal con-

tributions due to the EA wave are found to contribute largely to radiated, or real, rather than stored, or reactive, energy. This is seen in the plots of figure 6. The physical interpretation is that the EA electron motion is caused to be largely in phase with the density perturbations and this contributes to real power flow. This is maximized with the homogeneous medium model and a large resistive component results. This is discussed further in the next two sections.

As stated at the beginning of this section, the particular case presented here was chosen to allow a comparison with the model discussed in the next section and not because of its physical reality. The sheath is somewhat wider and the wall potential somewhat lower than in the cases considered later. Further comparison between the different boundary conditions and the models will therefore be considered throughout this section.

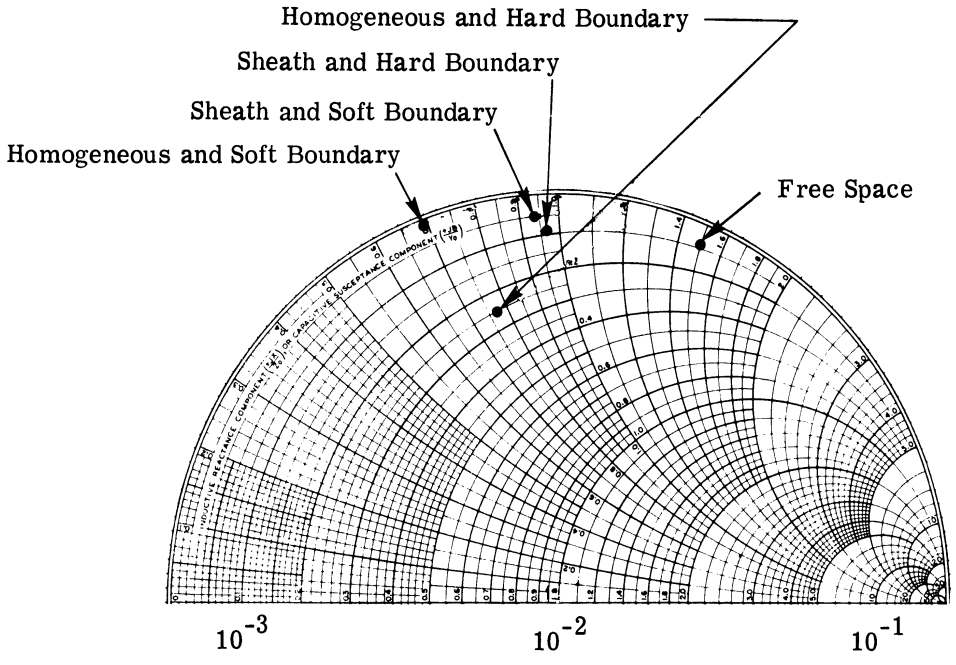

Model	G_t	B_t
Free Space	0.962	14.486
Homogeneous and Soft Boundary	0.155	6.894
Homogeneous and Hard Boundary	2.506	7.63
Sheath and Soft Boundary	0.525	9.3
Sheath and Hard Boundary	0.955	9.52

FIGURE 8. DIPOLE TERMINATING ADMITTANCE Y_t (millimhos).
Sheath, plasma, and sphere parameters are given in table III.

6.3. COMPARISON OF INHOMOGENEOUS PLASMA MODELS

6.3.1. INFLUENCE OF ASSUMED DENSITY VARIATIONS. Two models of the static sheath have been employed in the numerical integrations performed in these studies; typical static electron density and potential profiles for these two sheath models are shown in figure 9. The parameters for both sets of curves are given in table VI. The model labeled "standard" is defined by equation 175; the model labeled "special" is defined by

$$\frac{\omega_p^2(r)}{\omega^2} = 1 - \frac{r_0^2}{r^2}$$

where

$$r_0^2 = \left[1 - \frac{\omega_p^2(r_1)}{\omega^2}\right] r_1^2 \tag{177}$$

The static potential and electric field for both models are obtained from equations 90 and 91 respectively. In the standard model the static electric field as well as the static potential are found to be zero at the outer sheath edge; in the special model the electric field had to be set equal to zero by subtracting the outer sheath edge value. This special model choice was dictated by the desire to obtain an expression for the modal admittances which could be expressed in closed form; only this choice was found to lead to coupled equations for which such a solution is possible (as explained in section 2.3), although the d-c electric field had to be ignored. Numerical calculations being necessary to include the effects of the electric field, the first calculations were also performed with the special model. However, this form has very limited usefulness because, in contrast to the actual behavior, the sheath thickness increases as the plasma frequency increases. Nevertheless this early form was very useful in eliminating errors in the computer program, obtaining an appreciation of the importance of EM and EA wave coupling in an inhomogeneous plasma and simplifying the method of computation. The entire range of these early numerical studies will not be presented since data for the standard model discussed in the preceding section and in the remainder of this section is of greater physical interest.

A comparison of modal admittances for the two models with the hard boundary condition is shown in figure 9b; the data for these curves are given in table VI. The most interesting feature is the obvious similarity of the results for quite different sheath electron density profiles. The differences that exist (loop size and location) are better explained in the context of the investigations to be reported in sections 6.3.2-6.3.4, in which the sheath thickness and wall potential are varied. The soft boundary condition results display a similar correspondence.

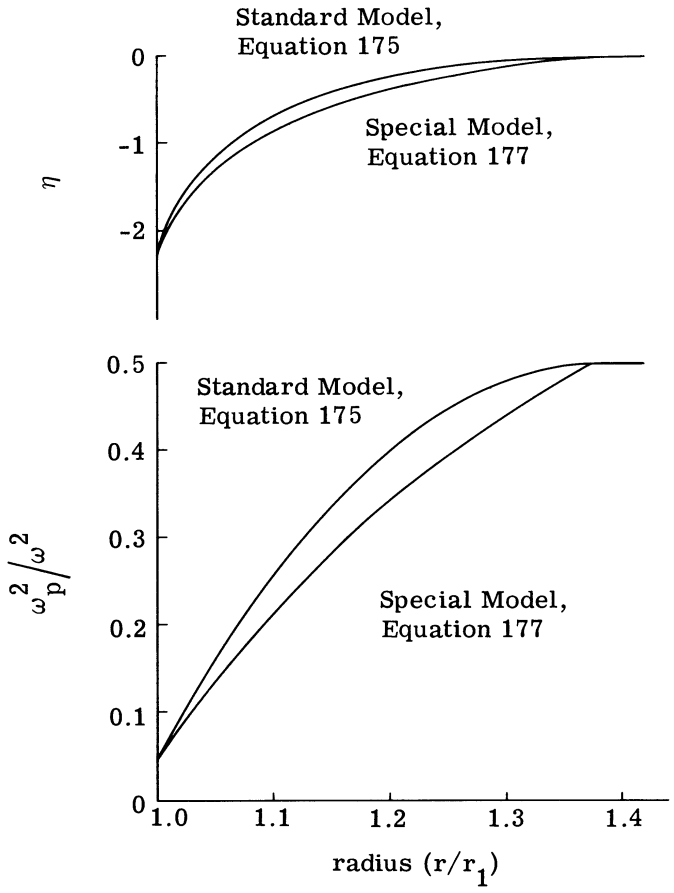

(a) Static electron density and potential profiles in the sheath

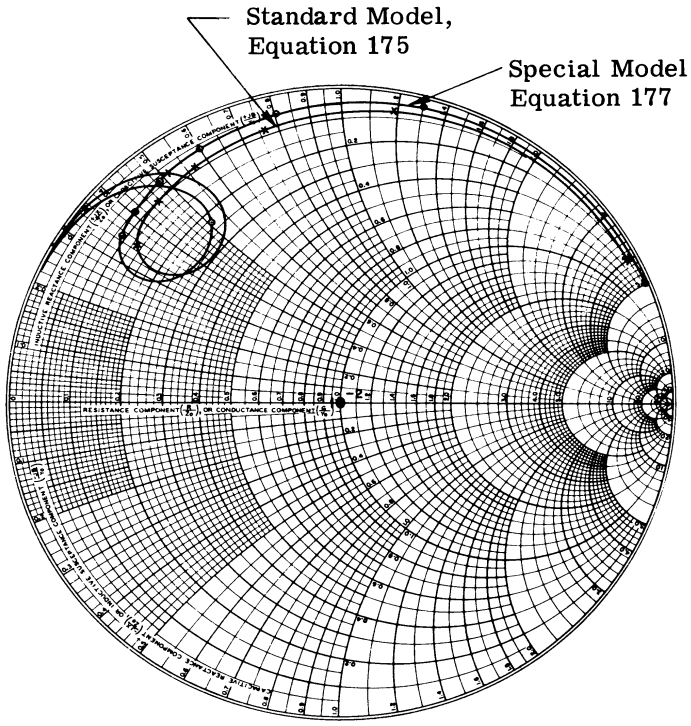

(b) Y_n for the hard boundary

FIGURE 9. COMPARISON OF TWO SHEATH MODELS. Sheath, plasma, and sphere parameters are given in table VI.

TABLE VI. PARAMETERS AND ADMITTANCES FOR COMPARISON OF STANDARD MODEL (EQUATION 175) AND SPECIAL MODEL (EQUATION 177)

(a) Sheath, Plasma and Sphere Parameters

$r_2/r_1 = 1.3784$, $r_0/r_1 = 0.95$, $\omega_p^2(r_2)/\omega^2 = 0.5$, $\omega_p^2(r_1)/\omega^2 = 0.05$, $\eta_w = -2.3$, $v_0/c = 1/32$, $k_0 r_1 = 0.5$

(b) Admittances

	Special Model		Standard Model		Standard Model (no electric field)	
n	G_n	B_n	G_n	B_n	G_n	B_n
1	0.2418	4.298	0.2901	4.020	0.1903	4.130
3	0.0444	1.296	0.0782	1.197	0.0201	1.223
5	0.0545	0.814	0.0841	0.755	0.0328	0.761
7	0.0632	0.601	0.0921	0.564	0.0448	0.555
9	0.0725	0.481	0.1011	0.459	0.0576	0.435
11	0.0825	0.409	0.1096	0.397	0.0720	0.354
13	0.0903	0.357	0.1341	0.344	0.0977	0.263
15	0.2287	0.5026	0.0636	0.524	0.2089	0.804

An interesting result is obtained when the d-c electric field is neglected in the standard model. This was accomplished in the computer program by simply setting the single term containing the electric field in equation 23 equal to zero. In the inhomogeneous sheath surrounding a physical dipole a d-c electric field must exist; however, density inhomogeneities can be supported by gravity or temperature gradients. The relative importance of electric field and density gradient effects is therefore an interesting question. Modal admittances for the hard and soft boundary conditions are compared in figure 10 for the standard model (parameters are given in table III), with and without the d-c electric field. This type of plot has been used because the curves would be indistinguishable on a Smith Chart. It must be emphasized that the conductance and susceptance scales differ by a factor of ten in this plot. For low orders, the d-c electric field is seen to add considerably to the modal conductances. However, for the 15th mode (with the hard boundary assumption), the d-c electric field apparently "inhibits" radiation. Since this mode obviously makes an important contribution to the total conductance, the total conductance can be either increased or decreased with an electric field. In the present case there is a decrease in G_t from 0.95×10^{-3} to about 0.75×10^{-3} without the electric field. Also important in this comparison is the fact that the degree of excitation of various modes has been altered; it might be anticipated therefore that the radiation pattern would be altered more than the terminating admittance. Similar results have been obtained in other cases that have been attempted, but the above example should suffice to demonstrate the necessity of including the electric field. Since the homogeneous media analyses cannot include the influence of an electric field, neither the radiation patterns nor the input admittance obtained with that model should be expected to be in agreement with the inhomogeneous medium results.

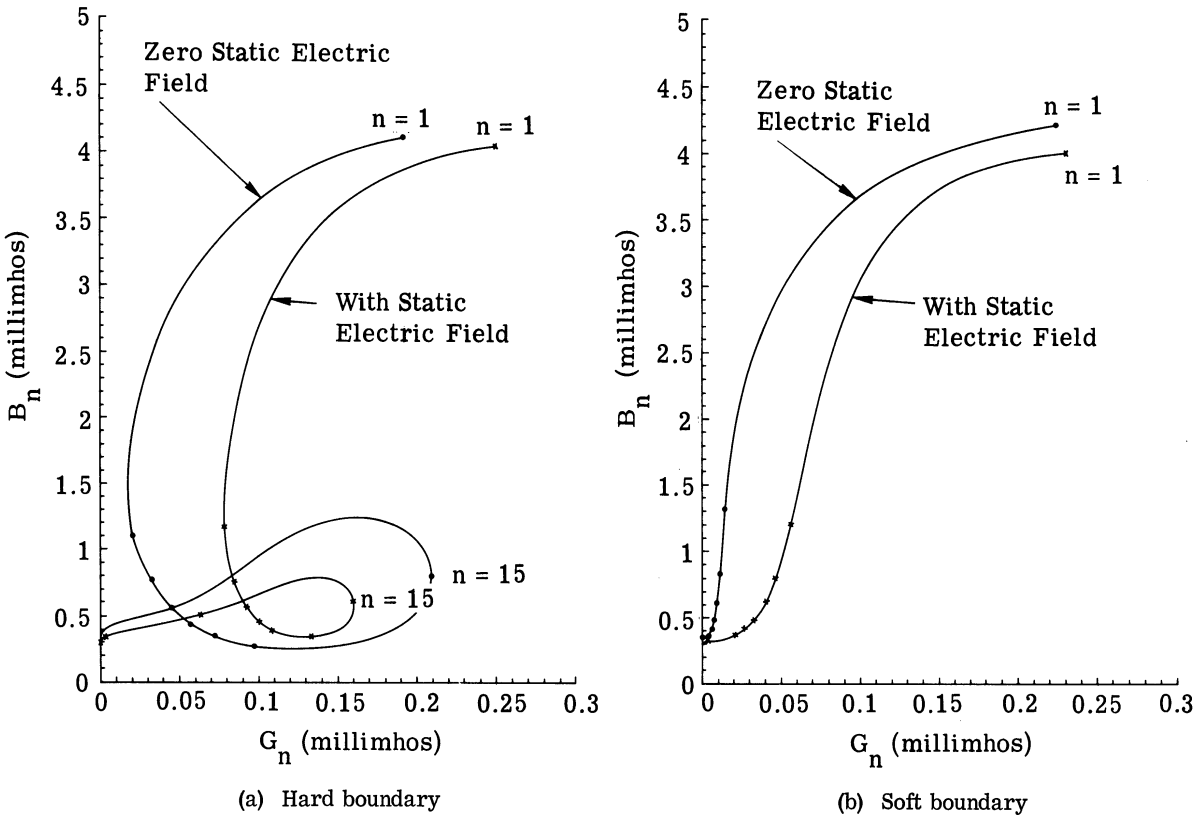

(a) Hard boundary

(b) Soft boundary

FIGURE 10. EFFECT OF STATIC ELECTRIC FIELD ON Y_n. Sheath, plasma, and sphere parameters are given in table VI, standard model.

It is also of interest to compare "analytical" and "numerical" results in order to obtain an estimate of the accuracy of the numerical integration technique. One case is compared in table VII. The analytical results were obtained using the analytical forms of section 2.3 and the set of six boundary equations given in sections 4.2 and 4.3. The details of this will not be given since the method is fairly standard. The numerical results were obtained for the same simple analytical model, but using the integration techniques described in the previous section. It should be noted that these data are obtained for the unrealistic case, $v_0/c = 0.1$, and should not be compared with the data given in section 6.2 or above.

Results for this simple case were also obtained on a desk calculator and integrated on an analog computer (for only n = 1); these results were in excellent agreement with the data in table VII. The discrepancy between the techniques is negligible; for smaller values of v_0/c, and larger orders of n, the agreement should not be expected to be as good. This expected decrease in accuracy for larger orders is due to the large magnitudes of the "trial" solutions, as seen in table IV. Nevertheless, it is apparent that the method of integration is correct and only minor errors should be expected due to the method of solution.

TABLE VII. COMPARISON OF TECHNIQUES OF SOLUTIONS; SOFT BOUNDARY CONDITION. $v_0/c = 0.1$; $\omega_p(r_2)/\omega = 0.707$; $r_0 = r_1$; $(\omega_p(r_1)/\omega = 0)$

	Analytical Results		Numerical Integration Results	
	G_n	B_n	G_n	B_n
n=1	4.362454(-4)	4.617575(-3)	4.362453(-4)	4.617574(-3)
3	4.470334(-5)	1.455706(-3)	4.470329(-5)	1.455706(-3)
5	3.905162(-6)	9.238822(-4)	3.905152(-6)	9.238826(-4)
7	2.714829(-8)	6.765825(-4)	2.714823(-8)	6.765826(-4)

In conclusion, it has been found that the exact nature of the d-c sheath electron density and potential profiles is of secondary importance in determining the modal admittances. The differences that do exist in the results are believed to be caused by the magnitude of the d-c electric field. This effect is the subject of the next several sections.

6.3.2. EFFECTS OF VARYING THE ASSUMED SHEATH THICKNESS WITH A CONSTANT WALL POTENTIAL. This section discusses the consequences of incorrectly specifying the sheath thickness. This is not a study of the effects of physically varying the wall potential and thereby changing the sheath size; discussion of that phenomenon is contained in section 6.3.4. To study the effect of varying the sheath thickness, the case defined in table VIII will be considered. The case discussed in sections 6.2 and 6.3.1 differed from this one in having a smaller wall potential and therefore a higher electron density at the radiator.

TABLE VIII. PARAMETERS FOR FIGURES 11 AND 12

$\frac{r_2}{r_1}$ varied as below $\qquad \frac{\omega_p^2(r_2)}{\omega^2} = 0.50$

$\eta_w = -3.5 \left(e^{\eta_w} = 0.03 \right) \qquad \frac{v_0}{c} = \frac{1}{32}$

$\frac{\omega_p^2(r_1)}{\omega^2} = 0.015 \qquad k_0 r_1 = 0.50$

$$\begin{pmatrix} r_2 r_1 \\ \Delta r/\lambda_D \end{pmatrix} = \begin{pmatrix} 1.147 \\ 2.9 \end{pmatrix}, \begin{pmatrix} 1.295 \\ 5.7 \end{pmatrix}, \begin{pmatrix} 1.589 \\ 11.5 \end{pmatrix}, \begin{pmatrix} 1.884 \\ 17.3 \end{pmatrix}$$

A plot of the electron density and potential variations for this case is given in figure 11a. The plots of modal admittance data obtained using both the hard and soft boundary conditions for these four sheath thicknesses are shown in figure 12a and b. It is seen that the assumed sheath thickness is an important parameter for both of the assumed boundary conditions, the size of the loop increases as the sheath becomes narrower. In addition, the modal conductances increase with decreasing sheath thickness for both boundary conditions so that the total terminating admittances are strongly affected as seen in figure 11b. It is important to note that the homogeneous medium result with the hard boundary (data given in fig. 8) appears as a logical limiting value for the sheath cases as the sheath width is decreased. Similar results were observed in a preliminary investigation with only low orders of n for a higher wall potential and larger thermal velocity.

The conclusion to be drawn from these plots is that EA wave excitation is strongly influenced by the degree (thickness) of the inhomogeneity. It must again be emphasized that figures 11 and 12 represent an artificial situation in which the sheath thickness varies but wall potential does not.

6.3.3. EFFECT OF VARYING THE WALL POTENTIAL WITH CONSTANT SHEATH THICKNESS. In this section, results are presented for the variation in terminating admittance as the normalized wall potential takes on the values -2.3, -3.0, -3.5, and -4.6, which is a sufficient change to vary the density at the radiator from 0.1 to 0.01 of its value in the homogeneous region. The other parameters are given in table IX and are the same as in section 6.3.2. Again it must be emphasized that the sheath thickness is being kept constant (at $\Delta r/r_1 = 0.2946$) here. Thus, this investigation cannot be interpreted as covering the variation that would exist with changes in the dipole d-c potential, which is the subject of section 6.3.4.

A plot of the electron density and potential profiles that have been considered is shown in figure 13a. The dominant feature of the d-c potential and electron density profiles seen in figure 13a is that they are only slightly different. The modal admittance plots shown in figure 14a and b are also virtually the same with one exception. As can be seen in figure 14b, the large potential case ($\eta_w = -4.6$) with the soft boundary condition does have a markedly different behavior from the other cases. This is interpreted as meaning that there is an electric field above which the electroacoustic wave is more strongly excited when the soft boundary condition is assumed. It is probable that the strong influence seen here would be partially counteracted, in practice, by a change in sheath thickness; this is the subject of section 6.3.4.

For the hard boundary condition (fig. 14a), the points lie between those plotted and are therefore essentially on the curve which is drawn; this curve is specifically for the $\eta_w = -3.5$ case. The total terminating admittance variation with wall potential is shown in figure 13b where it is seen that relatively minor variations are predicted (noting again that the sheath thickness is assumed constant.)

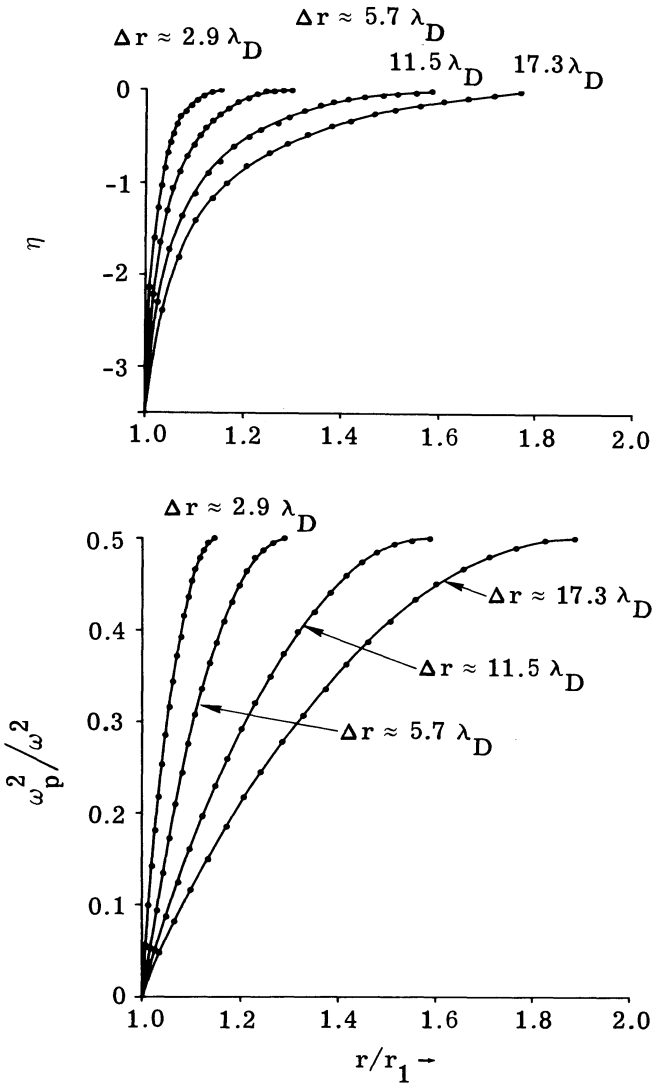

(a) Static electron density and potential profiles in the sheath

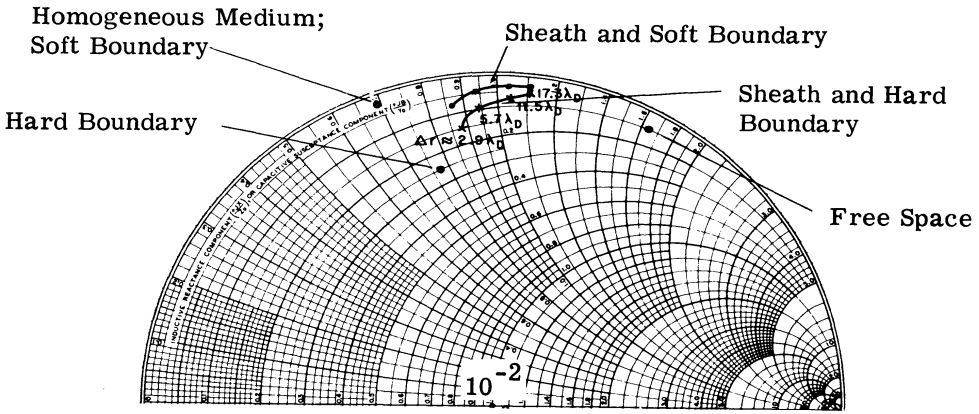

Debye Lengths	Soft Boundary		Hard Boundary	
	G_t	B_t	G_t	B_t
2.9	0.848	8.7*	1.687	8.89
5.7	0.739	9.5*	1.166	9.37
11.5	0.383	10.3	0.703	10.46
17.3	0.310	11.1	0.542	11.08

* Estimated (within 0.1)

(b) Y_t for hard and soft boundaries (millimhos)

FIGURE 11. COMPARISON OF SEVERAL SHEATH THICKNESSES (CONSTANT WALL POTENTIAL). Sheath, plasma, and sphere parameters are given in table VIII.

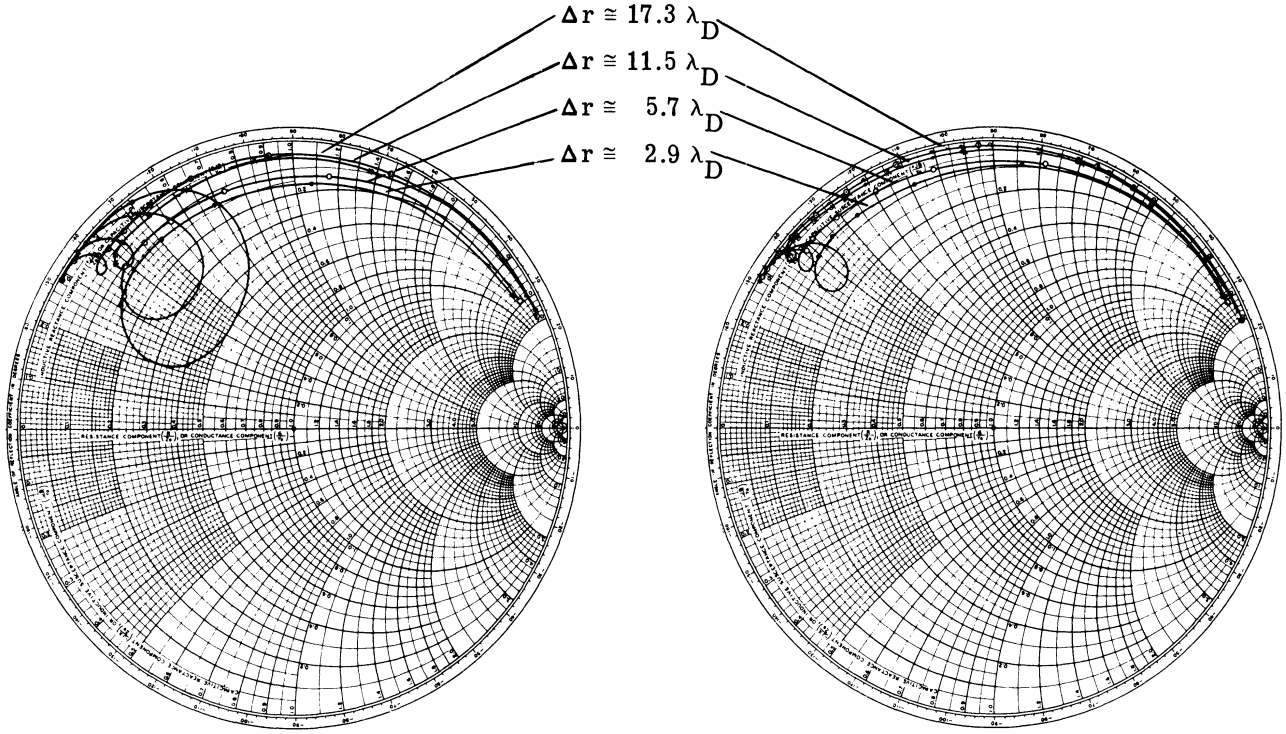

(a) Hard boundary

(b) Soft boundary

FIGURE 12. Y_n FOR VARIOUS SHEATH THICKNESSES (CONSTANT WALL POTENTIAL). Sheath, plasma, and sphere parameters are given in table VIII.

TABLE IX. PARAMETERS FOR FIGURES 13 AND 14

$$\frac{r_2}{r_1} = 1.295(\Delta r \approx 5.7\lambda_D) \qquad v_0/c = \frac{1}{32}$$

$$\omega_p^2(r_2)/\omega^2 = 0.50 \qquad k_0 r_1 = 0.50$$

$$\eta_w = -2.3, -3.0, -3.5, -4.6$$

$$\omega_p^2(r_1)/\omega^2 = 0.05, 0.025, 0.015, 0.005$$

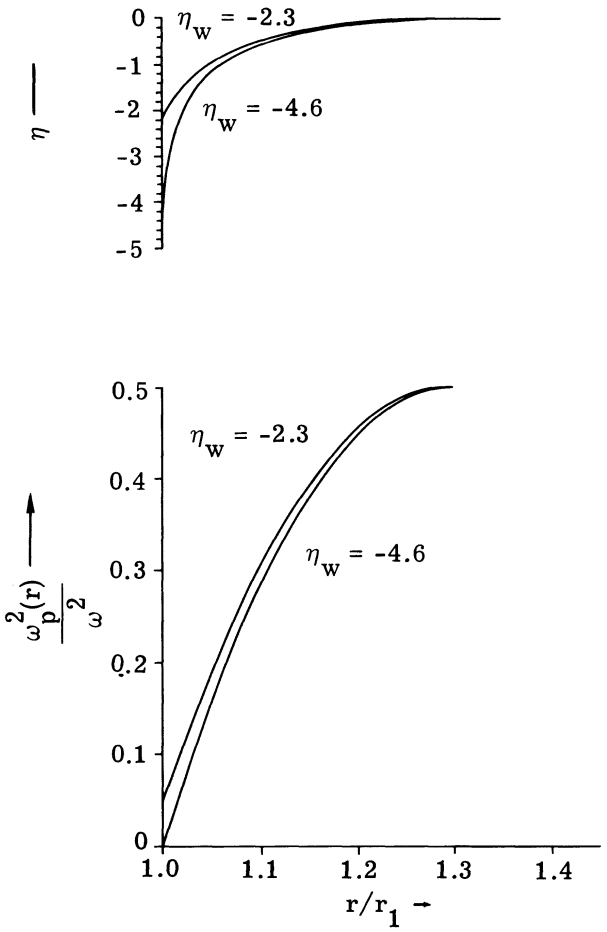

(a) Static electron density and potential profiles

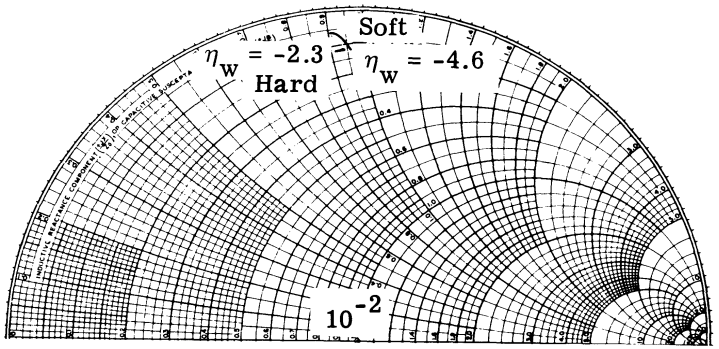

	Soft Boundary		Hard Boundary	
	G_t	B_t	G_t	B_t
-2.3	0.678	9.0*	1.223	9.25
-3.0	0.753	9.2*	1.179	9.33
-3.5	0.739	9.5*	1.166	9.37
-4.6	1.12	9.57	1.143	9.40

*Estimated (within 0.1)

(b) Y_t

FIGURE 13. COMPARISON OF VARIOUS WALL POTENTIALS (WITH CONSTANT SHEATH THICKNESS). Sheath, plasma, and sphere parameters are given in table IX.

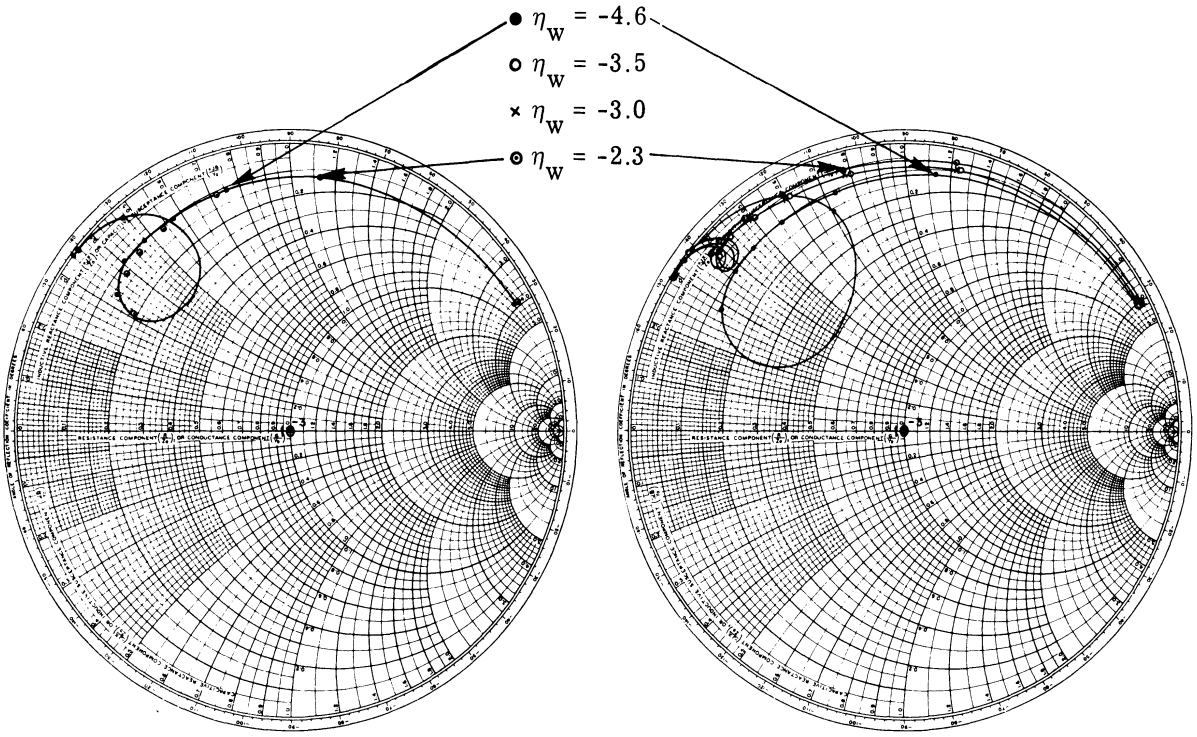

(a) Hard boundary

(b) Soft boundary

FIGURE 14. Y_n FOR VARIOUS WALL POTENTIALS (WITH CONSTANT SHEATH THICKNESS). Sheath, plasma, and sphere parameters are given in table IX.

6.3.4. EFFECT OF VARYING BOTH WALL POTENTIAL AND SHEATH THICKNESS. This section contains results obtained by varying both the wall potential and sheath thickness; in the preceding two sections each of these parameters was varied while the other was held constant. In order to illustrate a more realistic case, the thermal velocity was dropped by a factor of 10 from its previous value (from 0.03125c to 0.003125c). It is then necessary to drop the electromagnetic size of the sphere (from $k_0 r_1 = 0.5$ to 0.05) in order to keep the maximum order which needs to be calculated to a realistically small number. The results to be presented were obtained for a normalized plasma frequency of $\sqrt{0.833}$. This value was chosen to illustrate the point to be made here; the main influence of increasing the wall potential is to widen the sheath and thereby decrease the efficacy of the plasma in reducing the apparent size of the radiator. These other parameters are given in table X.

The range of assumed density and potential profiles that was considered is shown in figure 15; the values of sheath thickness, although smaller than the theoretical values, conform to the variations discussed in section 3. Because the chosen variation in sheath thickness was only approximate, the results can only be considered as qualitative. Nevertheless, the termi-

nating admittance results shown in figure 15b show several dominant and interesting features (that could be deduced from the separate results in sections 6.3.2 and 6.3.3). First, the susceptance markedly increases as the wall potential increases, much the same as was found for a constant wall potential when increasing the sheath thickness. Secondly, the results for the two assumed boundary conditions approach each other, which is similar to the results obtained for a constant sheath thickness when varying the wall potential, but not for the case of constant wall potential when varying the sheath thickness. Finally, there was a decidedly uniform behavior in the results for the hard boundary condition and a scattering of points for the soft boundary condition. This behavior was also noted in the modal plots which are not presented here. This is due to the somewhat arbitrary combinations of sheath thickness and wall potential that were chosen. It thus appears that the electric field strongly influences the generation of the EA waves. The hard boundary condition guarantees the existence of the EA wave and the terminating admittance is modified mainly by the increase in sheath size. However, the soft boundary condition leads to results that are more critically dependent on the details of the model and consistent results are obtained only in a general sense.

In conclusion, it is seen that in an experimental test of the influence of the EA wave, the effect of increasing the radiator potential would be mainly observed as an increasing input susceptance. Simultaneously, a decreasing conductance would be a good proof for the essential correctness of the hard boundary condition. The converse could not necessarily be interpreted as a verification of the correctness of the soft boundary condition; the radiation conductance in a cold plasma increases as the sheath size increases.

TABLE X. PARAMETERS FOR FIGURE 15

$\omega_p^2(r_2)/\omega^2 = 0.833,\ v_0/c = 1/320,\ k_0 r_1 = 0.05$

$\eta_w = -2.0, -3.5, -5.0, -7.0, -10.0$

$r_2/r_1 = 1.05, 1.08, 1.11, 1.15, 1.20$

$\omega_p^2(r_1)/\omega^2 = 8.33(-2), 2.5(-2), 5.7(-3), 7.5(-4), 3.8(-5)$

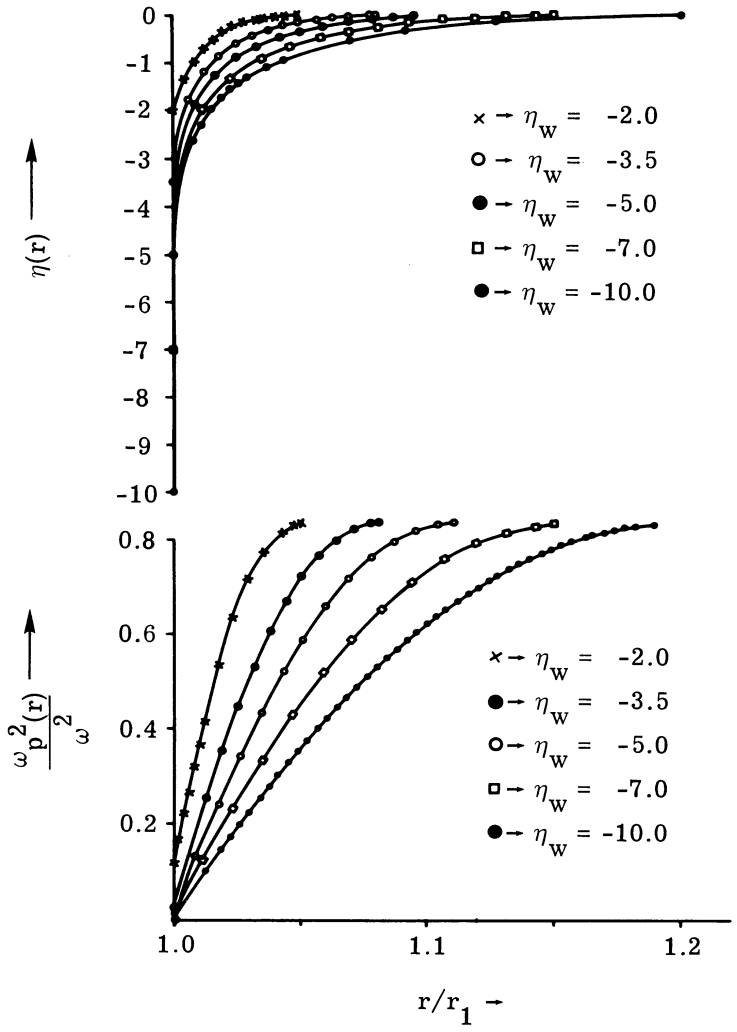

(a) Static electron density and potential profiles in the sheath

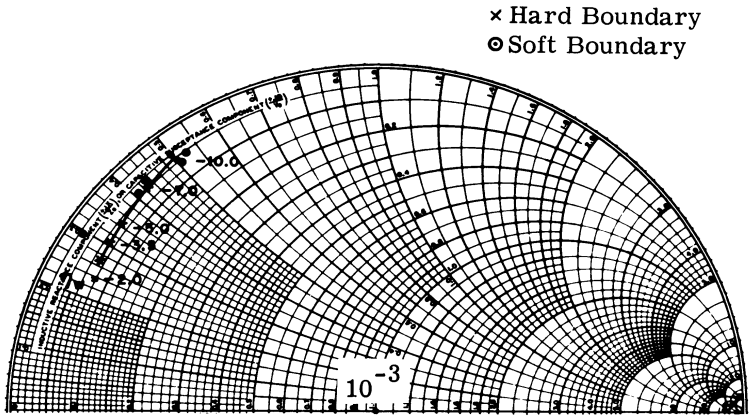

		Soft Boundary		Hard Boundary	
η_w	r_2/r_1	G_t	B_t	G_t	B_t
-2.0	1.05	0.0228	0.29*	0.0718	0.273
-3.5	1.08	0.0596	0.41*	0.0701	0.301
-5.0	1.10	0.0559	0.43*	0.0679	0.349
-7.0	1.15	0.0607	0.517	0.0637	0.432
-10.0	1.20	0.0573	0.518	0.0573	0.518

*Estimated (within .01)

(b) Y_t

FIGURE 15. COMPARISON OF VARIOUS WALL POTENTIALS (WITH VARIOUS SHEATH THICKNESSES). Sheath, plasma, and sphere parameters are given in table X.

6.4. EFFECT OF VARYING THE HOMOGENEOUS MEDIUM PARAMETERS

6.4.1. EFFECT OF VARYING ELECTRON DENSITY. In the typical solution of section 6.2, modal impedance results were discussed in the context of the homogeneous medium so that the separation into EA and EM components could be more readily displayed. Similarly, in the present section, the homogeneous medium result is discussed first because it gives an upper limit to the conductance values as well as an indication of the region of "interesting" plasma frequencies. Calculated modal and terminating admittances for this homogeneous medium case are presented in figure 16 as functions of plasma frequency; $v_0/c = 0.03125$ and $k_0 r_1 = 0.5$. The data for this figure are given in table XI. The loop in the terminating admittance plot is a direct result of the individual loops in the modal admittance plots. As the plasma frequency is increased, the dominant point (the thirteenth) moves counterclockwise on the modal admittance loop. A maximum conductance is thus exhibited for $\omega_p/\omega = 0.77\left(\omega^2/\omega_p^2 = 1.69\right)$.

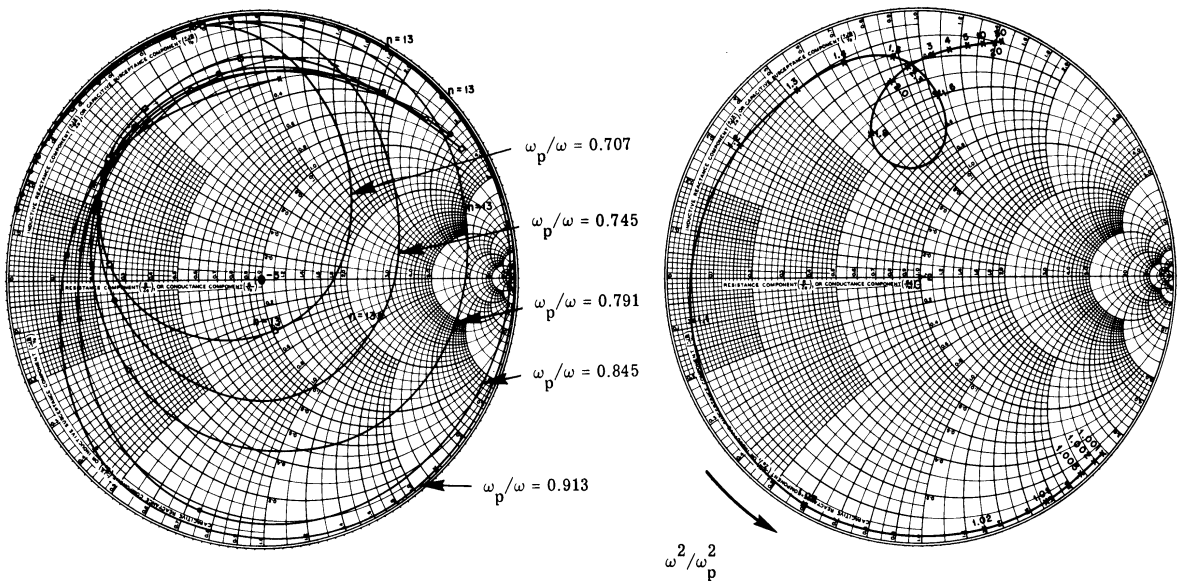

(a) Y_n (b) Y_t

FIGURE 16. Y_n AND Y_t FOR VARIOUS PLASMA FREQUENCIES (HOMOGENEOUS MEDIUM). Parameters: $v_0/c = 0.03125$, $k_0 r_1 = 0.5$, Y_t data given in table XI.

Returning to the inhomogeneous medium model, the modal plots for a range of different plasma frequencies and the two assumed boundary conditions are displayed in figure 17a and b. The parameters for these cases are given in table XII. The density and potential profiles associated with these cases, and the terminating admittances, are shown in figure 18a and b. The general similarity between the loops in the admittance results for the inhomogeneous and

TABLE XI. Y_t FOR VARIOUS PLASMA FREQUENCIES (HOMOGENEOUS MODEL); Parameters: $v_0/c = 0.03125$, $k_0 r_1 = 0.5$, Y_t data is plotted in figure 16b.

ω^2/ω_p^2	G_t	B_t
1.001	0.0251	-2.5181
1.002	0.0359	-2.3995
1.005	0.0598	-2.1398
1.01	0.0927	-1.7639
1.02	0.1477	-1.3043
1.05	0.2793	-0.5861
1.1	0.4574	-0.0969
1.2	0.7628	0.3110
1.3	1.0350	0.5292
1.4	1.2663	0.6043
1.5	1.6736	0.9257
1.6	3.8928	1.0859
1.8	3.9469	0.6299
2.0	2.5060	0.7633
2.3	2.0670	0.8926
3.0	1.9004	1.0467
4.0	1.7330	1.1420
5.0	1.5650	1.2312
10.0	1.2419	1.3167
20.0	1.0980	1.3860
50.0	1.0150	1.4234

homogeneous medium models is readily apparent. There is an increase in "modal" looping for the soft boundary results at the larger plasma frequencies resulting in a greater similarity between the hard and soft boundary conditions. This is also evident in the terminating admittance results shown in figure 18b. It is important to note again that the inhomogeneous medium leads to a smaller electroacoustic wave influence than does the homogeneous medium model. The existence of a terminating admittance loop is obviously important for diagnostics (both of electron density and temperature); further comment on this is deferred to the discussion of the effect of thermal velocity in section 6.4.2. However, the loop in the terminating admittance plot is again a consequence of the loop in the modal admittance plots. Physically, this means that a resonance occurs in which the electroacoustic wave "fits" the sphere optimally and maximum radiative transfer is able to take place. This is discussed further in section 6.4.2.

6.4.2. EFFECT OF VARYING THERMAL VELOCITY. Following the procedure used in section 6.4.1, the homogeneous medium case will be discussed first. This is especially important because of the complexity of the variation of each modal admittance value as the thermal velocity is changed. A different presentation of the modal admittance variation is given in

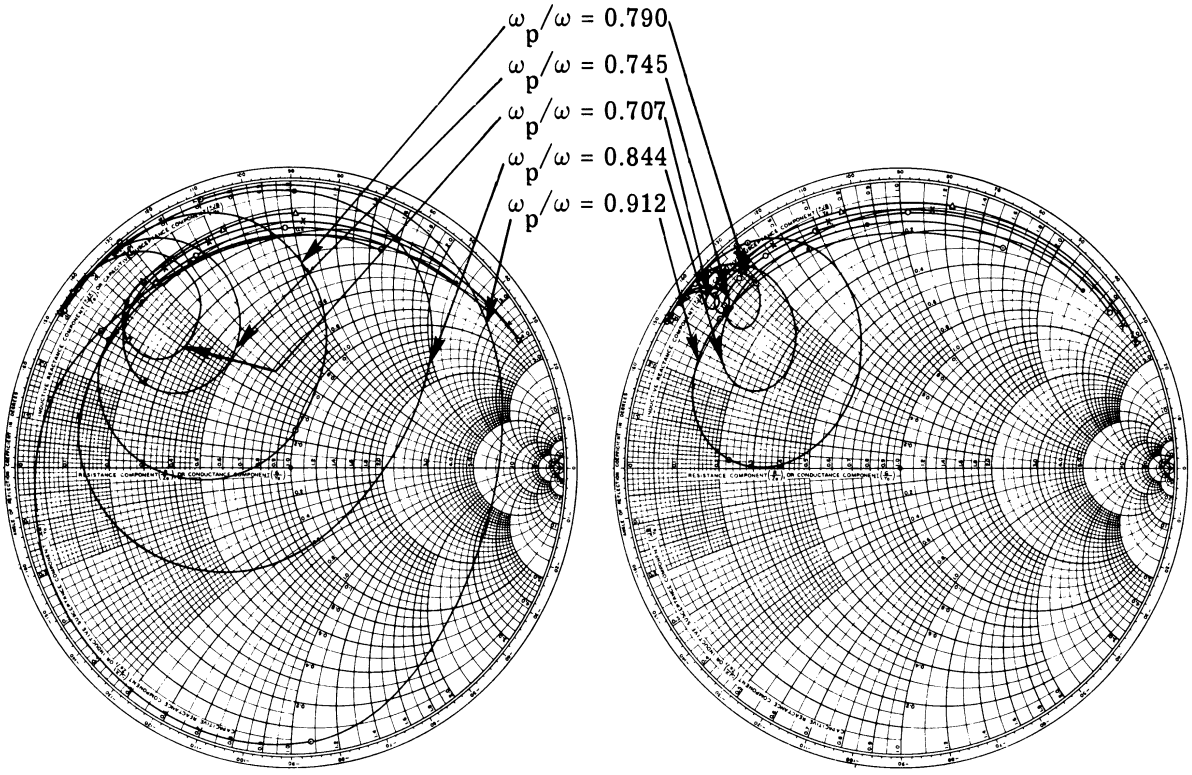

(a) Hard Boundary (b) Soft Boundary

FIGURE 17. Y_n FOR VARIOUS VALUES OF ω_p/ω. Sheath, plasma, and sphere parameters are given in table XII.

TABLE XII. PARAMETERS FOR FIGURES 17 and 18

$$\eta_w = -3.5,\ \omega_p^2(r_1)/\omega^2 = 0.015\ \omega_p^2(r_2)/\omega^2,\ k_0 r_1 = 0.50$$

$$\omega^2/\omega_p^2(r_2) = 1.2,\ 1.4,\ 1.6,\ 1.8,\ 2.0$$

$$\omega_p(r_2)/\omega = 0.912,\ 0.844,\ 0.790,\ 0.745,\ 0.707$$

$$r_2/r_1 = 1.228,\ 1.247,\ 1.264,\ 1.280,\ 1.295$$

figure 19a; in this plot (for $\omega_p/\omega = 0.707$ and $k_0 r_1 = 0.5$), each mode is shown on its own circular arc in the region where the mode has its maximum conductance value. With this modal admittance plot, it is apparent that the terminating admittance should be a very rapidly varying function of the thermal velocity; this terminating admittance variation is shown in figure 19b with the data given in table XIII. An alternative description of this rapid variation is given in figure 20 where the terminating conductance is plotted as a function of the thermal velocity. This rapidly varying plot (and Y_t in fig. 19b) was obtained from figure 19a by estimating the

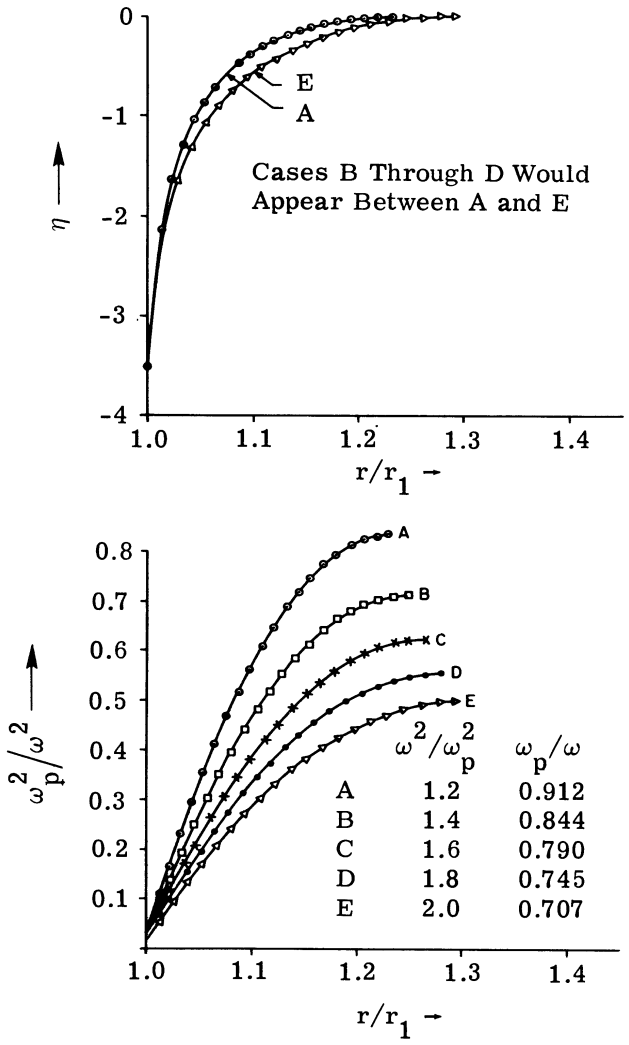

(a) Static electron density and potential profiles in the sheath

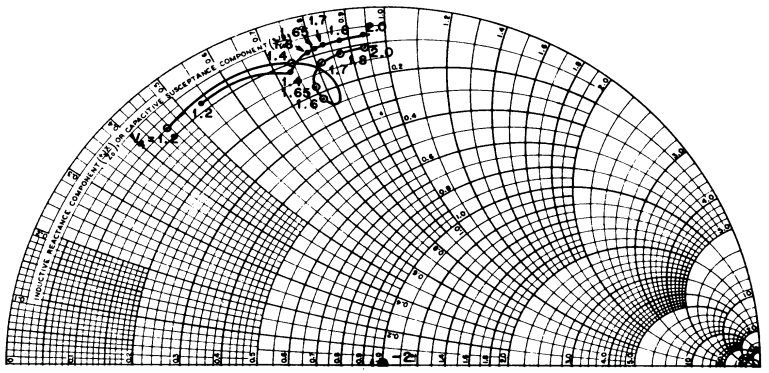

ω^2/ω_p^2	Soft Boundary		Hard Boundary	
	G_t	B_t	G_t	B_t
1.2	0.838	5.8*	0.790	4.55
1.4	1.039	7.5*	1.131	7.43
1.6	0.819	8.3*	2.132	7.74
1.8	0.787	8.9*	1.194	8.63
2.0	0.739	9.5*	1.166	9.37

*Estimated (within 0.1)

(b) Y_t (millimhos)

FIGURE 18. COMPARISON OF VARIOUS PLASMA FREQUENCIES. Sheath, plasma, and sphere parameters are given in table XII.

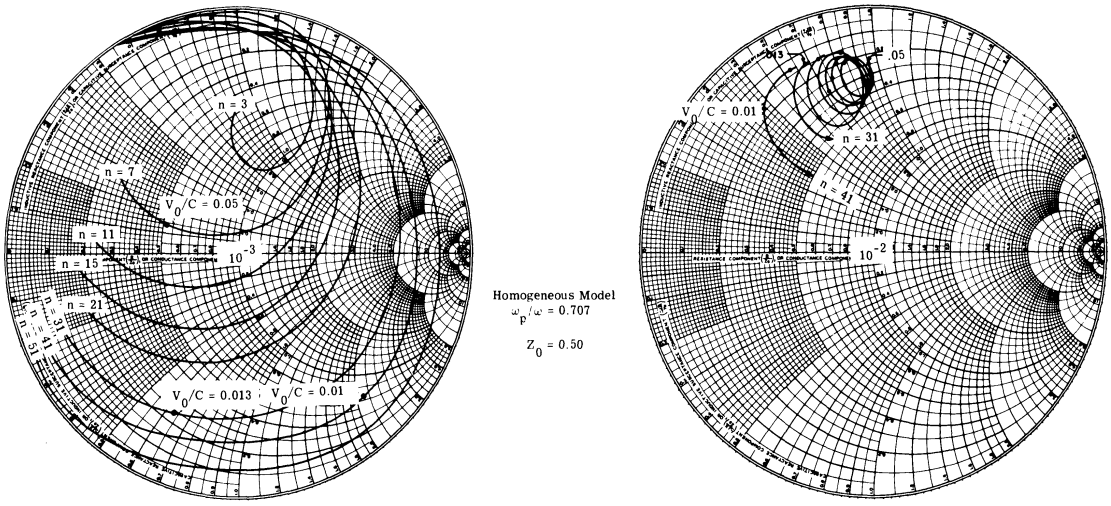

(a) Y_n (b) Y_t

FIGURE 19. Y_n AND Y_t FOR VARIOUS THERMAL VELOCITIES (HOMOGENEOUS MODEL). Parameters: $\omega_p/\omega = 0.707$, $k_0 r_1 = 0.5$, Y_t data given in table XIII.

TABLE XIII. Y_t DATA FOR VARIOUS THERMAL VELOCITIES (HOMOGENEOUS MODEL)
Parameters: $\omega_p/\omega = 0.707$, $k_0 r_1 = 0.707$. This data is plotted in figure 19b.

v_0/c	G_t	B_t
0.008	1.276	5.18
0.009	1.249	6.25
0.011	1.484	6.03
0.012	1.498	8.18
0.013	1.469	6.88
0.014	1.650	6.54
0.015	1.663	6.75
0.016	1.575	7.36
0.017	1.789	8.50
0.018	3.546	6.14
0.019	1.694	7.42
0.020	4.100	8.91
0.0225	2.262	9.01
0.025	3.123	9.23
0.0275	2.961	7.30
0.03	1.948	8.22
0.03125	2.506	7.83
0.0325	2.026	8.47
0.05	2.406	9.55
0.075	2.741	9.17

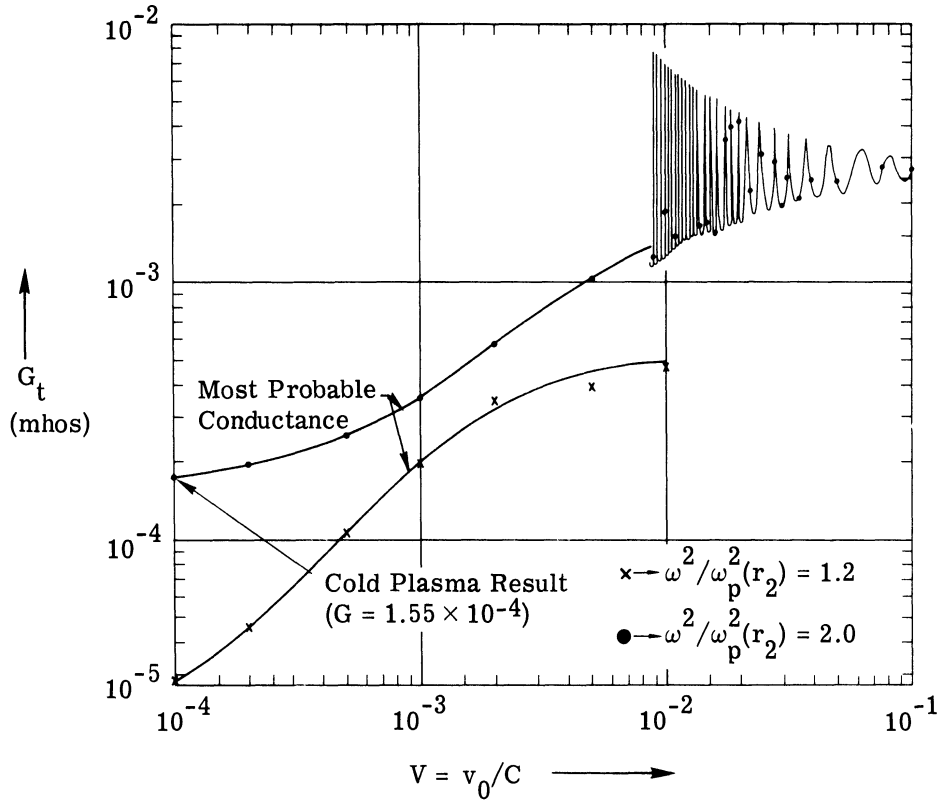

FIGURE 20. TERMINATING CONDUCTANCE FOR VARIOUS THERMAL VELOCITIES (HOMOGENEOUS MODEL). Parameters: ω_p/ω = 0.707, $k_0 r_1$ = 0.5, G_t data given in table XIII.

thermal velocity at which a particular modal admittance would make its maximum contribution. By using an estimated maximum contribution, this approximate curve could be deduced from the limited amount of data available. The data for the modal admittances show which mode is contributing most heavily to the terminating admittance. As an example, it is found (see fig. 19a) that when v_0/c = 0.01 it is the 41st mode which is contributing while the 39th and 43rd have conductances less than 1/10 as large. This resonance does not occur when the angular periodicity of the fields corresponds to the electroacoustic wavelength. For v_0/c = 0.01, with the parameters given in figure 19, the circumference in plasma wavelengths is

$$k_p a = \sqrt{1 - 1/2}\ 0.5 \cdot 100 = 35.35$$

For the order n = 35, it is found that the electroacoustic resistance (not conductance) is a maximum. Because of the EM modal capacitance, however, the total conductance maximizes when the EM and EA reactive contributions cancel; in this case for n = 41. Because only odd integers are involved in the summation, the conductance curve takes on this rapidly varying shape as first one, and then another of the modes, assumes importance.

Because of the large amount of time required to calculate the inhomogeneous medium results, it is not practical to investigate the large number of cases shown for the homogeneous medium. As an alternative, table XIV and figure 21 give Y_n values for three inhomogeneous medium cases, that were calculated for thermal velocities of $v_0/e = 0.030$, 0.03125, and 0.0325 and the other parameters given in table XIV. Points on the modal loops are rotated counterclockwise on the Smith Chart as for the homogeneous medium cases (and the loop becomes somewhat larger) as the thermal velocity decreases. The plot of the terminating admittances would show, for both assumed boundary conditions, a small portion of a loop. From figures 19-21 it is apparent that an experimental study of the location and behavior of these admittance loops must include an accurate knowledge of the electron temperature.

TABLE XIV. MODAL ADMITTANCES FOR VARIOUS THERMAL VELOCITIES, INHOMOGENEOUS MEDIUM

Parameters: $\omega_p^2(r_2)/\omega^2 = 0.50$ $\quad v_0/c = 0.03, 0.03125, 0.0325$

$\eta_w = -3.5, \quad k_0 r_1 = 0.50 \quad r_2/r_1 = 1.283, 1.295, 1.306$

Soft Boundary

	$v_0/c = 0.03$		$v_0/c = 0.03125$		$v_0/c = 0.0325$	
n	G_n	B_n	G_n	B_n	G_n	B_n
1	0.3892	3.988	0.3985	4.066	0.4079	4.023
3	0.0875	1.212	0.0904	1.222	0.0933	1.231
5	0.0666	0.784	0.0684	0.791	0.0700	0.798
7	0.0538	0.597	0.0548	0.603	0.0556	0.608
9	0.0441	0.489	0.0447	0.493	0.0452	0.497
11	0.0381	0.416	0.0392	0.420	0.0406	0.424
13	0.0404	0.370	0.0409	0.381	0.0343	0.394
15	7.4(-3)	0.345	2.6(-3)	0.339	9.2(-4)	0.336
17	1.1(-4)	0.293	3.5(-5)	0.292	1.1(-5)	0.292

Hard Boundary

	$v_0/c = 0.03$		$v_0 = 0.03125$		$v_0/c = 0.0325$	
n	G_n	B_n	G_n	B_n	G_n	B_n
1	0.4095	3.850	0.4213	3.863	0.4331	3.875
3	0.1232	1.153	0.1289	1.160	0.1346	1.168
5	0.1113	0.738	0.1163	0.744	0.1212	0.750
7	0.1063	0.562	0.1108	0.568	0.1151	0.573
9	0.1018	0.464	0.1057	0.469	0.1096	0.474
11	0.0979	0.396	0.1028	0.399	0.1092	0.402
13	0.1155	0.331	0.1461	0.330	0.2046	0.349
15	0.1507	0.550	0.0296	0.448	7.2(-3)	0.441
17	6.6(-4)	0.361	1.8(-4)	0.350	5.2(-5)	0.342

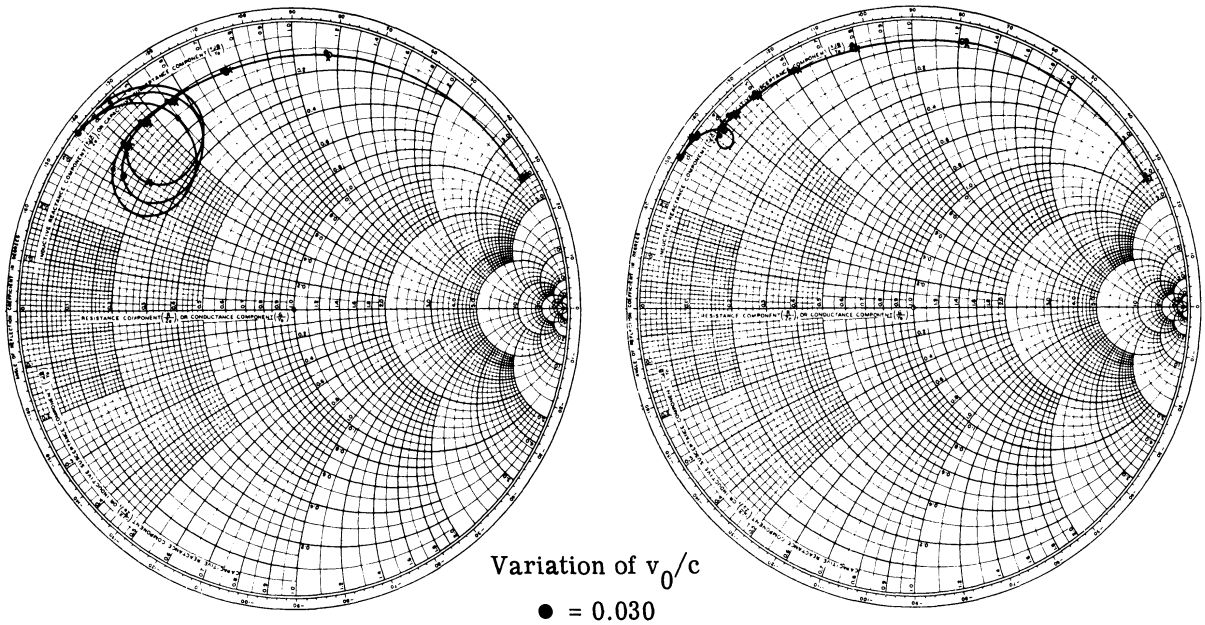

FIGURE 21. MODAL ADMITTANCE FOR VARIOUS THERMAL VELOCITIES (INHOMOGENEOUS MEDIUM). Sheath, plasma, and sphere parameters and Y_n data are given in table XIV.

The conclusion to be reached here is that the thermal velocity is a very important parameter. In all of the data reported above, the gap angle would only slightly effect the terminating conductance. For smaller v_0/c, the terminating conductance is affected by the gap angle and the looping features illustrated above would not occur. This is discussed in section 7.2 and appendix IV.

6.4.3. INFLUENCE OF RADIATOR SIZE. A good deal of data was obtained with different radiator sizes, especially for the homogeneous medium model. This homogeneous medium data need not be presented here, since the results are largely contained in the work of Wait [18] and are not of a fundamentally new or illuminating nature. As would be expected, the conductances and susceptances both decrease (as $k_0 r_1$) as the radiator is made smaller. For the first mode alone, the results follow those expected of the EM wave, but for all higher modes, the results are dominated by the EA contribution. In the location of points on the modal admittance plots, however, the dominant parameter is not $k_0 r_1$ or even $z_1 = k_0 r_1 \sqrt{1 - \frac{\omega_p^2}{\omega^2}}$, but rather $z_2 = k_0 \frac{c}{v} r_1 \sqrt{1 - \frac{\omega_p^2}{\omega^2}}$. Since variations of z_2 with v_0/c and ω_p^2/ω^2 have been demonstrated in sections 6.4.1 and 6.4.2, there is little need to indicate the type of variation found with $k_0 r_1$.

Similar EM and EA effects were indicated in the inhomogeneous medium results. The data obtained in section 6.3.4 is a good example of this, where the free space radiator size and thermal velocity were dropped by a factor of 10 in order to retain accuracy. The only notable modification in the results was in the reduction of the modal admittance values by a factor of ten (almost exactly).

6.5. INFLUENCE OF BOUNDARY CONDITIONS

The only variable remaining to be discussed is the boundary condition at the radiator. Throughout the preceding presentation, only results for the hard and soft conditions have been shown. When the electron density near the radiator is small, it has been shown that these two conditions predict nearly identical input admittances. However, for larger electron densities near the wall (lower wall potentials), the soft boundary condition leads to an appreciably smaller input conductance.

An alternative formulation of the boundary condition suggested by Cohen [14] was discussed in section 4; that is, at the radiator

$$T_4 = Y_A T_1 + Y_B Y_2$$

It was shown in section 4 that Y_A and Y_B are real, negative numbers and that a possible choice is

$$Y_A = -\frac{n(n+1)}{1 - \frac{\omega_p^2}{\omega^2}}$$

$$Y_B = -\frac{1}{1 - \frac{\omega_p^2}{\omega^2}}$$

The terminology "bilinear admittance condition" to describe the relationship defined above is especially appropriate since the modal admittances defined by (169) can be put in the form (using (131))

$$Y_n = +j \frac{2\pi\omega\epsilon_0 r_1}{N_n}\left[P_n^1(0)\right]^2 \frac{C_{32} + Y_B C_{34}}{C_{12} + Y_B C_{14} + Y_A C_{42}}$$

This can be written in the well known "bilinear transformation" form

$$w = (az + b)/(cz + d)$$

where z takes on the value Y_A or Y_B (depending on which is being varied) and a, b, c, d define

the transformation in terms of the calculated quantities C_{ab}. In either case, it can be shown that a variation along the real axis (real Y_A or Y_B) in the z-domain leads to a circle in the admittance or w-domain. For the case where z is purely real, the radius of the circle is given by [46]

$$R_q = |(ad - bc/2Im(\bar{c}d)|$$

and the center by

$$W_q = i(a\bar{d} - b\bar{c})/2Im(\bar{c}d)$$

The purpose of this section is to illustrate an example of the type of circular domains that are obtained as shown in figure 22a for the order n = 1. This data was obtained for arbitrary values of Y_A and Y_B as well as the "calculated value" of Y_A and Y_B given above. The model parameters are given in table XV. The center and radius for the case $Y_A = 0.1$ were also calculated, using the above equations, and agreed with values obtained from figure 22a. For this order the circles for various values of Y_A are well separated; for larger orders they were virtually indistinguishable.

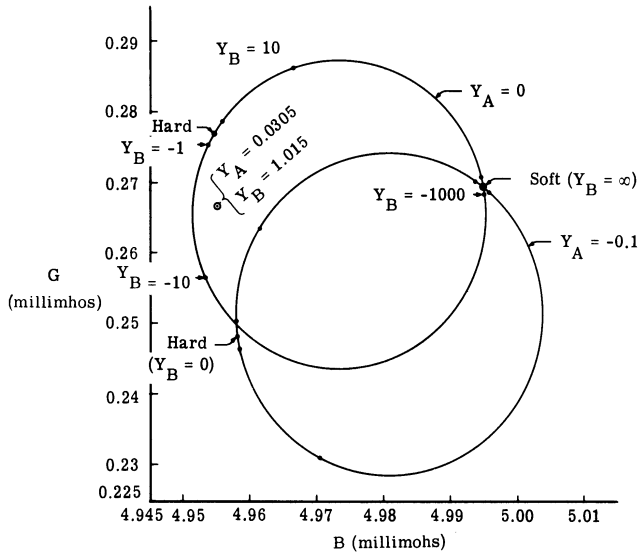

(a) Detail for n = 1

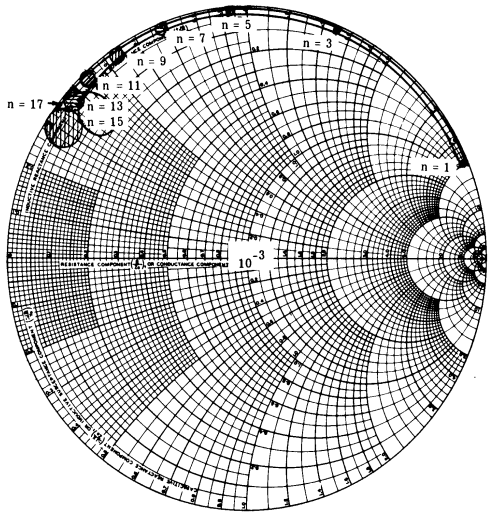

(b) Smith chart representation

FIGURE 22. MODAL ADMITTANCES FOR VARIOUS BOUNDARY CONDITIONS (INHOMOGENEOUS MEDIUM). Sheath, plasma, and sphere parameters and Y_n data are given in table XV.

TABLE XV. MODAL ADMITTANCES FOR VARIOUS BOUNDARY CONDITIONS, INHOMOGENEOUS MEDIUM

Parameters: $r_2/r_1 = 1.884$, $\omega_p^2(r_2)/\omega^2 = 0.5$, $\eta_w = -3.5$

$\omega_p^2(r_1)/\omega^2 = 0.015$, $v_0/c = 0.03125$, $k_0 r_1 = 0.5$

	Soft Boundary			Hard Boundary				Calculated Y_A, ($Y_B = -1.0152$)		
n	G_n	B_n	ΔB_n	G_n	B_n	ΔB_n	Y_A	G_n	B_n	ΔB_n
1	0.26980	4.9946	1.2554	0.27698	4.9544	1.2956	-0.03046	0.26638	4.9550	1.2950
3	0.00867	1.5221	0.3009	0.02113	1.4992	0.3237	-0.18273	0.01445	1.4984	0.3245
5	0.00759	0.9482	0.1260	0.02371	0.9267	0.1475	-0.45683	0.01703	0.9257	0.1485
7	0.00679	0.6937	0.0692	0.02726	0.6732	0.0897	-0.8528	0.02035	0.6719	0.0911
9	0.00596	0.5484	0.0435	0.3191	0.5295	0.0624	-1.3705	0.02459	0.5277	0.0642
11	0.00505	0.4543	0.0294	0.03816	0.4383	0.0454	-2.0101	0.03024	0.4356	0.0481
13	0.00395	0.3883	0.0206	0.04847	0.3782	0.0308	-2.7715	0.03948	0.3740	0.0350
15	0.00226	0.3394	0.0148	0.06696	0.3563	-0.0021	-3.6547	0.05752	0.3468	0.0075
17	0.00027	0.3004	0.0121	0.00741	0.3502	-0.0378	-4.6597	0.00666	0.3403	-0.0278
19	1.4(-6)	0.2687	0.0107	1.6(-5)	0.2922	-0.0127	-5.7865	1.0(-5)	0.2857	-0.0062
21	9.9(-8)	0.2435	0.0094	4.7(-7)	0.2596	-0.0067	-7.0352	5.9(-7)	0.2544	-0.0016

The radii of the circles for larger orders can be deduced from the Smith Chart plot (for $Y_A = 0$) as shown in figure 22b and given in table XV; their relative size (but not shape) is distorted in this presentation. The eight circles shown ($n \leqq 15$) are of similar size but increase for values of n greater than fifteen. However, for these large circles, the points for the hard and soft boundary cases fall very close together and near the free-space values. Thus, for all practical purposes, the boundary conditions do not seem to be influential upon orders $n >> k_p r_1$.

It has thus been shown in this section that the assumed boundary condition is an important factor in determining the modal, and therefore the terminating, admittance values. No unequivocal choice of boundary condition has been demonstrated and the only possible conclusion is that this remains an important area for future work.

6.6. SUMMARY OF TERMINATING ADMITTANCE RESULTS

In the preceding sections, admittance calculations were presented as a function of each of the parameters of the analysis. From these calculations, the following conclusions can be drawn about the influence of each parameter:

(1) The particular form of electron density (sec. 6.3.1): a measurable but not dominant factor.

(2) Sheath thickness (sec. 6.3.2): very important in its influence on susceptance, somewhat less so for conductance.

(3) Wall potential (sec. 6.3.3 and 6.3.4): when only the wall potential was varied, the differences were not too important, especially for low potentials. It was even found in section 6.3.1

that ignoring the electric field altogether (but not the density gradient) led to modal admittances that were markedly different only for orders near $k_p r_1$. When the wall potential and sheath size were varied together, as would occur in an experiment, the dominant effect was on the input susceptance which could be attributed to the change in sheath size alone. It is also important to note that, for large negative wall potentials, the hard and soft boundary assumptions led to essentially identical terminating admittances.

(4) Electron density in the homogeneous region (sec. 6.4.1): a critical density (or plasma frequency) exists for which the terminating conductance is a maximum: otherwise the effect is largely the usual alteration of the electrical size of the sphere. However, depending on the boundary assumption and other parameters, a loop may be predicted on the Smith Chart plot as the external (homogeneous) medium electron density is varied. It was also noted, reminiscent of the multiple resonance phenomenon, that the susceptance goes to zero at a normalized plasma frequency less than unity.

(5) Thermal velocity (sec. 6.4.2): a very important parameter, having an influence on both susceptance and conductance. For "high" thermal velocities, rapid looping is found on a Smith Chart plot as the thermal velocity is varied slightly. With "low" thermal velocities, the influence of the EA wave is much diminished. The criterion for high and low is that the terminating admittance will not be damped because of the decay of the higher orders due to the finite width of the gap. That is, the influential orders are for $n \sim k_p r_1$, but these orders may not be influential for wide gaps as shown in figure 3.

(6) Radiator size (sec. 6.4.2): does not have any appreciable effect on the forms of the results other than that to be observed for the electromagnetic mode alone and the gap condition discussed above. The important parameter is the ratio of the size of the radiator in EA wavelengths to the size in EM wavelengths, which is to say that the thermal velocity is most important.

(7) Assumed boundary condition (sec. 6.5 and throughout): a very important difference is generally noted between the results for different assumed radiator conditions (hard and soft). The results for the two conditions used become more similar for larger wall potentials (or with the assumption of thinner sheaths). However, the influence of the EA wave is always calculable, even for the least influential boundary conditions, as long as the electron thermal velocity is high.

7
SPATIAL VARIATIONS

7.1. INTRODUCTION

The results of the input admittance computations contained in the preceding section answered the basic question posed at the beginning of this study:

What is the influence of a finite electron temperature on the terminating admittance of a plasma-imbedded spherical dipole?

The presentation of conclusions based on these results is deferred to the next section. A further insight into the character of the EA wave and its influence on input admittance can be obtained from a brief presentation of the angular and radial field variations near the sphere. These field variations need not be calculated to obtain the input admittance, but are found by a straightforward extension of the techniques presented in the last section.

It is shown in appendix V that the influence of EA waves on input admittance is quite apt to be masked by the influence of collision frequencies, so that the use of some other phenomena is indicated if excitation of the EA wave is to be unequivocally detected. However, since diagnostics is not the major concern of this study, more attention will be devoted to understanding how these fields affect the input admittance and only secondarily with the possible detection of the EA wave.

7.2. ANGULAR VARIATION OF SURFACE FIELDS

The technique for calculating the field magnitudes at the radiator were given in section 4. The total surface fields (including the angular variation) can thus be obtained from (15); the variables T_{5n} and T_{6n} can be obtained from (18) or (19). When the plasma is assumed homogeneous, the fields can be specified directly, as has been done in section 2.4, with the constants obtained in section 4.4. In all models, the variable T_{3n} (proportional to tangential electric field) is specified as being zero everywhere but at the gap. In general, the variable T_{4n} at the radiator can be specified as

$$T_{4n}(r_1) = Y_A T_{1n}(r_1) + Y_B T_{2n}(r_1)$$

Elastic reflection ($T_{4n}(r_1) = 0$) is obtained by using $Y_A = Y_B = 0$; zero perturbed electron density ($T_{4n}(r_1) = 0$) can be obtained by assuming $Y_A = 0$, $Y_B = \infty$. Thus, each of the variables $T_{jn}(r_1)$ are readily obtainable, and the total surface fields, as a function of angle, are repeated for convenience from (15) as (replacing the suppressed subscript, i.e., $T_{jn}(r_1) = T_j(r_1)$)

$$H_\phi(r_1, \theta) = \sum_n{}' T_{1n}(r_1) P_n^1(\cos\theta) = S_1(r_1, \theta) \tag{178}$$

$$\frac{v_0^2}{i\omega}\rho(r_1, \theta) = \sum_n{}' T_{2n}(r_1) P_n(\cos\theta) = S_2(r_1, \theta)$$

$$i\omega\epsilon_0 r_1 E_\theta(r_1, \theta) = \sum_n{}' T_{3n}(r_1) P_n^1(\cos\theta) = S_3(r_1, \theta) \qquad \text{(equation continued)}$$

$$\rho_0 r v_r(r_1, \theta) = \sum_n{}' T_{4n}(r_1) P_n(\cos\theta) = S_4(r_1, \theta)$$

$$\rho_0 r v_\theta(r_1, \theta) = \sum_n{}' T_{5n}(r_1) P_n^1(\cos\theta) = S_5(r_1, \theta)$$

$$i\omega\epsilon_0 r_1 E_r(r_1, \theta) = \sum_n{}' T_{6n}(r_1) P_n(\cos\theta) = S_6(r_1, \theta)$$

The only complication in performing these computations arises because of the large number of terms needed to specify the tangential electric field. Fortunately this problem exists only at the gap; a smaller number of terms suffices to specify the field at other angles. Because tables of the Legendre functions are available only for $n < 50$ and for angles that are multiples of 2.5 degrees, the summations given above were performed on the digital computer. The Legendre functions were obtained by using standard recursion formulas (appendix I) with double precision techniques. Agreement with published tables was excellent. The homogeneous medium computer analysis was modified to obtain the angular variation directly. A smaller number of terms was used with the inhomogeneous medium model, because of the excessive computer time required for the calculations.

The results for the homogeneous medium model with a hard boundary are shown in figures 23-26, for $k_0 r_1 = 0.5$, $\omega_p/\omega = 1/\sqrt{2}$ and $\frac{v_0}{c} = 1/32$. In each case, N_{max} was taken as ninety-nine, so that fifty terms were used in equations 178. The fields were calculated at five degree intervals for θ between zero and eighty degrees and at one degree intervals from eighty-one to ninety degrees. The equations used to obtain these results are (67) through (72) for the homogeneous plasma model. To facilitate comparison with the terminating admittances results given in section 6, "admittance" units are used in plotting. These admittance units are denoted with a prime.

The conversion factor is obtained from equation 169 as

$$2\pi\omega\epsilon_0 r_1 = 2\pi \cdot \frac{\omega\sqrt{\mu_0\epsilon_0 r_1}}{\sqrt{\frac{\mu_0}{\epsilon_0}}} = \frac{2\pi \cdot k_0 r_1}{120\pi}$$

For $k_0 r_1 = 0.5$, we then have

$$S_j' = S_j/120$$

Figure 23 shows the real and imaginary parts of the four, non-zero, surface fields, S_1, S_2, S_5, S_6, for a four degree gap. The first point of interest is that the fields S_1 (magnetic

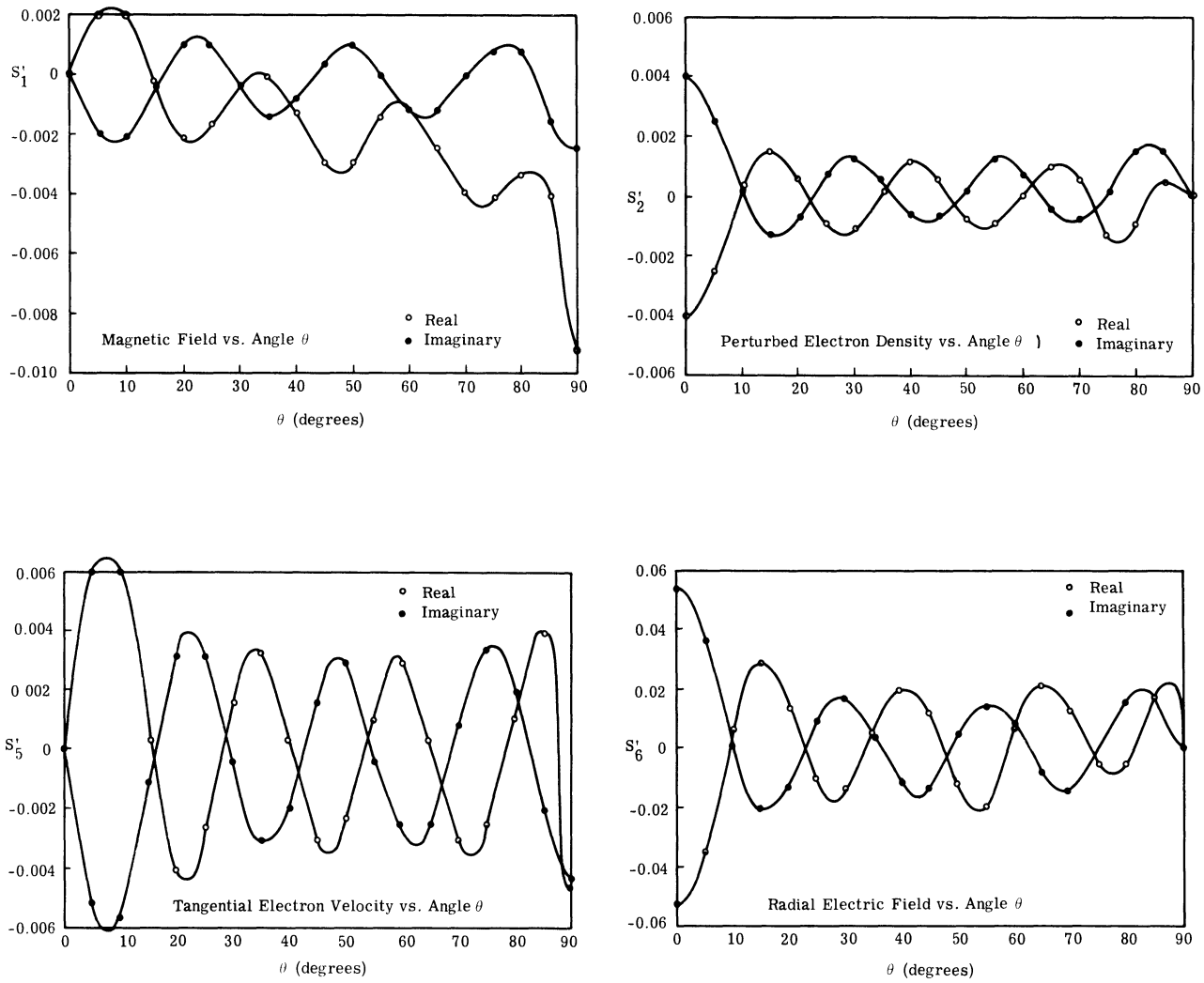

FIGURE 23. NORMALIZED REAL AND IMAGINARY COMPONENTS OF THE NON-ZERO SURFACE FIELDS (HOMOGENEOUS MEDIUM, HARD BOUNDARY). Parameters: $\omega_p^2/\omega^2 = 0.5$, $v_0/c = 0.03125$, $k_0 r_1 = 0.5$.

field) and S_5 (tangential velocity) are zero at the poles and maximum at the gap center, whereas the variables S_2 (perturbed density) and S_6 (radial electric field) have opposite characteristics: zero at the gap center and maximum at the poles. Secondly, there is a marked phase difference between pole and gap for each variable; S_1 and S_5 have a phase angle of -45^o at the poles but an angle near -160^o at the gap; S_2 and S_4 have a phase angle of -225^o at the poles but near -315^o ($+45^o$) at the gap. This shift of -90^o is especially apparent in the rapid variation of the real components of S_5 and S_6 near the gap. Thirdly, the rapidly varying fields seem to have an appreciable magnitude as might be expected with this unrealistic homogeneous medium model. The variable S_1 (related to magnetic field) is also, of course, related to the surface current (see equation 241). The real part of the variable S_1 (or the current) is not strongly influenced by the varying term near the gap. It is this quantity which is used to obtain the in-

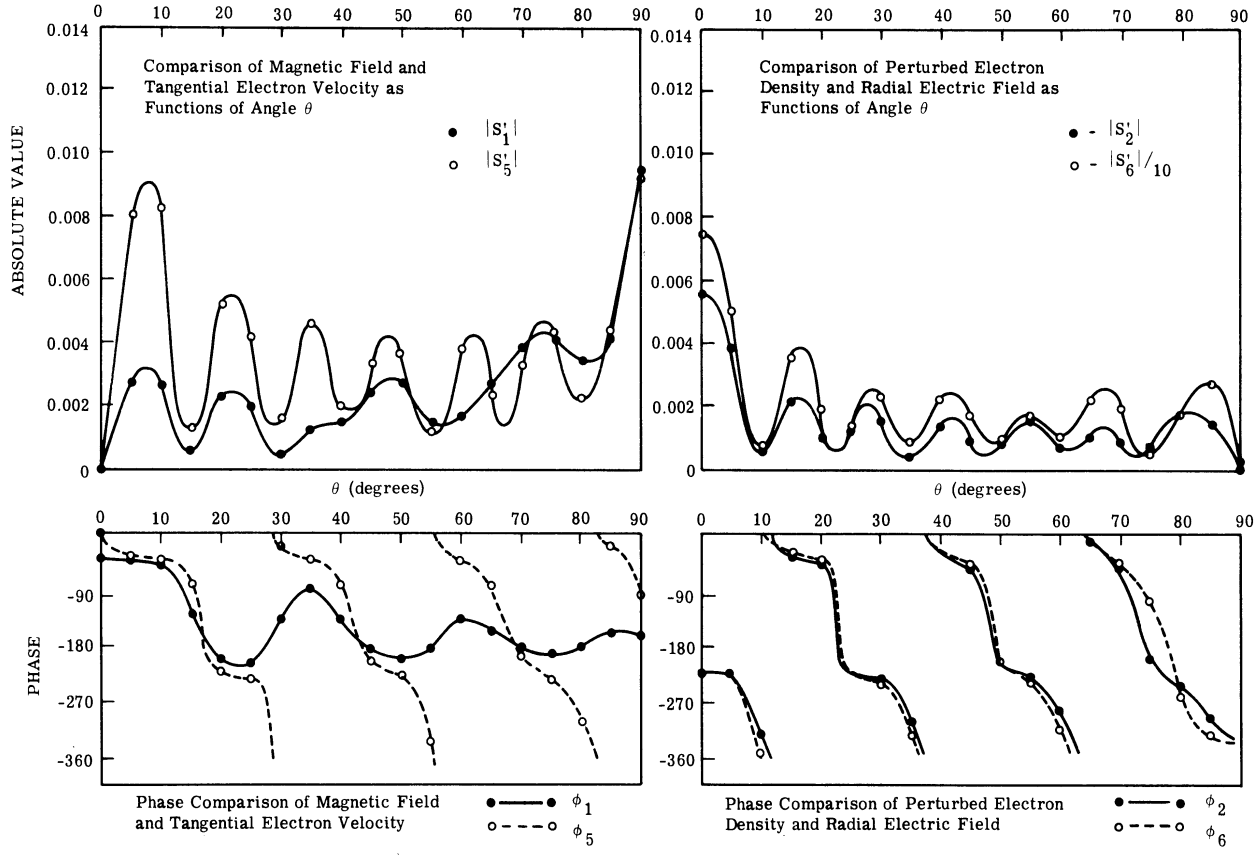

FIGURE 24. AMPLITUDE AND PHASE OF THE NORMALIZED NON-ZERO SURFACE FIELDS (HOMOGENEOUS MEDIUM, HARD BOUNDARY). Parameters: $\omega_p^2/\omega^2 = 0.5$, $v_0/c = 0.03125$, $k_0 r_1 = 0.5$.

put susceptance and which was previously noted to be only slightly influenced by the EA wave. The imaginary component of S_1 at the gap is, however, strongly affected in agreement with the result noted for the input conductance which is obtained from this quantity. It is obvious from these plots of angular variation that the looping on the Smith Chart discussed in section 6.2 results from changes in the "electroacoustic size" of the radiator. Thus, as ω_p/ω or v_0/c change, the radiation properties do not depend only on the EA wave "fitting" the sphere exactly. Rather, the EM capacitance must be cancelled by the EA inductance. Alternatively stated, the EA modal resistance is largest for n = 11 ($k_p a \approx 11.3$ in this case) but the overall modal conductance is largest for n = 13. The interaction of these angular variations is clearly seen in this and succeeding figures as a "beating" of the two strong harmonics.

Figure 24 displays the same information in a form in which the quantities might be measured: amplitude and phase. The magnetic field (S_1) and tangential velocity (S_5) are shown together to emphasize their similarities; the same reason groups the perturbed density (S_2) and the radial electric field (S_6). In all cases, there is a rapid change in amplitude of the oscillations near the poles, accompanied by a rapid change in phase. A similar amplitude and phase variation is seen on a long radiating transmission line such as a slotted waveguide.

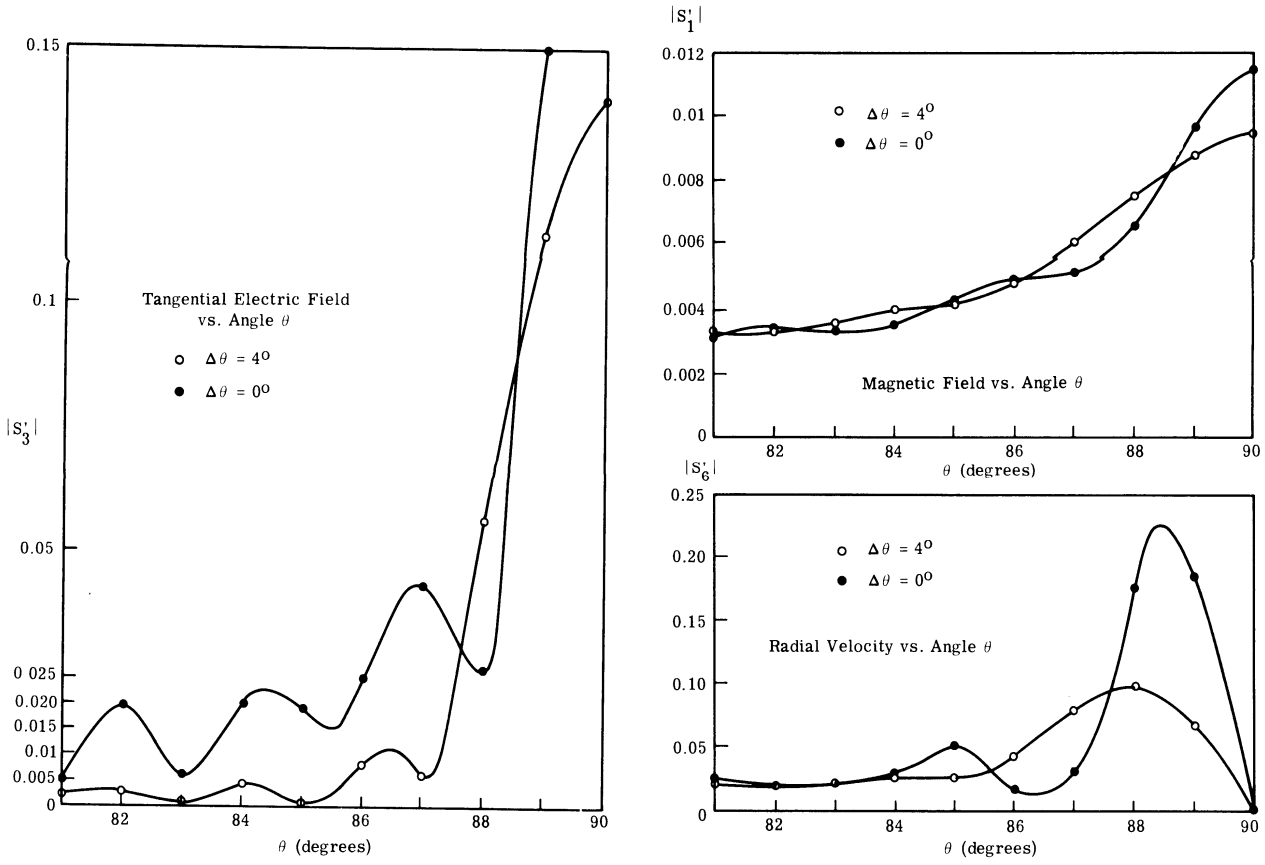

FIGURE 25. MAGNITUDE OF THE NORMALIZED TANGENTIAL ELECTRIC AND MAGNETIC FIELDS AND RADIAL VELOCITY FOR GAP ANGLES OF 4^{o} AND 0^{o} (HOMOGENEOUS MEDIUM). Parameters: $\omega_p^2/\omega^2 = 0.5$, $v_0/c = 0.0315$, $k_0 r_1 = 0.5$.

Figure 25 indicates the field variation for angles nearer to the gap by plotting the magnitudes of the normalized tangential electric field (S_3), the magnetic field (S_1), and the radial electric field (S_6) for assumed gap angles of zero degrees and four degrees. Because the imaginary components are always rapidly convergent for both gap angles, the differences in magnitudes reflect differences in the real component, which does not converge rapidly. However, it can be seen that for angles somewhat removed from the gap, the differences are not great. Although the series is only slowly convergent when the gap is assumed small, the first hundred terms offer a good approximation. In fact, it can be shown that a proper number of terms is on the order of $2/\Delta\theta$. The seriousness of excluding terms in the series for small gap angles is therefore not great (at least for the purposes of understanding the angular field variations).

Figure 26 presents the variation of the real and imaginary magnetic field (S_1) components for the sheath model (with both hard and soft boundary) as well as the homogeneous medium model (hard boundary) discussed above. As mentioned earlier, sufficient accuracy could not

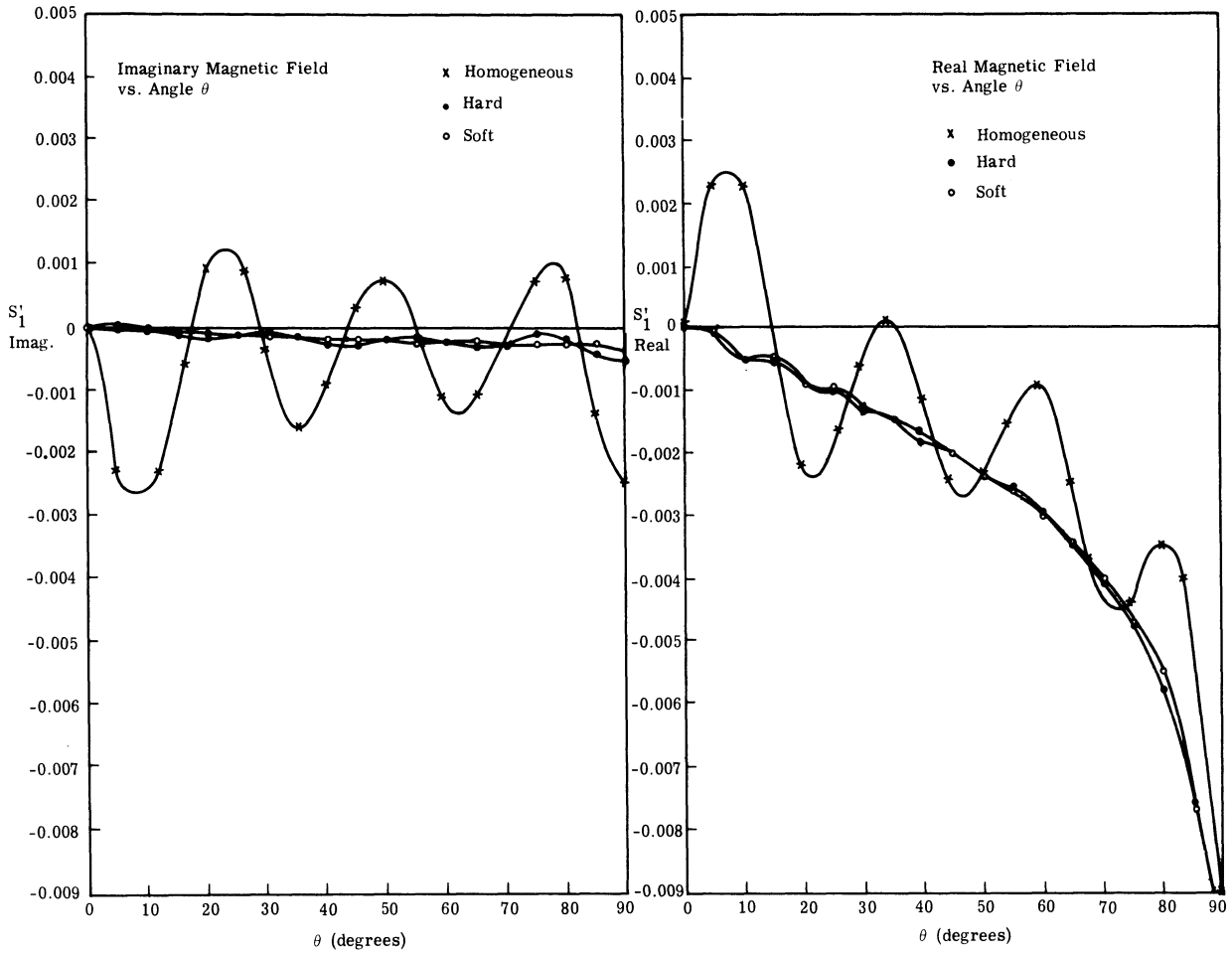

FIGURE 26. REAL AND IMAGINARY COMPONENTS OF NORMALIZED MAGNETIC FIELD VS. ANGLE θ (INHOMOGENEOUS MEDIUM). Parameters: Both models: $\omega_p^2(r_2)/\omega^2 = 0.5$, $v_0/c = 0.03125$, $k_0 r_1 = 0.5$. Sheath model: $\eta_w = 3.5$, $\omega_p^2(r_1)/\omega^2 = 0.015$, $r_2^1 r_1 = 1.884$.

readily be retained with the numerical integration procedures to warrant calculating the results for the large orders used in the homogeneous medium analysis. The surface field results of the inhomogeneous model were therefore computed using terms only up to $N_{max} = 35$. The case used for this comparison is shown in figure 2 and also in figure 12 as the thickest sheath model, $\left(\omega_p^2(r_2)/\omega^2 = 0.5\ ,\ v_0/c = 1/32,\ \eta_w = -3.5,\ r_2/r_1 = 1.884\right)$. Even though only a small number of terms were retained, the imaginary values were obtained with a high degree of accuracy because of their rapid convergence. Using the results described above for the homogeneous medium model allowed a rather accurate estimate of the proper convergent answer for the real component, especially for angles not too close to the poles or equator. It can be seen that the homogeneous medium and sheath models exhibit different magnitudes of EA amplitude variations. The phase variation is largely dictated by this imaginary component for

the inhomogeneous medium models since the real component is dominated by the non-oscillatory EM component. However, it is seen in figure 26 that near the pole ($\theta = 0^{o}$) the phase variation is considerably different for the two boundary conditions since the oscillatory, or EA, portion of the real component of the current, or magnetic field, differs for the two assumed boundary conditions. This observation might be useful as a technique for an experimental test of the assumed boundary conditions; several current probes (loops) or a moveable probe could be used near the poles to measure the angular phase variation if prior experimentation indicated the presence of even a small EA component.

A further comparison of results for the inhomogeneous medium model is shown in figure 27, where the absolute values of the fields S_1, S_2, S_5, and S_6 are compared with those for the homogeneous medium model. The major differences for each of these variables are:

(1) S_1 - magnetic field. The amplitude of the variations is much reduced for both boundary conditions with the inhomogeneous medium model. The larger amplitude of the field at $\theta = 90^{o}$ (near the gap) when the sheath is considered has been previously noted as a larger input susceptance corresponding to an "electrically larger" sphere. The hard and soft boundary conditions give virtually identical results.

(2) S_2 - perturbed electron density. For the soft boundary condition, this field is zero. For the hard boundary condition, the calculated values are also much smaller than for the homogeneous medium model; on the graph a scale change of ten was necessary to display both results. In addition, the amplitude of the variations is somewhat reduced relative to the mean value although for the inhomogeneous medium model the amplitude is found to be relatively larger near the gap.

(3) S_5 - tangential electron velocity. This is the variable for which the most striking differences between the three cases may be noted. The results for a cold plasma would be similar to those for the soft condition: zero everywhere except at the gap. For the hard boundary condition, a much smaller velocity is noted for the sheath model (with ripples of smaller amplitude) than with the homogeneous medium model.

(4) S_6 - radial electric field. This variable is much the same for all three cases. This fact indicates that a radial probe (used for detection of radial electric fields) would not be helpful in testing the validity of the boundary conditions. However, the large amplitude ripples in the radial electric field could be readily detected. This might prove most useful as a test of the presence of an EA wave, since these ripples would not exist in a cold plasma.

S_3 (tangential electric field) which should be zero except at the gap was also calculated with $N_{max} = 35$. It alternated in sign and was generally less than two percent as large as at the gap (see also fig. 25). S_4 (radial electron velocity) is only non-zero for the soft case. It was

found to be very small everywhere except near the poles where it had its largest calculated value of $|S_4| = 0.63 \times 10^{-3}$; it is therefore not shown.

In conclusion, it has been found that rapid angular variations of the fields is the dominant feature of EA wave excitation. Certain of the fields are more strongly affected than others by the two assumed boundary conditions. It also seems that EA wave excitation might best be tested with a moveable radial probe.

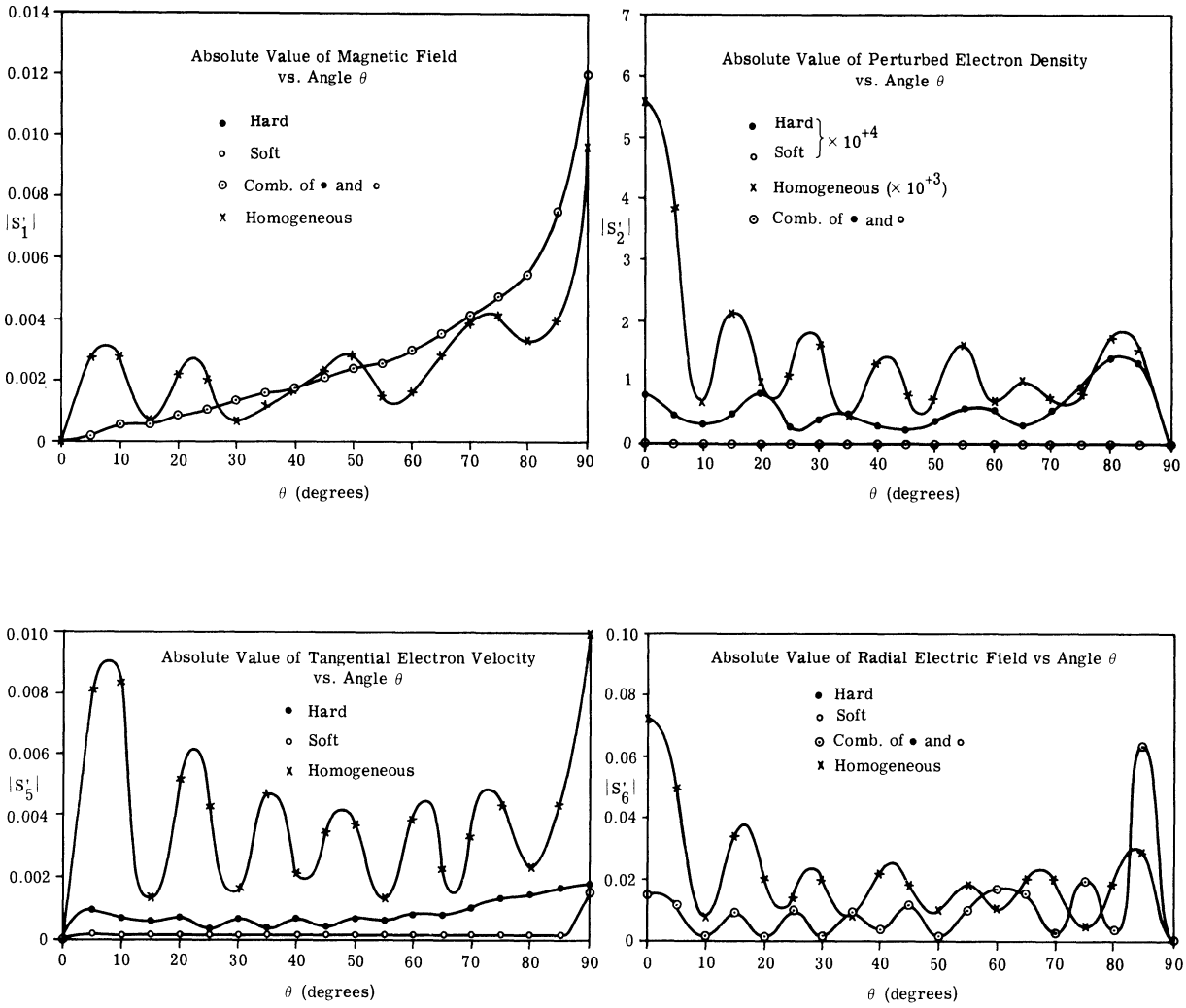

FIGURE 27. COMPARISON OF MAGNITUDE OF SURFACE FIELDS (INHOMOGENEOUS). Parameters: Both models: $\omega_p^2(r_2)/\omega^2 = 0.5$, $v_0/c = 0.03125$, $k_0 r_1 = 0.5$. Sheath model: $\eta_w = -3.5$, $\omega_p^2(r_1)/\omega^2 = 0.015$, $r_2/r_1 = 1.884$.

7.3. CALCULATION OF RADIAL VARIATIONS

Angular variations of the fields at the radiator were presented for a "typical" case in the preceding section 7.2. In this section for the same case, the radial variations are shown for $\theta = 0^o, 45^o, 90^o$. These are presented mainly to get an appreciation of the influence of inhomogeneities in exciting the EA wave and to compare the two assumed boundary conditions. However, there are a few features of the results that are to be presented that might also be useful for diagnostic purposes. The potential and density profiles are shown in figures 2 and 12.

The following results were obtained by numerically integrating the defining equations for each value of n, using the calculated initial conditions. An earlier example for only the mode n = 1 was shown in figure 5. In the present example, the total field was obtained by multiplying each of the calculated radial modal values by the appropriate Legendre function; as indicated in equation 178. As stated earlier, the real and imaginary contributions could be summed separately because of the normalization employed. The imaginary values could be accurately summed since they rapidly decrease for values of n greater than $z_2 = \frac{c}{v_0} k_0 r_2 \sqrt{1 - (\omega_p/\omega)^2}$. However, because of the small number of orders that could be summed, interpolation was necessary to obtain the plotted values of the real component, and the results are therefore accurate only to within several percent. Fortunately, the higher order modes also decay rapidly as the distance from the radiator increases, so that the accuracy of points near the outer sheath edge is reasonably good. Comparisons with figures 26 and 27 may be made by dividing by 120.

The results of these calculations are shown in figures 28 and 29. In each case, the six numbered points are separated by five equal logarithmic increments through the sheath. The separation of points for this case is $\frac{1}{5} \ell n \frac{r_2}{r_1} = 0.127$. So the six positions are $\frac{r}{r_1} = 1.0, 1.135, 1.289, 1.463, 1.660$, and 1.884. The 1st and 6th points refer respectively to the radiator and sheath edge. Both hard and soft assumed boundary conditions are shown in each case. Figure 28 shows the results at 0^o and 90^o; figure 29 shows only the variation of 45^o. The data at 0^o and 90^o is abbreviated because the EM (S_1 and S_3) and EA (S_2 and S_4) variables are respectively zero at these angles for all radii. An examination of the figures reveals these facts:

(1) At both 90^o and 45^o, the magnetic fields (S_1) for each boundary condition are virtually indistinguishable and therefore not suitable for diagnostics.

(2) The tangential electric fields (S_3) are quite similar at 90^o but are different at 45^o because of the slow rate of increase of the imaginary component near the radiator with the soft boundary condition. A probe such as a moveable, slender θ-directed dipole might be able to sense such a difference.

(3) The perturbed electron density at $\theta = 0^o$ is found to be much larger with the hard boundary condition than with the soft. However, at 45^o they are more nearly of equal size, even

though the soft condition demands that the perturbed density start at zero. This difference could only be used for diagnostics with a sensor for perturbed density; none seems to exist.

(4) The radial electron velocity at 0^{o} and 45^{o} exhibits much the same behavior as did the perturbed electron density. Even though the radial velocity vanishes at 0^{o} with the "hard" boundary condition, it rapidly grows and is in fact larger than that predicted with the soft boundary condition before progressing halfway through the sheath. The variations at 45^{o} display a greater similarity and would not seem to be distinguishable experimentally even were a velocity detector available.

In summary, these radial variation plots clearly indicate the excitation of the EA wave and even some hope for experimentally verifying the boundary conditions. They are presented, however, mainly to help in understanding the nature of the sheath mode conversion and the small effect previously found in the input admittance.

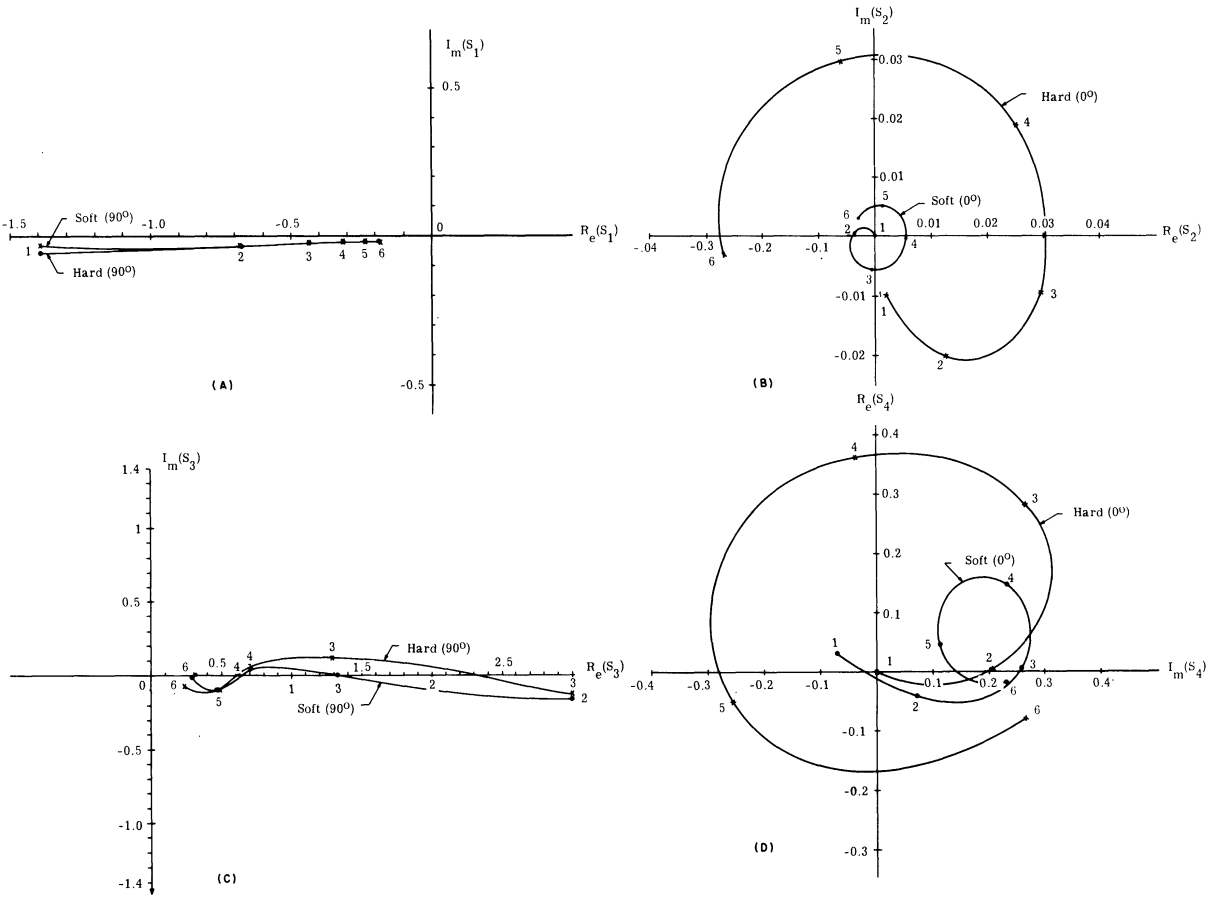

FIGURE 28. RADIAL VARIATIONS OF TOTAL FIELDS AT 0^{o} and 90^{o} (INHOMOGENEOUS MEDIUM). Parameters: $\omega_p^2(r_2)/\omega^2 = 0.5$, $v_0/c = 0.03125$, $\eta_w = -3.5$, $k_0 r_1 = 0.5$.

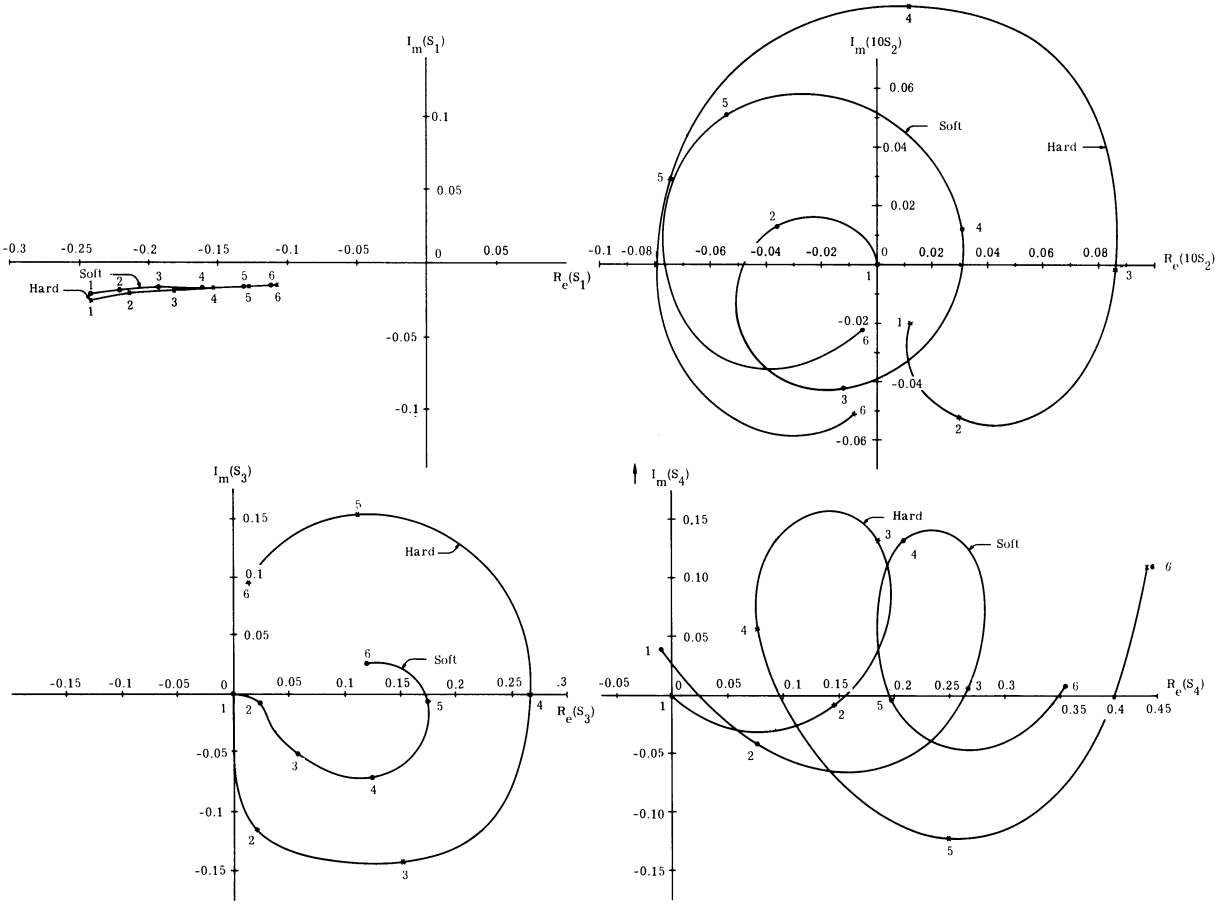

FIGURE 29. RADIAL VARIATIONS OF TOTAL FIELDS AT 45° (INHOMOGENEOUS MEDIUM). Parameters: $\omega_p^2(r_2)/\omega^2 = 0.5, v_0/c = 0.03125, \eta_w = -3.5\ k_0 r_1 = 0.5$.

8
DISCUSSION

8.1. REVIEW OF APPROACH

The purpose of this study has been to answer the specific question posed in section 1.1:

What is the influence of boundary conditions, electron density inhomogenieties, and d-c electric fields on the terminating admittance of a spherical dipole in a warm plasma?

To achieve this result, it was necessary to examine the basic equations and include terms that are left out in the usual homogeneous medium analyses. It was found that the equations decoupled into two sets with the assumption that the dipole excitation is symmetric ($\partial/\partial\phi = 0$). The assumption of zero electron drift velocity (or zero d-c current) made the problem tractable and a set of four coupled first order, ordinary differential equations was finally obtained. It was possible to present explicit solutions in two special cases but in order to answer the ques-

tion above for the general case, numerical integration of the four differential equations was necessary. Section 3 specified a plasma sheath model which is based on Langmuir probe theory. A discussion was given in section 4 and in appendixes III and VI of several alternative proposed boundary conditions at the radiator and the shortcomings of the standard assumption of elastic electron reflection. A technique was also presented there for obtaining the correct radiator values of the four variables. By using these proper values as the starting values of the numerical integration, the angular and radial field variations can be determined. However, the main interest is in the terminating admittance as discussed in section 5. It was necessary to obtain a difference series because of the poor rate of convergence of the original series (discussed in appendix IV). Numerical results for the modal and terminating admittances with the numerous parameters of the problem are covered in section 6.

8.2. CONCLUSIONS

The most interesting effect of the electron thermal motion in the dipole analysis is seen in a previously unreported type of resonance. This resonance occurs because of the possibility of cancelling the capacitive electromagnetic energy storage with inductive electron motion energy storage associated with the electroacoustic wave. Thus as operating frequency, plasma frequency or thermal velocity are altered, the electroacoustic size of the sphere may become optimally matched to the electromagnetic size so as to permit maximum power transfer into the plasma (or maximum terminating conductance).

The condition for maximum terminating conductance is <u>not</u> that there be an integral number of electroacoustic wavelengths around the sphere. It was found that the angular periodicity of all the fields at resonance was more rapid than would be obtained for the electroacoustic wavelength. Alternatively stated, the largest contribution to these fields occurs when the mode number is somewhat larger than, rather than equal to, the normalized electroacoustic size of the sphere. A second consequence of the electron thermal motion is that the terminating susceptance is zero when the operating frequency is greater than the plasma frequency, rather than when they are equal as with a cold plasma.

The variation of the terminating admittance with all of the parameters of the problem appears as a loop or multiple loops in a Smith Chart presentation. The magnitude and location of these loops can be easily established for a model that approximates the plasma as a homogeneous compressible medium and that assumes elastic electron reflection at the radiator. Although this highly unrealistic homogeneous medium model has been used in this study to understand the gross aspects of the problem, it should not be used for interpretation or prediction of measured values. Equally important is the fact that an argument can be made against the assumption that the electrons are elastically reflected at the radiator since the results do not reduce to the cold plasma results as the thermal velocity decreases.

In this study an attempt has been made to avoid these difficulties by considering the effects of a realistic inhomogeneous sheath on the terminating admittance and discussing several alternative types of radiator boundary conditions (elastic electron reflection, zero perturbed electron density,and Cohen's bilinear admittance relation). Relatively little is known about actual sheath profiles, so that the representation that has been chosen (that the static electron density in the sheath varies as the square of the distance from the outer sheath edge) must still be considered approximate.

It was found that the resonances cited above were a strong function of the electron thermal velocity; slight changes were sufficient to cause multiple looping in the Smith Chart presentation. Changes in operating and plasma frequency or radiator radius also cause (slower) looping. Any minor errors in the specification of the sheath do not seem to be serious; the most critical parameter seems to be the assumed sheath thickness rather than the form of the density profile or the wall potential.

The most important conclusion that can be reached about the effect of an actual sheath is that the terminating susceptance will be increased significantly over that predicted by the homogeneous compressible plasma model. This can be readily visualized by thinking of the electron deficient region as counteracting the efficacy of the plasma in reducing the electromagnetic size of the radiator. As an example, a sheath resembling that given in figure 18 for $\omega_p/\omega = 0.707$ would lead to an admittance which, based on homogeneous medium theory, would be obtained for $\omega_p/\omega = 0.57$. Thus, plasma diagnostics relying on homogeneous medium theories can be expected to be appreciably in error.

The second major effect of the inhomogeneous sheath is to make the terminating admittance results for the hard and soft boundary conditions more nearly similar. The effects are now caused by mode conversion due to the inhomogeneity as well as by conversion necessary to satisfy the hard boundary condition. As an example of this effect in one case, the ratio of terminating conductances obtained for the hard and soft radiator boundary assumptions was found to be 75 for the homogeneous medium model but only 2.5 for the sheath model. Although the predicted effects are measurable, it must be remembered that the calculated conductances are still comparable to the free space values. The calculated effects are in fact quite modest compared to those predicted with linear dipoles by assuming certain current distributions.

In the seventh section, several interesting results were found from a study of the spatial field variations. The most important result of the calculations as a function of the angle θ was finding large-amplitude variations (with angle) of the radial electric field regardless of model or boundary condition; measurement of this field would seem to be the most promising means of detecting the excitation of an EA wave. The radial calculations showed a very rapid phase variation with distance of the fields most strongly influenced by the EA wave, perturbed electron

density and radial electron velocity. The most promising method for experimentally distinguishing between different boundary conditions seems to be in detecting the radial variation of the tangential electric field near the radiator (fig. 29).

In addition, it is shown in appendix V that the effect of including collisions in the linear dipole analysis also leads to increased conductance. Thus, in view of the relatively small effects and the uncertainty in boundary conditions, the final conclusion must be that the detection of the excitation of electroacoustic waves in laboratory plasmas through measurement of the terminating admittance will probably be equivocal.

8.3. FUTURE WORK

The basic question to be answered in future EA wave excitation investigations must be that of the proper model of the plasma sheath especially including the proper boundary condition at the radiator. It is believed that the present work is the first antenna analysis to seriously investigate the standard assumption of the hard boundary condition. Since the main interest in this analysis was on the influence of the inhomogeneous sheath on the terminating admittance, no detailed determination of perturbed electron behavior at the radiator boundary was attempted. It would seem that electron absorption should be studied, but there does not seem to be any convenient way to concisely express this condition. Possibly a boundary condition can be obtained from the kinetic approach and then transformed (using Cohen's bilinear admittance relation) into the hydrodynamic treatment.

Secondly, it might be hoped that someone would find a way to study the influence on the fields and terminating admittance of the drift velocity and/or stress tensors in the inhomogeneous plasma since these are undoubtedly of some importance. However, it also seems that the best hope for further advances must come from the kinetic treatment of wave propagation through the sheath even if entirely numerical.

A final suggestion for further work is that future investigations obtain some experimental data for the excitation of the EA wave. It would seem that moveable radial and tangential probes and exceedingly small collision frequencies would be essential for the reasons given above. It is strongly urged that this experimental investigation be performed with a sphere. The important influence of the sheath cannot be conveniently included in the analysis for any other finite shape.

Appendix I
MATHEMATICAL RELATIONS

I.1. VECTOR IDENTITIES AND OPERATORS

The following vector identities were used to obtain the results in section 2 [47]:

$$\rho_T(\vec{v}_T\cdot\nabla)\vec{v}_T = \frac{\rho_T}{2}\nabla(\vec{v}_T\cdot\vec{v}_T) - \rho_T\vec{v}_T\times(\nabla\times\vec{v}_T) \tag{179}$$

$$\nabla\times(\nabla\times\vec{H}) = \nabla(\nabla\cdot\vec{H}) - \nabla\cdot\nabla\vec{H} \tag{180}$$

$$\nabla\times\nabla\rho = 0 \tag{181}$$

$$\nabla\cdot\nabla\times\vec{A} = 0 \tag{182}$$

For the special case when $\frac{\partial}{\partial\phi} = 0$, the following vector operators in spherical coordinates are useful:

$$\nabla\rho = \hat{r}\frac{\partial\rho}{\partial r} + \hat{\theta}\frac{1}{r}\frac{\partial\rho}{\partial\theta} \tag{183}$$

$$\nabla\cdot\vec{v} = \frac{1}{r^2}\frac{\partial}{\partial r}\left(r^2 v_r\right) + \frac{1}{r\sin\theta}\frac{\partial}{\partial\theta}(v_\theta\sin\theta) \tag{184}$$

$$\nabla\times\vec{H} = \frac{\hat{r}}{r\sin\theta}\frac{\partial}{\partial\theta}(H_\phi\sin\theta) - \frac{\hat{\theta}}{r}\frac{\partial}{\partial r}(rH_\phi) + \frac{\hat{\theta}}{r}\left[\frac{\partial}{\partial r}(rH_\theta) - \frac{\partial}{\partial\theta}H_r\right] \tag{185}$$

$$\nabla^2\rho = \frac{1}{r^2}\frac{\partial}{\partial r}\left(r^2\frac{\partial\rho}{\partial r}\right) + \frac{1}{r^2\sin\theta}\frac{\partial}{\partial\theta}\left(\sin\theta\frac{\partial\rho}{\partial\theta}\right) \tag{186}$$

$$\nabla^2(H_\phi\hat{\phi}) = \hat{\phi}\left[\left(\frac{1}{r^2}\frac{\partial}{\partial r}r^2\frac{\partial H_\phi}{\partial r}\right) + \frac{1}{r^2\sin\theta}\frac{\partial}{\partial\theta}\left(\sin\theta\frac{\partial H_\phi}{\partial\theta}\right) - \frac{H_\phi}{r^2\sin^2\theta}\right] \tag{187}$$

I.2. WAVE EQUATIONS AND SOLUTIONS

For the special case when the external medium is homogeneous, the wave equations 44 and 45 become

$$\left[\frac{1}{R_1}\frac{d}{dr}\left(r^2\frac{dR_1}{dr}\right) + k^2r^2\right] + \left[\frac{1}{\Theta_1\sin\theta\,d\theta}\left(\sin\theta\frac{d\Theta_1}{d\theta}\right) - \frac{1}{\sin^2\theta}\right] = 0 \tag{188}$$

$$\left[\frac{1}{R_2}\frac{d}{dr}\left(r^2\frac{dR_2}{dr}\right) + k_p^2r^2\right] + \left[\frac{1}{\Theta_2\sin\theta\,d\theta}\left(\sin\theta\frac{d\Theta_2}{d\theta}\right)\right] = 0 \tag{189}$$

Because the bracketed terms in both equations are respectively independent of θ and r, they must each be equal to a constant. Standard forms are obtained if the second bracket is set equal to -n(n + 1) so that the angular equations are

$$\frac{1}{\sin\theta}\frac{d}{d\theta}\left(\sin\theta\frac{df_2}{d\theta}\right)+\left[n(n+1)-\frac{m^2}{\sin^2\theta}f_2\right]=0 \tag{190}$$

where m = 1 and 0, respectively for the θ_1 and θ_2 equation and f_2 symbolizes both Θ_1 and Θ_2.

An alternative standard form is obtained by letting $\eta = \cos\theta$, so that

$$(1-\eta^2)\frac{d^2f_2}{d\eta^2}-2\eta\frac{df_2}{d\eta}+\left[n(n+1)-\frac{m^2}{1-\eta^2}\right]f_2=0 \tag{191}$$

The solution in either case is the Legendre function $f_2 = P_n^m(\cos\theta) = P_n^m(\eta)$. The independent solutions $Q_n^m(\cos\theta)$ do not apply to physical fields in a complete spherical domain since they become infinite at $\eta = \pm 1$.

The radial functions in both equations satisfy

$$\frac{1}{z^2}\frac{d}{dz}\left(z^2\frac{df_1}{dz}\right)+\left[1-\frac{n(n+1)}{z^2}\right]f_1=0 \tag{192}$$

with the solution f_1 (replacing R_1 and R_2) as a linear combination of the spherical Bessel functions $j_n(z)$ and $n_n(z)$ with z = kr or $k_p r$, respectively. An alternative form of this solution often appears in the literature as

$$f_1 = \frac{1}{\sqrt{z}}Z_{n+1/2}(z) \text{ or } \sqrt{\frac{\pi}{2z}}Z_{n+1/2}(z) \tag{193}$$

where $Z_p(z)$ satisfies the cylindrical Bessel equation

$$\frac{d^2Z_p}{dz^2}+\frac{1}{z}\frac{dZ_p}{dz}+\left(1-\frac{p^2}{z^2}\right)Z_p=0 \tag{194}$$

Schelkunoff [2] gives still another form

$$H_\phi = \frac{R}{r}\frac{d\Theta}{d\theta} \tag{195}$$

$R(r) = A_n Jn_n(kr) + B_n Nn_n(kr)$, where R(r) satisfies the equation

$$\frac{d^2R}{dr^2}+\left[k^2-\frac{n(n+1)}{r^2}\right]R=0 \tag{196}$$

His forms are related to the above by

$$Jn_n(kr) = krj_n(kr) = \sqrt{\frac{\pi}{2}}\sqrt{kr}\,J_{n+1/2}(kr) \tag{197}$$

In the analysis of section 2 and thereafter, the spherical Hankel function forms are used, i.e.

$$h_n^{(1)}(z) = j_n(z) + in_n(z) \tag{198}$$

and the superscript (1) is suppressed when possible.

I.3. PROPERTIES OF THE ANGULAR FUNCTIONS

The Legendre functions were calculated using the recursion formula

$$(n+1)P_{n+1}(\cos\theta) = (2n+1)\cos\theta P_n(\cos\theta) - nP_{n-1}(\cos\theta) \tag{199}$$

with the starting values

$$P_0(\cos\theta) = 1$$

$$P_1(\cos\theta) = \cos\theta$$

The associated Legendre functions were then obtained from

$$P_n^1(\cos\theta) = \frac{1}{\sin\theta}\left\{(n-1)\cos\theta P_n(\cos\theta) - (n+1)P_{n-1}(\cos\theta)\right\} \tag{200}$$

Also important was the value

$$P_{1+2\ell}^1(0) = \frac{(-1)^\ell(2+2\ell)!}{(2^{1+2\ell})\ell!(1+\ell)!} \tag{201}$$

The definitions of the associated Legendre functions that are used in this analysis are

$$\frac{d}{d\theta}(P_n(\cos\theta)) = -P_n^1(\cos\theta) \tag{202}$$

$$\frac{1}{\sin\theta}\frac{d}{d\theta}\left(\sin\theta P_n^1(\cos\theta)\right) = n(n+1)P_n(\cos\theta) \tag{203}$$

It is important to note that the negative sign in (202) is not always used; the present choice is consistent with Stratton [3, 47].

I.4. PROPERTIES OF THE RADIAL FUNCTIONS

The only combination of the spherical Hankel functions that is necessary for computations is denoted

$$H_2(n) = \frac{z\frac{d}{dz}h_n(z)}{h_n(z)} \tag{204}$$

In order to compute H_2 accurately, it was necessary to develop a recursion formula as follows: Two standard forms are [48]

$$z \frac{d}{dz} h_n(z) = -(n + 1)h_n(z) + zh_{n-1}(z) \tag{205}$$

$$zh_{n+1}(z) = nh_n(z) - z \frac{d}{dz} h_n(z) \tag{206}$$

By dropping the order of the second form and dividing by $z^2 h_{n-1}(z)$,

$$\frac{1}{z} \frac{h_n(z)}{h_{n-1}(z)} = \frac{(n - 1)}{z^2} - \frac{\frac{d}{dz} h_{n-1}(z)}{zh_{n-1}(z)} \tag{207}$$

Dividing the first form by $h_n(z)$ and inserting this last equation gives

$$H_2(n) = \frac{z \frac{d}{dz} h_n(z)}{h_n(z)} = -(n + 1) + \frac{z^2}{(n - 1) - H_2(n - 1)} \tag{208}$$

With this form, it is apparent that for $n > z^2$, $H_2(n) \rightarrow -(n + 1)$. Since only odd n are needed in the final summation, it is convenient to drop the subscripts again to obtain $H_2(n - 1)$ in terms of $H_2(n - 2)$ and thereby obtain

$$H_2(n) = -(n + 1) + \frac{1}{\frac{(2n - 1)}{z^2} + \frac{1}{H_2(n - 2) - (n - 2)}} \tag{209}$$

where the starting value for n = 1 is easily shown to be

$$H_2(1) = \frac{-(2 + z^2) + iz^3}{(1 + z^2)} \tag{210}$$

This method was checked against an independent calculation using cylindrical Bessel function forms given by Watson [49] for the case of equal order and argument. The Watson formula, stated to be good to 7-digit accuracy for $n > 50$, gave a result that agreed within 10^{-5} percent with the recursion formula result for n = 97, x = 97.5. Examples of calculated values of $H_{2n}(2)$ are given in table XVI. The arguments used here are for the homogeneous medium and sheath models discussed in section 6.2. It should be noted how rapidly the imaginary contribution decreases for $n > z$, which is the term contributing to the modal conductances.

TABLE XVI. VALUES OF $H_{2n}(z)$ USED IN SECTION 6.2 The signs on the imaginary components should be reversed for use with the $e^{+j\omega t}$ time convention.

	$H_2(0.3535)$		$H_2(11.314)$		$H_2(0.4873)$		$H_2(15.59)$	
n	Re	Im	Re	Im	Re	Im	Re	Im
1	-1.889	+i.0393	-1.008	+i11.23	-1.808	0.0935	-1.004	15.53
3	-3.975	+i2.99(-6)	-1.050	+i10.78	-3.95	+i2.76(-5)	-1.206	+i15.21
5	-5.986	+i1.191(-11)	-1.146	+i9.93	-5.97	+i4.02(-10)	-1.069	+i14.61
7	-7.990	+i9.14(-18)	-1.351	+i8.58	-7.98	+i1.116(-15)	-1.146	+i13.70
9	-9.993	+i2.20(-24)	-1.843	+i6.55	-9.99	+i9.73(-22)	-1.281	+i12.43
11	-11.994	+i2.16(-31)	-3.21	+i3.72	-11.99	+i3.46(-28)	-1.537	+i10.67
13	-13.995	+i1.024(-38)	-6.41	+i1.011	-13.99	+i5.91(-35)	-2.09	+i18.29
15	-15.996	+i---	-10.29	+i0.0872	-15.99	+i---	-3.47	+i5.13
17	-17.996	+i---	-13.42	+i2.86(-3)	-17.99	+i---	-6.60	+i1.864
19	-19.997	+i---	-16.10	+i4.71(-5)	-19.99	+i---	-10.92	+i0.275
21	-21.997	+i---	-18.57	4.49(-7)	-21.99	+i---	-14.60	+i0.01679

Appendix II
HYDRODYNAMIC EQUATIONS

The usual "hydrodynamic equations" were presented without derivation in the second chapter as equations 6 and 7. A brief review of their derivation is necessary, however, since they are generally used neither with an inhomogeneous medium nor with an electric field, nor a drift velocity. The basic equation for this derivation is the Boltzmann equation; the following discussion follows that of Spitzer [39].

The Boltzmann equation gives the time rate of change of the particle density as a function of the particles' position, velocity,and encounters with other particles. The particle density (electrons or ions), $f(\vec{r}, \vec{v}, t)\, dx\, dy\, dz\, dv_x\, dv_y\, dv_z$ is the number of particles in the volume $dx\, dy\, dz$ centered at $\vec{r}$ and whose velocities lie in the intervals dv_x, dv_y, dv_z centered at $\vec{v}$. Thus,

$$\frac{df}{dt} = \frac{\partial f}{\partial t} + \sum_j \frac{\partial f}{\partial x_j}\frac{dx_j}{dt} + \sum_j \frac{\partial f}{\partial v_j}\frac{dv_j}{dt} = \left(\frac{\partial f}{\partial t}\right)_{\text{collision}} \tag{211}$$

or since $v_j = \dfrac{dx_j}{dt}$ and $F_j = m\dfrac{dv_j}{dt}$,

$$\frac{\partial f}{\partial t} + \sum_j v_j \frac{\partial f}{\partial x_j} + \sum_j \frac{F_j}{m}\frac{\partial f}{\partial v_j} = \left(\frac{\partial f}{\partial t}\right)_{\text{collision}} \tag{212}$$

This equation would be exclusively used in studies of the EA wave were it not so difficult to obtain solutions. The alternative is to use this equation to obtain hydrodynamic or "macroscopic" equations from which solutions may be more readily obtained. Thus macroscopic quantities (denoting all but the density $n(\vec{r}, t)$ by underlining) may be defined as

$$n(\vec{r}, t) = \iiint_{-\infty}^{+\infty} f(\vec{r}, \vec{v}, t)\, dv_x dv_y dv_z \tag{213}$$

$$\underline{\vec{v}}(\vec{r}, t) = \frac{1}{n(\vec{r}, t)} \iiint_{-\infty}^{+\infty} \vec{v} f(\vec{r}, \vec{v}, t)\, dv_x dv_y dv_z \tag{214}$$

and in general any macroscopic quantity $\underline{Q}(\vec{r}, t)$ is obtained from the arbitrary function $Q(\vec{v})$ as

$$\underline{Q}(\vec{r}, t) = \frac{1}{n(\vec{r}, t)} \iiint_{-\infty}^{+\infty} Q(\vec{v}) f(\vec{r}, \vec{v}, t)\, dv_x dv_y dv_z \tag{215}$$

The macroscopic equations are obtained by multiplying both sides of equation 212 by $Q(\vec{v})$ $dv_x dv_y dv_z$ and integrating over velocity space as in equations 213 through 215. Because $Q(\vec{v})$ is assumed independent of $\vec{r}$ and t, then the first two terms become

$$\frac{\partial}{\partial t} \iiint_{-\infty}^{+\infty} Q(\vec{v}) f(\vec{r}, \vec{v}, t)\, dv_x dv_y dv_z = \frac{\partial}{\partial t}(n\underline{Q}) \tag{216}$$

$$\frac{\partial}{\partial x_j} \iiint_{-\infty}^{+\infty} Q(\vec{v}) v_j f(\vec{r}, \vec{v}, t)\, dv_x dv_y dv_z = \frac{\partial}{\partial x_j}(n\underline{v_j Q}) \tag{217}$$

By integrating by parts and noting that $f(\vec{v}, \vec{r}, t)$ is zero for $v_j = \pm\infty$, the third term becomes

$$-\frac{1}{m} \iiint_{-\infty}^{+\infty} f(\vec{r}, \vec{v}, t) \frac{\partial}{\partial v_j} \left\{ F_j(\vec{r}, \vec{v}) Q(\vec{v}) \right\} dv_x dv_y dv_z \tag{218}$$

The integral of the collision term on the right hand side will be denoted as I_Q. Thus (212) can be integrated to give

$$\frac{\partial}{\partial t}(n\underline{Q}) + \sum_j \frac{\partial}{\partial x_j}(n\underline{v_j Q}) - \sum_j \frac{n}{m} \frac{\partial}{\partial v_j}(\underline{F_j Q}) = I_Q \tag{219}$$

The continuity equation is obtained as the simplest form of this equation when $Q = 1$. The third term in (219) disappears with the restriction of the analysis to forces for which $\partial F_j / \partial v_j \equiv$; this does not exclude magnetic forces. The right hand side, $I_Q = I_1$, must vanish since collisions cannot change the particle density. Thus (219) gives

$$\frac{\partial n}{\partial t} + \nabla \cdot (n\underline{\vec{v}}) = 0 \tag{220}$$

The force equation (often called the equation of motion or momentum transfer) is obtained by letting $\vec{Q} = m\vec{v}$, so (219) gives $\left(\text{using } \frac{\partial}{\partial v_j}(F_j v_j) = F_j\right)$

$$\frac{\partial}{\partial t}(nm\underline{\vec{v}}) + \nabla\cdot(nm\underline{\vec{v}\vec{v}}) - n\underline{\vec{F}} = \iint m\vec{v}\left(\frac{\partial f}{\partial t}\right)_{coll.} dv_x\, dv_y\, dv_z \tag{221}$$

The first term of (221) can be rewritten using (220):

$$m\frac{\partial}{\partial t}(n\underline{\vec{v}}) = mn\frac{\partial\underline{\vec{v}}}{\partial t} + m\underline{\vec{v}}\frac{\partial n}{\partial t} = mn\frac{\partial\underline{\vec{v}}}{\partial t} - m\underline{\vec{v}}\nabla\cdot n\underline{\vec{v}} \tag{222}$$

By dividing the velocity into macroscopic and random parts

$$\vec{v} = \underline{\vec{v}} + \vec{w}, \qquad (\text{hence } \underline{\vec{w}} \equiv 0) \tag{223}$$

The second term of (221) may be rewritten as

$$\nabla\cdot(nm\underline{\vec{v}\vec{v}}) = \nabla\cdot(nm[\underline{\vec{v}\vec{v}} + \underline{\vec{w}\vec{w}}]) = m\underline{\vec{v}}\nabla\cdot n\underline{\vec{v}} + mn\underline{\vec{v}}\cdot\nabla\underline{\vec{v}} + \nabla\cdot\psi \tag{224}$$

where $\psi = nm\underline{\vec{w}\vec{w}}$ is defined as the stress tensor and will be further discussed below. The third term of (221) may be replaced by

$$\vec{F} = -e(\vec{E} + \mu\underline{\vec{v}} \times \vec{H}) - m\nabla\phi_g \tag{225}$$

where $\vec{E}$ and $\vec{H}$ are the electric and magnetic field strengths; ϕ_g is the gravitational potential which will hereafter be ignored as will the magnetic forces. The right hand side of (221) would be zero if all particles were identical, but a net momentum exchange could occur when collisions with other particles are considered; this term will be dropped in this analysis with the assumption that collision frequencies are very low. Combining (221) through (225) then gives

$$mn\frac{\partial\underline{\vec{v}}}{\partial t} + mn\underline{\vec{v}}\cdot\nabla\underline{\vec{v}} + ne\vec{E} + \nabla\cdot\psi = 0 \tag{226}$$

Other "hydrodynamic" equations could be obtained by using other functions of $\vec{v}$ for $\vec{Q}(\vec{v})$. For the present purpose, this is not necessary with the assumption that the stress tensor ψ has only equal, diagonal elements. This is equivalent to assuming an isotropic, scalar pressure p, so that

$$\nabla\cdot\psi = \nabla p \tag{227}$$

The scalar pressure assumption cannot be rigorously defended; in fact, Tidman and Boyd [50] have presented interface boundary conditions involving a tensor pressure. However, Parker, Nickel, and Gould [51] have successfully used scalar pressures in predicting resonances in non-uniform, cylindrical plasma columns. The main reason for using scalar pressures, though, is the extreme difficulty, if not impossibility, of solving any radiation problem with the inclusion of a stress tensor.

This development essentially completes the derivation of the hydrodynamic equations. Equations (220) and (226) can be put in the forms (6) and (7) by adding the subscript "T," deleting the underlining (since all quantities are now averaged), and using $\rho_T = -en_T$. Thus we have

$$\nabla\cdot(\rho_T\vec{v}_T) + \frac{\partial\rho_T}{\partial t} = 0 \tag{6}$$

$$\rho_T\left[m\left(\frac{\partial\vec{v}_T}{\partial t} + (\vec{v}_T\cdot\nabla)\vec{v}_T\right) + eE_T\right] - e\nabla\rho_T = 0 \tag{7}$$

It is possible to write a similar set of hydrodynamic equations for the ions; it is not necessary to do so in this analysis since they are presumed to experience no RF perturbations. However, there are still more variables than equations. The remaining relationship comes from an assumption about the "equation of state." Landau [52] was the first to show, using the kinetic approach, that the longitudinal wave experiences small damping in the frequency region to which we have restricted ourselves ($\lambda >> \lambda_D$). This thus justifies the standard assumption that the compression is reversible (constant entropy) and one can use the adiabatic equation of state

$$\frac{p_T}{p_0} = \left(\frac{n_T}{n_0}\right)^\gamma \tag{228}$$

where γ is the abiabatic constant. Thus,

$$\nabla p_T = \nabla p_0\left(\frac{n_T}{n_0}\right)^\gamma = \nabla n_0 kT_e\left(1 + \frac{n}{n_0}\right)^\gamma \cong \nabla(n_0 kT_e + \gamma nkT_e) = kT_e\nabla n_0 + \gamma kT_e\nabla n, \tag{229}$$

using the perfect gas law ($p_0 = n_0 kT_e$) and the small signal assumption ($n << n_0$).

Using the well known [39] relation that $\gamma = (2 + m)/m$, where m is the number of degrees of freedom, then $\gamma = 3$ for the present case of one-dimensional compression. Hok [53] has also obtained this result from the series of moment equations demanding constant entropy.

In the manipulations given in section 2, it is advantageous to put the results in terms of the rms thermal velocity, v_0. For a Maxwellian distribution, this gives

$$\frac{1}{2}mv_0^2 = \frac{3}{2}kT_e \tag{230}$$

so that

$$\nabla p_T = \frac{1}{3}mv_0^2\nabla n_0 + mv_0^2\nabla n \tag{231}$$

An area of confusion that exists on this form was pointed out to the author by Professor Hok. Although v_0 is termed the rms velocity above, other authors call this or similar symbols

the "sound" or "acoustic" velocity. With this nomenclature, one can go between (229) and (231) with the definition: $mv_0^2 = \gamma kT_0$. However this definition will not be correct when v_0 is termed the rms velocity. Similar caution is indicated in the definition of Debye length given in section 3. In both cases, the extension of these results to cases when $\gamma \neq 3$, could cause serious confusion.

Appendix III
BOUNDARY CONDITIONS

III.1. INTRODUCTION

Boundary conditions at both inner and outer sheath edges were presented in section 4 without derivation. The conditions at the outer sheath edge have been used by many authors for much less restrictive models; their derivation in section III.2 shows the importance of the restrictions used in this study. One of the conditions at the inner sheath edge is much more dubious; in fact, three different suggested conditions are studied in sections 6 and 7. Justification for these radiator conditions were given in section 4; possible approaches to a derivation are given in section III.3. An extension of this material for the vacuum-plasma boundary is contained in appendix VI.

III.2. BOUNDARY CONDITIONS AT THE OUTER SHEATH EDGE

This section is devoted to the case where the static or d-c electron density is continuous, although the gradient of the density is not, at first, restricted. This is a model close to that existing in an actual sheath as opposed to artificial step discontinuities used in all previous radiation analyses and discussed in appendix VI. The boundary conditions given previously for special cases by numerous authors [14, 54] are

$$\hat{n} \times [\vec{H}_2 - \vec{H}_1] = 0 \tag{232}$$

$$\hat{n} \times [\vec{E}_2 - \vec{E}_1] = 0 \tag{233}$$

$$\hat{n} \cdot [\vec{v}_2 - \vec{v}_1] = 0 \tag{234}$$

$$p_2 - p_1 = 0 \tag{235}$$

Previous derivations of these boundary conditions have not included the d-c electric field or drift velocity; it is therefore necessary to show how these might influence the boundary conditions as well as to illustrate the limitations in their use. Since these conditions are often justified by heuristic arguments it is also important to appreciate the limitations and alternatives to these arguments.

The derivation of the first two boundary conditions above does not differ essentially from that given by Stratton [47]. The derivation of (100) begins with equation 10:

$$\nabla \times \vec{H}_T = \rho\vec{v} + \rho\vec{u}_0 + \epsilon_0 \frac{\partial \vec{E}}{\partial t}$$

Since this equation holds on each side of the boundary shown in figure 30a, the equation may be scalar multiplied by $\hat{n}_0 da$ and integrated over the area shown. The first term is replaced by using Stokes' Theorem; e.g., Stratton [47, p. 6],

$$\int_{S_0} (\nabla \times \vec{A}) \cdot \hat{n}_0 \, da = \int_{C_0} \vec{A} \cdot \vec{ds} \tag{236}$$

where C_0 is the closed path surrounding the rectangular area S_0 shown in figure 30a. This gives

$$\int_{C_0} \vec{H} \cdot \vec{ds} = \int_{S_0} [\rho_0 \vec{v} + \rho\vec{u}_0] \cdot \hat{n}_0 da + \epsilon_0 \int_{S_0} \frac{\partial \vec{E}}{\partial t} \cdot \hat{n}_0 \, da \tag{237}$$

This equation may be approximated by

$$(\vec{H} \cdot \hat{\tau}_1 + \vec{H} \cdot \hat{\tau}_2) \, \Delta s + \text{contributions from ends} = \left[\rho_0 \vec{v} + \rho\vec{u}_0 + \epsilon_0 \frac{\partial \vec{E}}{\partial t}\right] \cdot \hat{n}_0 \, \Delta s \, \Delta \ell \tag{238}$$

By contracting the path to lie infinitesimally close to the boundary surface, the end contributions become vanishingly small. The first term on the right may contribute to a surface current; in the present example, these contributions to the current density are assumed finite and it can be

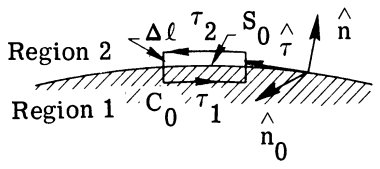

(a) For the tangential boundary conditions

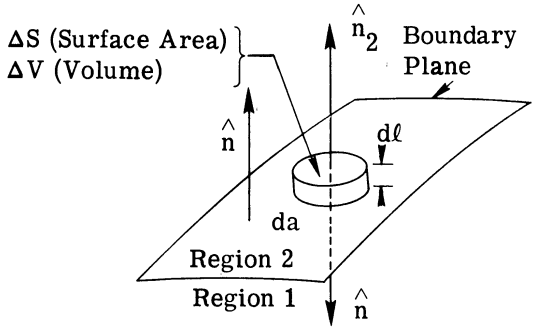

(b) For the normal boundary conditions

FIGURE 30. BOUNDARY CONDITION DIAGRAMS.

seen that all terms on the right hand side vanish as $\Delta\ell \to 0$ since all the terms and their derivatives are bounded. Since

$$-\hat{\tau}_1 = \hat{n}_0 \times \hat{n} = \hat{\tau}_2 \tag{239}$$

then in the limit as $\Delta\ell \to 0$,

$$\hat{n} \times (\vec{H}_2 - \vec{H}_1) = 0 \tag{240}$$

It can be noted for use in the next section that at a perfect conductor, the surface current $\vec{J}_s$ should be included in equation 10. In the limit of vanishing $\Delta\ell$, one would then obtain

$$\hat{n} \times (\vec{H}_2 - \vec{H}_1) = \lim_{\Delta\ell \to 0} \vec{J}_s \, \Delta s \, \Delta\ell = \vec{K} \tag{241}$$

An entirely analogous integration of equation 5 leads to the familiar equation for continuity of tangential electric fields.

$$\hat{n} \times (\vec{E}_2 - \vec{E}_1) = 0 \tag{242}$$

It is important to note here that boundary conditions on the normal components of these vectors would be somewhat redundant. Since the divergence of a curl of a vector is identically zero, taking divergences of equations (10) and (11) give for the a-c components

$$\nabla\cdot(\rho_0\vec{v} + \rho\vec{u}_0) + \nabla\cdot\epsilon_0\frac{\partial\vec{E}}{\partial t} = 0 \tag{243}$$

$$\nabla\cdot\mu_0\frac{\partial\vec{H}}{\partial t} = 0 \tag{244}$$

Since Gauss' Theorem states

$$\int_V \nabla\cdot\vec{A}\,dV = \int_S \vec{A}\cdot\hat{n}\,da \tag{245}$$

where V is the volume enclosed by the surface S shown in figure 30b, then a volume integration of (243) gives

$$\epsilon_0\frac{\partial}{\partial t}\int_S \vec{E}\cdot\hat{n}\,da = -\int_V \nabla\cdot(\rho_0\vec{v} + \rho\vec{u}_0)\,dV \tag{246}$$

The term on the right may be replaced, using (12):

$$\nabla\cdot(\rho_0\vec{v} + \rho\vec{u}_0) = -\frac{\partial\rho}{\partial t} - \frac{\partial Q_s}{\partial t} \tag{247}$$

where $Q_s (\neq Q^s)$ has been included to allow for possible surface charges. Dropping the time derivatives, (246) may be approximated by

$$\epsilon_0(\vec{E}\cdot\hat{n}_1 + \vec{E}\cdot\hat{n}_2)\Delta Q + \text{contributions from the walls} = (\rho + Q_s)\Delta\ell\,\Delta a \tag{248}$$

The first term on the right vanishes as $\Delta\ell \to 0$ since ρ is assumed finite. The term $Q_s \Delta\ell\, \Delta a$ approaches $\sigma \Delta a$ if surface charges exist. Consequently, since $\hat{n}_1 = -\hat{n}_2 = \hat{n}$, then

$$\hat{n}\cdot(\vec{E}_2 - \vec{E}_1) = -\frac{\sigma}{\epsilon_0} \tag{249}$$

In the nomenclature being used here, the electron charge is taken as -e, so that electron charge densities are negative quantities (i.e., $\rho_0 = -|e|n_0$). Similarly Q_s and σ are defined as negative quantities for excess electron density.

The familiar boundary condition on normal magnetic flux density follows in a similar fashion from (244):

$$\hat{n}\cdot(\vec{B}_2 - \vec{B}_1) = 0 \tag{250}$$

Equation 250 provides the same information for the purpose of evaluating constants as does (242), as indeed it must with the same starting equation. Equation 249, however, provides somewhat more information than (241) since another of the basic equations (continuity) was used in its derivation. A similar volume integration of the continuity equation 274 gives

$$\int_S (\rho_0\vec{v} - \rho\vec{u}_0)\cdot\hat{n}\,da = -\int_V \left(\frac{\partial\rho}{\partial t} + \frac{\partial Q_s}{\partial t}\right) dV \tag{251}$$

or

$$\hat{n}\cdot\left[(\rho_0\vec{v} + \rho\vec{u}_0)_2 - (\rho_0\vec{v} + \rho\vec{u}_0)_1\right] = \frac{\partial\sigma}{\partial t} \tag{252}$$

A combination of (249) and (252) gives a continuity of current condition

$$\hat{n}\cdot\left[\left(\rho_0\vec{v} + \rho\vec{u}_0 + \epsilon_0\frac{\partial\vec{E}}{\partial t}\right)_2 - \left(\rho_0\vec{v} + \rho\vec{u}_0 + \epsilon_0\frac{\partial\vec{E}}{\partial t}\right)_1\right] = 0 \tag{253}$$

This result is not in any sense new since it is obtainable directly from (243). It is obviously redundant with (240), whereas either (249) or (252) provide new information.

Before further comment on the nature of the surface density σ, it is desirable to discuss boundary conditions derivable from the remaining fundamental equation—the force equation 13:

$$m\rho_0\left[\frac{\partial\vec{v}}{\partial t} + u_0\nabla v_r + v_r\nabla u_0\right] + m\rho u_0\nabla u_0 - m\rho_0 u_0\hat{r}\times(\nabla\times\vec{v}) + \rho_0 e\vec{E} + \rho e E_0\hat{r} + m v_0^2\nabla\rho = 0$$

It is obvious that all realistic models require continuity of the d-c parameters, ρ_0, E_0, and u_0. In the present analysis it is necessary, in order to solve the problem, that the quantities E_0, u_0, and ∇u_0 vanish in the exterior regions and, therefore, also in the internal region at the

boundary. With the models analyzed in this study, these assumptions about the boundary region give (at the boundary) the simpler equation

$$\rho_0 m \frac{\partial \vec{v}}{\partial t} + \rho_0 e\vec{E} + m v_0^2 \nabla\rho = 0 \tag{254}$$

If this equation is integrated along the line $\Delta\ell$ shown in figure 30a, then

$$\int_{\ell_1}^{\ell_2} \rho_0 m \frac{\partial \vec{v}}{\partial t}\cdot\hat{n}\, d\ell + \int_{\ell_1}^{\ell_2} \rho_0 e\vec{E}\cdot\hat{n}\, d\ell + m v_0^2 \int_{\ell_1}^{\ell_2} \nabla\rho\cdot\hat{n}\, d\ell = 0 \tag{255}$$

where ℓ_1 and ℓ_2 are points on $\Delta\ell$ close to and on opposite sides of the interface. The last term can be rewritten as

$$\int_{\ell_1}^{\ell_2} \frac{d\rho}{d\ell}\, d\ell = \int_{\rho_1}^{\rho_2} d\rho = \rho_2 - \rho_1 \tag{256}$$

As the length $\Delta\ell$ shrinks to zero, equation 255 may then be approximated as

$$\hat{n}_2\cdot\left[\left(\rho_0 m \frac{\partial \vec{v}}{\partial t} + \rho_0 e\vec{E}\right)_2 + \left(\rho_0 m \frac{\partial \vec{v}}{\partial t} + \rho_0 e\vec{E}\right)_1\right]\frac{\Delta\ell}{2} + m v_0^2(\rho_2 - \rho_1) = 0 \tag{257}$$

Since this is a line rather than volume integration, the left hand terms do not lead to surface density terms as in equations 249 and 252. As the length $\Delta\ell$ shrinks to zero, the first terms disappear (since all quantities are presumed finite), giving

$$\rho_2 - \rho_1 = 0 \tag{258}$$

The condition in (258) is more often presented as a dynamic condition—namely, that the boundary would move were the pressures (and therefore the densities) not made equal. From the above derivation it is seen that it is necessary for the d-c electric fields and velocities to vanish at the boundary to obtain this condition. Furthermore, it would seem that the heuristic reasoning that forces be balanced should include electric as well as pressure forces. This line of reasoning (not used, of course, in acoustics) would lead to an entirely different result if the normal electric field were not continuous.

The boundary conditions derived above are believed to be exhaustive; no further conditions seem possible. Nevertheless they are of little value with $\sigma \neq 0$ since there is no a priori method of specifying this quantity. However, when the medium is continuous as in the present example, it is obvious that there is no mechanism for supporting a surface charge and the following familiar boundary conditions are obtained:

$$\hat{n} \times (\vec{H}_2 - \vec{H}_1) = 0 \tag{240}$$

$$\hat{n} \times (\vec{E}_2 - \vec{E}_1) = 0 \tag{241}$$

$$\hat{n} \cdot (\vec{v}_2 - \vec{v}_1) = 0 \qquad \text{(see (252))}$$

$$\rho_2 - \rho_1 = 0 \tag{258}$$

With the present assumption of continuous electron density and zero d-c electric fields and drift velocity at the interface, these conditions are simple mathematical statements that all fields are continuous across the interface. Alternatively stated, there is no coupling at the interface between EM and EA modes with a realistic continuous electron density. A further modification, appropriate to the spherical radiator study, is given in section 4.2.

III.3. RADIATOR CONDITIONS

In order to completely specify the solution to the radiator problem it is necessary to specify two conditions at the radiator. One obvious condition is that the tangential electric field vanishes except at the gap; this is discussed in section 5.1. In past analyses [17, 18], it has been assumed that elastic reflection of electrons is the second necessary condition. However, this condition cannot be analytically defended, nor can any other be rigorously derived as in the previous section.

The basic problem is that the continuity and force equations cannot be presumed valid in the limit of an infinitely conducting metal. However, assuming that the infinitely conducting metal can be approximated by the electron gas model used in the preceding appendix, and assuming zero field quantities in the infinitely conducting metal, then equation 252 would give for the surface continuity equation

$$\hat{n} \cdot [\rho_0 \vec{v} + \rho \vec{u}_0]_{r_1} = \frac{\partial \sigma}{\partial t} \tag{259}$$

Quite obviously, one cannot obtain $\hat{n} \cdot \vec{v} = 0$ from this relation. On the other hand, the derivation leading to (258) would give the soft boundary condition

$$[\rho]_{r_1} = 0 \tag{260}$$

The final alternative used in section 6 is the Cohen bilinear admittance relation, with a short derivation there of a possible set of coefficients using this same analysis.

However, all of these derivations, or any similar one, rest on the decidedly non-physical assumption that all of the fields are zero inside the infinitely conducting metallic radiator. In fact, it is quite possible that the finite metallic conductivity and associated skin depth associated with a physical radiator play an important role in the actual boundary conditions. For these

reasons, further speculation on the actual boundary condition does not seem to be warranted and all three cases are studied. Fortunately, it is found that with an inhomogeneous sheath region, the calculated results are quite similar and the question is mainly of academic importance.

Appendix IV
LIMITING VALUE OF INPUT SUSCEPTANCE

The method of calculation of the modal admittances was described in section 5 for both the homogeneous and inhomogeneous medium models. These extensions of the techniques employed by Chu and Stratton [3] took into account both the electroacoustic wave and the sheath inhomogeneity. For the homogeneous medium model similar results were obtained by Wait [18], who restricted his attention, however, to the total input conductance. It was shown in section 6.2, that this total input conductance (for both models) can be obtained from a series that converges rapidly for orders larger than the normalized EA sheath size (i.e. $n > k_p r_2$). However, the total input susceptance does not converge rapidly; in fact, the series does not converge at all for the infinitesimal gap as pointed out by Chu and Stratton [3] in their original article. The techniques used to obtain a convergent solution are the subject of this appendix.

There are two features of the problem that make it possible to obtain a convergent solution. First, as shown in section 5.2, the individual modal contributions approach those for free space when $n > k_p r_2$. Then, because the free space values can be summed for finite gap angles, the total input susceptance can be obtained for any gap angle from the known modal values for the infinitesimal gap.

Mathematically, the first feature can be stated as

$$\sum_{n=1}^{\infty}{}' B_n = -\omega C_t + \sum_{n=1}^{\infty}{}' (B_n + B_{0n}) = -\omega C_t + \sum_{n=1}^{N_m-2}{}' (\Delta B)_n - \sum_{n=N_m}^{\infty}{}' \frac{C_\Delta}{n^p} \qquad (261)$$

where B_{0n} and ωC_t are respectively the low frequency free space modal and input susceptances, $(\Delta B)_n$ are the differences between the calculated susceptances and the free space values, N_m is the largest order used in the calculations, and C_Δ and p are calculated parameters approximating the series from N to infinity. C_t is discussed below; it remains only to show how C_Δ and p are obtained and then used to give a correction term.

In each set of calculations presented in section 6, the sequence $\log (\Delta B)_n$ was plotted vs. $\log n$. For values of $n > k_p r_2$, a straight line was obtained whose slope is -p. For the homogeneous

medium, p was 3; for the inhomogeneous medium cases, values between 1.5 and 3 were obtained. The value C_Δ is then simply the final calculated difference value times N_m^p.

An upper bound to this correction term can be readily obtained, since (letting n = 2m + 1)

$$\sum_{n=N_m}^{\infty}{}' \frac{1}{n^p} = \frac{1}{2^p} \sum_{m=\frac{N_m}{2}}^{\infty}{}' \frac{1}{\left(m+\frac{1}{2}\right)^p} < \frac{1}{2^p}\int_{\frac{N_m}{2}}^{\infty} \frac{dx}{x^p} = \frac{1}{2^p(p-1)\left(\frac{N_m}{2}\right)^{p-1}} \tag{262}$$

Hence

$$\sum_{n=N_m}^{\infty}{}' \frac{C_\Delta}{n^p} < \frac{(\Delta B)_{N_m} N_m^p}{2^p(p-1)\left(\frac{N_m}{2}\right)^{p-1}} = \frac{N_m(\Delta B)_{N_m}}{2(p-1)} \tag{263}$$

In all the calculations that were made, this correction term never was more than a few percent of the value $\sum_{n=1}^{N_m}{}' (\Delta B)_n$. A major contribution, however, comes from the low frequency free space input capacitance C_t. Although Chu and Stratton [3] mentioned that a finite gap width would lead to a finite summation for B_{in}, the only person who seems to have discussed the problem is Schelkunoff [2].

Schelkunoff's approach was to note that, for low frequencies, the input admittance approaches the admittance of the capacitor formed by the hemispheres with the result previously given in equation 162:

$$C_t = \frac{2\mu_0 r_1}{\pi K^2} \sum{}' \frac{[P_n(\cos)]^2}{nN_n} \tag{264}$$

As ψ approaches $\pi/2$, K (defined by (146)) approaches $\sqrt{\mu_0/\epsilon_0}\left(\frac{\Delta\theta}{2\pi}\right)$. By expressing the Legendre function in an approximate trigonometric form and replacing the summation by an integral, Schelkunoff obtained

$$\omega C_t \cong \frac{k_0 r_1}{60\pi}(-\ell n\, \Delta\theta + 0.52) \tag{265}$$

In accordance with Schelkunoff's suggestion that the first terms be evaluated separately and the remainder expressed as an integral, a more accurate expression was obtained

$$\omega C_t = \frac{k_0 r_1}{60\pi}(-\ell n\, \Delta\theta + 2.0) \tag{266}$$

This last form was in much closer agreement with computer computations of (264) that retained terms up to n = 200. Because ωC_t is not influenced by the EA wave or the sheath, the representative value of 13.0×10^{-3} mhos (corresponding to about three degrees) was taken as a standard value in all of the data presented in section 6.

Appendix V
INFLUENCE OF COLLISION FREQUENCY

In order to simplify the analysis, it has been assumed, in the main body of this study, that the plasma is lossless. Although this is a standard assumption in EA wave analyses, it is not usually valid in laboratory plasmas nor for most lower ionospheric experiments. Therefore, it is important to understand the influence of collision frequencies, especially because the main effect of including collision frequencies is much like that resulting from the inclusion of EA wave effects: increased radiation resistance.

A discussion of the spherical dipole admittance analysis including collision effects, in conjunction with the EA wave, has been given by Wait [18]. Since Wait's numerical results are to be published soon, only a brief discussion of this problem need be given here. In figure 31, the modal conductances are shown for a range of collision frequencies where the compressibility of the plasma is ignored. These values were obtained at a desk calculator from equation 167 with the definition of propagation constant given below. For this model, a fairly large collision frequency is needed to materially affect the total conductance.

Rather than consider this further for the sphere, the same problem will be considered for a thin dipole. This is preferred here since the only available experimental evidence for the EA wave was obtained (Jackson, Kane and Whale [12]) in an ionospheric RF probe measurement using a thin cylindrical dipole. In the light of the negative results obtained in the present study, it is most important to determine whether the effects noted for the thin dipole in the Jackson, Kane and Whale experiments could not be explained by collision effects.

The basis for these calculations, which do not seem to have been presented in this form before, is the work of King, et al. [4]. By modifying their work slightly and using their nomenclatures, then the admittance of a short linear dipole may be expressed as

$$G(k) = \frac{2\pi}{\zeta_0 \psi_{d1}} \frac{(\beta h)}{(\beta_0 h)} \left\{ \frac{2\alpha}{\beta} \left[\beta h + \frac{2}{3}\beta^3 h^3 F\left(1 - \frac{\alpha^2}{\beta^2}\right) \right] + \frac{\beta^4 h^4}{3(\Omega - 3)} \left(1 - 10\frac{\alpha^2}{\beta^2} + 5\frac{\alpha^4}{\beta^4}\right) \right\} \tag{267}$$

$$B(k) = \frac{2\pi}{\zeta_0 \psi_{d1}} \frac{\beta h}{\beta_0 h} \left\{ \beta h \left(1 - \frac{\alpha^2}{\beta^2}\right) + \frac{1}{3}\beta^3 h^3 F\left(1 - 6\frac{\alpha^2}{\beta^2} + \frac{\alpha^4}{\beta^4}\right) - \frac{\beta^4 h^4}{3(\Omega - 3)} \frac{\alpha}{\beta} (5 - 10k^2 + k^4) \right\} \tag{268}$$

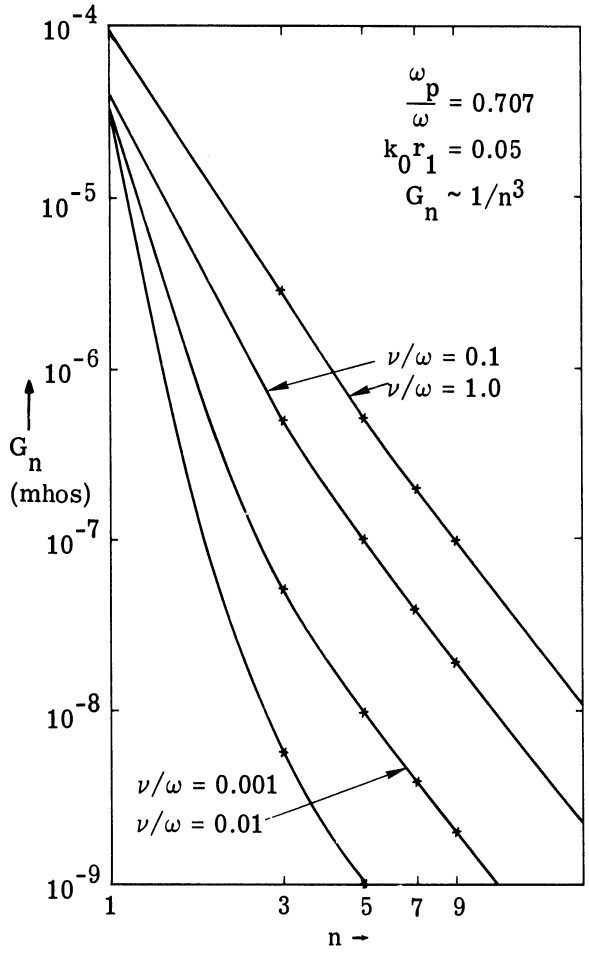

FIGURE 31. VARIATIONS IN MODAL CONDUCTANCE WITH VARIOUS COLLISION FREQUENCIES

where King's approximation $\zeta = \zeta_e / \left(1 - j\frac{\alpha}{\beta}\right)$ has not been employed, $F = 1 + 3\ \ell n\ 2 - 1/(\Omega - 3)$, $\Omega = 2\ \ell n \frac{2h}{a}$, $\psi_{d1} \cong 2\ \ell n\ (h/a) - 2$, $\zeta_0 = \sqrt{\mu/\epsilon}$, $\zeta_e = \zeta_0/\sqrt{\epsilon_r}$, h and a are antenna length and radius, respectively, G and B are antenna input conductance and susceptance, respectively, and $k = \beta - j\alpha$ defines the complex propagation constant where

$$\beta = \beta_0 \cdot \sqrt{(|K| + K_R)/2} \tag{269}$$

$$\alpha = \beta_0 \cdot \sqrt{(|K| - K_R)/2} \tag{270}$$

$$K_R = 1 - \frac{\left(\omega_p^2/\omega^2\right)}{1 + (\nu/\omega)^2},\ K_I = \frac{(\omega_p/\omega)^2 \cdot \nu/\omega}{1 + (\nu/\omega)^2},\ |K| = \sqrt{K_R^2 + K_I^2}$$

and

$$\beta_0 = \omega/c$$

This formula was calculated for a wide range of parameters in order to obtain the influence of collision frequency on the input conductance and resistance. The main parameters which are of interest are antenna length (see fig. 32), high collision frequency (see fig. 33), and low collision frequency (see figs. 34 and 35). In each case the variable is the normalized electron density or $\left(\omega_p^2/\omega^2\right)$.

The longer the antenna (or the higher the frequency) the greater will be the range of variation of the admittance as the plasma frequency is increased (as shown in fig. 32). Even for this relatively high collision frequency ($\nu/\omega = 0.3$), the antenna input susceptance is nearly zero at $\omega_p^2/\omega^2 = 1$ for all initial lengths. The value of input conductivity at this point is linearly related to the initial length, $\beta_0 h$.

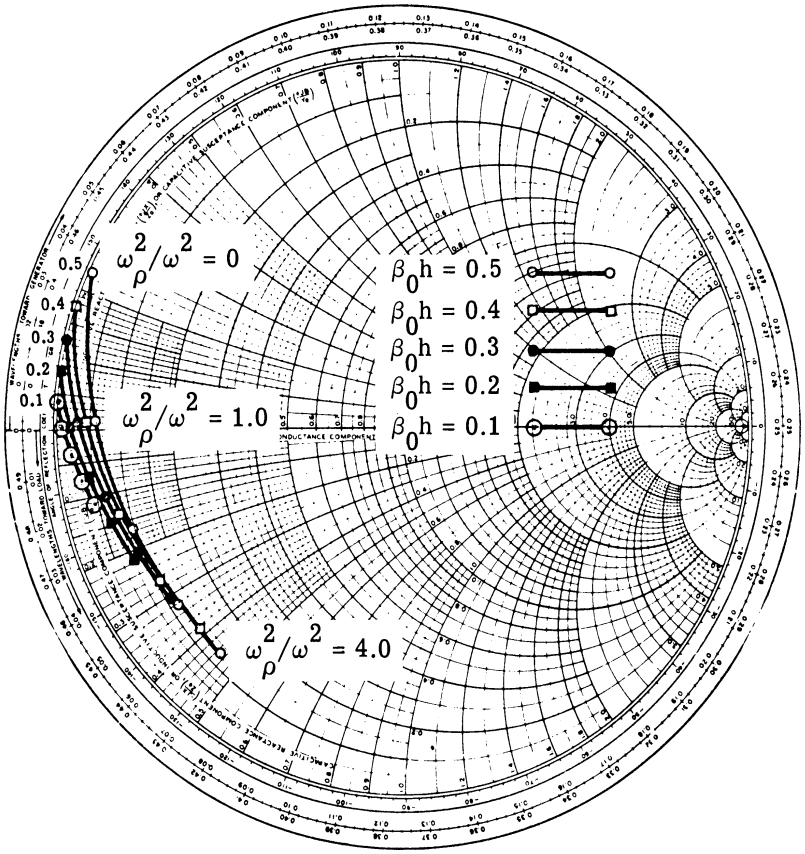

FIGURE 32. THEORETICAL MONOPOLE ANTENNA ADMITTANCE VS. PLASMA FREQUENCY WITH ANTENNA LENGTH AS A PARAMETER. Collision frequency is constant at $\nu/\omega = 0.3$; normalized electron density $\left(\omega_p^2/\omega^2\right)$ is the variable from 0 to 4.0; initial normalized antenna length $\beta_0 h$ is the parameter from 0.1 to 0.5; ratio of antenna diameter to length is in each case 1/10.

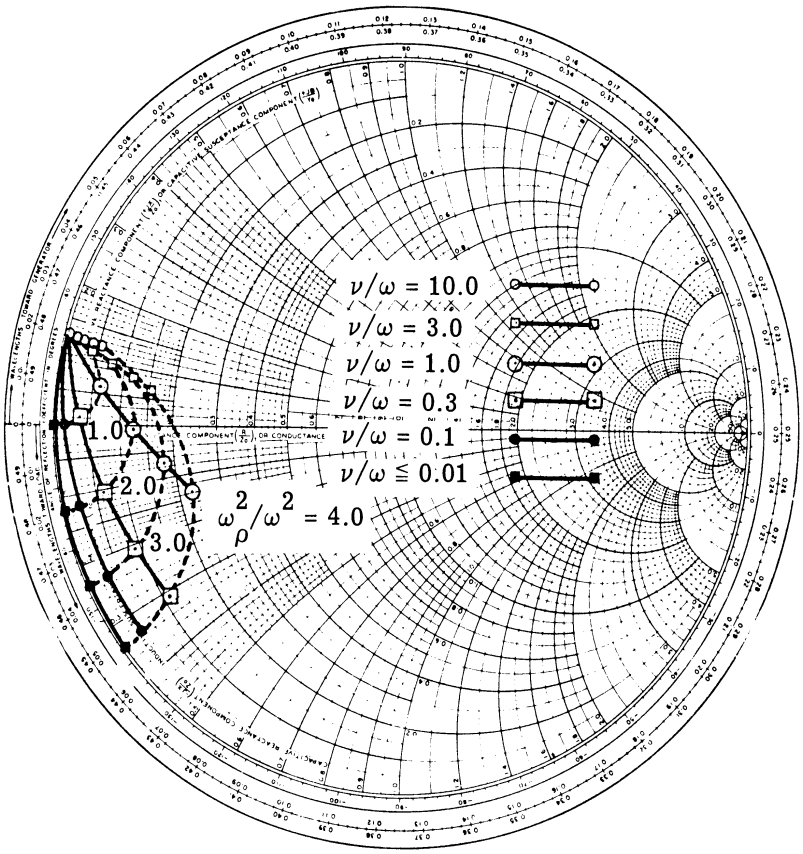

FIGURE 33. THEORETICAL MONOPOLE ANTENNA ADMITTANCE VS. PLASMA FREQUENCY WITH COLLISION FREQUENCY AS A PARAMETER. Normalized electron density $\left(\omega_p^2/\omega^2\right)$ is the variable from 0 to 4.0 (dashed lines); normalized collision frequency is the parameter from 0.01 to 10.0; the ratio of antenna diameter to length is in each case 1/10.

The antenna input admittance is not such a simple function of collision frequency (fig. 33). For very high collision frequencies ($\nu/\omega > 1$), little variation is found with increasing plasma frequency. Thus it can be seen that the variation in input susceptance is negligible for $\nu/\omega = 10$, even for $\omega_p^2/\omega^2 = 4.0$. However, the input conductance is a nearly linear function of plasma frequency for all of the collision frequencies shown in figure 33. A very interesting feature of the conductance is that it is maximum at any plasma frequency for equal collision and operating frequencies ($\nu/\omega = 1.0$). For collision frequencies considerably lower than the operating frequency ($\nu/\omega < 0.01$), the variation in input conductance cannot be seen on the Smith Chart, although lack of variation must not be assumed. The input susceptance is relatively unaffected by ν/ω for very low values.

Figure 34 gives the low collision frequency behavior of the conductance, again as a function of normalized electron density $\left(\omega_p^2/\omega^2\right)$. The interesting feature of this plot is that the input

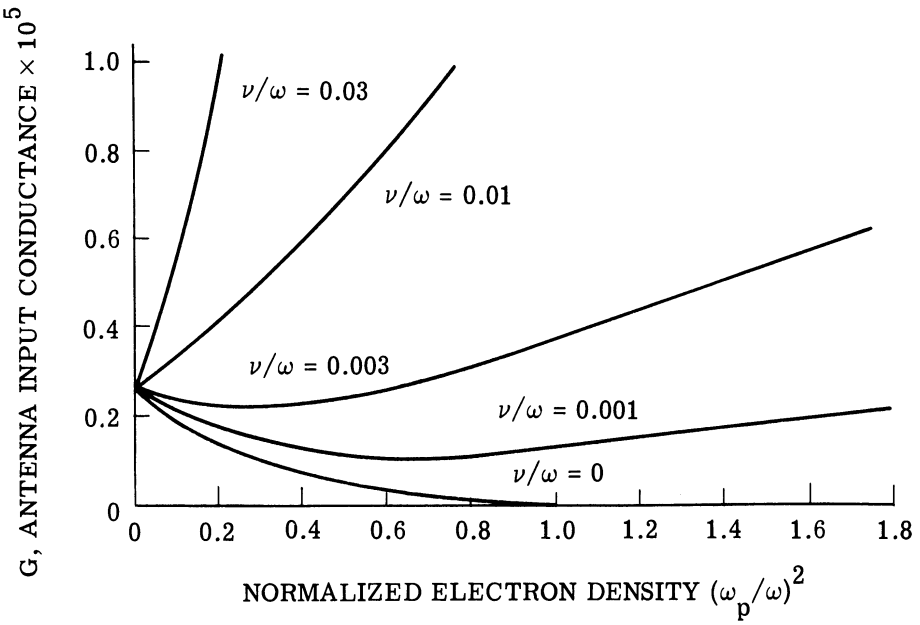

FIGURE 34. THEORETICAL MONOPOLE ANTENNA CONDUCTANCE VS. PLASMA FREQUENCY WITH COLLISION FREQUENCY AS A PARAMETER. Normalized initial antenna length is constant at 3.0; normalized electron density $\left(\omega_p^2/\omega^2\right)$ is the variable from 0 to 1.8; normalized collision frequency is the parameter from 0.001 to 0.03; ratio of antenna diameter to length is in each case 1/10.

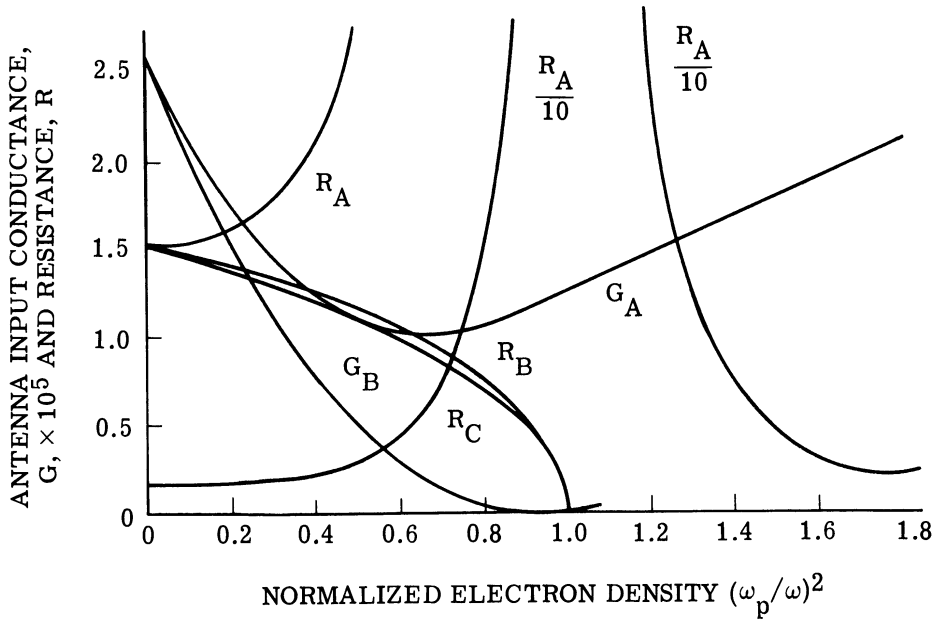

FIGURE 35. THEORETICAL CONDUCTANCES AND RESISTANCES FOR ZERO AND LOW COLLISION FREQUENCIES. (a) $\nu/\omega = 0.001$; same parameters as in figure 34. (b) $\nu/\omega = 0$; same parameters as in figure 34. (c) $\nu/\omega = 0$; radiation resistance calculations assuming same values at $\omega_p^2/\omega^2 = 0$.

conductance increases with increasing plasma frequency when the collision frequency is high enough. Equally significant is that, for a moderately low collision frequency such as $\nu/\omega = 0.003$, the conductance is almost independent of plasma frequency over a wide range of plasma frequencies.

The implications of this last result can be seen in figure 35, in which input resistances and conductances are plotted for the various cases indicated (note the superiority of admittance plots in this region). It can be seen that predictions of antenna input resistance based on zero collision-frequency results are open to serious doubt when the plasma is not sufficiently lossless. The experimental results obtained by Jackson, Kane, and Whale have indicated input resistances more nearly like the $\nu/\omega = 0.001$ case; that is, the input resistance was an increasing function of ω_p^2/ω^2, contrary to the prediction of the usual EM theory (assuming $\nu/\omega = 0$) that radiation resistance should decrease.

Although unstated, these authors apparently discounted electron collision with N_2 molecules, since the number of such encounters would indeed be quite low (perhaps about ten per second at altitudes near 250 km). They also evidently neglected collision frequencies with other particles; however, Mitra [55] states that collision frequencies of electrons with atomic oxygen particles of about 2×10^3/second at an altitude of 250 km are predicted and have been experimentally observed. Although this number is fairly low ($\nu/\omega \sim 0.4 \times 10^{-4}$), it is probably large enough to cause an increasing radiation resistance even at 250 km. Values of $\nu/\omega = 1.0 \times 10^{-3}$ predict a large increase in radiation resistance; only a moderate increase was observed in the Jackson, Kane, and Whale rocket experiment.

This calculation of the influence of collision effects on the input admittance and impedance of linear dipoles shows the importance of even small values of collision frequency. More importantly for the present study, it casts important doubts on the validity of the only experimental evidence that has been offered for the excitation of the EA wave; therefore greater credence is given to the theoretical predictions in this study for a small effect of the EA wave on antenna input admittance.

Appendix VI
MODIFICATION OF PREVIOUS EA WAVE EXCITATION

VI.1. INTRODUCTION

In this study, a small influence has been predicted of the EA wave on the terminating admittance at the spherical dipole. For this reason it is important to review those previous theories that have predicted a large influence. These theories are of two types: (1) modal analyses assuming elastic reflection and (2) Poynting vector method (assumed current distribution).

It is possible to make modifications in these theories that lead to a much reduced influence of the EA wave. These modifications are covered in the next two sections.

VI.2. MODAL ANALYSIS

All previous radiation analyses including a sheath and using a "modal" analysis seem to have employed models in which the electron density is zero inside the sheath and finite outside the sheath; the sheath is usually of zero thickness. In this category are the works of Hessel and Shmoys [17], Fejer [56] and Wait [18] for the spherical dipole, and Seshadri [57] for the linear slot on an infinite ground plane. In addition, this model has been used by investigators studying mode conversion at density discontinuities which is a subject that can be considered as part of the radiation problem. In this latter category are Kritz and Mintzer [54] and Cohen [14] who use one set of conditions and Tidman and Boyd [50, 58, 59] who use another set. When one of the densities is zero, the work of Field [19] and Yildiz [42] can be added. In this section, it is proposed to review this material briefly.

Needless to say, continuity of tangential magnetic and electric fields is common to most analyses. With the exception of the material by Tidman and Boyd, all of these references have another common characteristic — a boundary condition on the normal velocity. When neither density is zero, the requirement is one of continuity of velocity; when one is zero, the requirement is stated as "elastic reflection" — zero velocity at the boundary. The other common characteristic is that the electron pressure be continuous if neither density is zero, and that there be no condition on pressure if one of the densities is zero. Only one investigation has made any effort to include the actual sheath density variation — that is, the work of Tidman and Boyd. This is the main objection that must be voiced with all of these analyses — the steady state situation has not been fully included in the boundary conditions. As shown in appendix III, these variables play an important role in the boundary conditions. More importantly, when the density is discontinuous, there does not seem to be any justification for demanding either continuity of radial velocity or elastic reflection.

The justification that has been offered for the elastic reflection condition is its applicability in the field of acoustics. This would seem to be an inappropriate reason, since the analogy with acoustics should not be carried too far (at least a priori). Especially important is the concept of surface charge, which is neither useful nor valid in the theory of acoustics; more will be said of this in the following.

The one investigation that has not suggested the use of elastic reflection is the work of Tidman and Boyd [50]. However, it is believed that another discrepancy exists in their work which is equally important. In their series of three papers, a condition on continuity of normal current replaces the velocity condition. In appendix III, this is shown to be derivable from the same

equation that gives continuity of tangential magnetic field and should therefore be redundant with that condition. This was not noted in [58] but was noted in [50], without comment about their previous error. In this latter reference, a sufficient number of conditions were still available since they required continuity of the two transverse components of the pressure tensor. Their work will therefore be of value only in those cases where the pressure is considered as a tensor in the homogeneous region—a condition not usually employed and not used in this analysis. Without a pressure tensor, they do not have enough boundary conditions, because they have added unknown variables. An alternative formulation is given below.

A case that apparently has not been considered before for vacuum-plasma boundaries with EA waves gives a radically different answer from that given by other investigators. It is widely and successfully used in electron beam analyses, having been first discussed by Hahn [60]: the investigation reported here and in appendix III was suggested by G. Hok. In this approach, electron motion is permitted at the discontinuity. The main feature is that continuity of current is assured by means of an equivalent surface charge. The dynamic and kinematic conditions are automatically satisfied since the media and the average boundary interface are assumed to be stable. Since electron motion is now to be permitted at the interface as well as in the main body of the plasma, the electrons will experience small excursions into the region in which the time average of the density is assumed zero. However, the boundary conditions cannot be specified along this rippled boundary. Since the motion of the electrons leads to charge density perturbations at the boundary, this motion is interpreted as leading to an equivalent surface charge. It should also be noted that at the rippled boundary (not the average or unperturbed position) the normal velocity condition is satisfied ($\hat{n}\cdot\vec{v} \equiv 0$).

This approach would seem consistent with the Kritz and Mintzer approach [54] in which a surface charge is allowed, as opposed to that of Field [19] and those others who used elastic reflection. However, there is a difference between the surface charge concepts when one of the media is a vacuum and elastic reflection is still demanded. When the condition of continuity of normal velocity is replaced by elastic reflection, there can be no surface charge since by definition the electrons are presumed to experience no RF motion at the boundary. On the other hand, the conditions given by Kritz and Mintzer can be reduced in another manner, by retaining the concept of surface charge rather than continuity of velocity. Thus the condition in (103) is replaced by

$$\hat{n}\cdot(\rho_{02}\vec{v}_2) = \frac{\partial\sigma}{\partial t} \tag{271}$$

or

$$\hat{n}\cdot(\rho_{02}\vec{\xi}_2) = \sigma \tag{272}$$

where

$$\vec{v}_2 = \frac{\partial \vec{\xi}_2}{\partial t} \tag{273}$$

Perhaps the best justification of this approach, which differs so radically from that given in previous work is that this is the result obtained for the cold plasma. In none of the previous analyses has it been pointed out that continuity of velocity or "elastic reflection" are concepts alien to the theory of cold plasmas.

The question must then be asked—is there another possible boundary condition? Introducing the concept of surface charge did not provide a condition but rather a new variable. Continuity of normal electric field, of course, also introduces surface charge, but this is a redundant condition. This leaves only continuity of pressure which of course assures the nonexcitation of the EA wave since the EA-wave magnitude in the vacuum region must vanish. This result will be seen to be in accord with modifications of previous assumed current approaches discussed in the next section. However, the result is not meant as proof of nonexcitation of the EA wave but only to show that an equally realistic model can be presented in which the EA wave gives no contribution. This is also considered to be evidence of the importance of retaining the actual d-c sheath behavior.

The conclusions reached in this section are:

(1) Elastic reflection is not realistic.
(2) Introduction of a surface charge is a logical consequence of the integration of the continuity equation when a d-c discontinuity exists.
(3) The EA wave is not excited in this model and therefore has no influence on the input admittance.

VI.3. "POYNTING" VECTOR METHOD

As stated earlier, the homogeneous plasma analyses are divided into two types: (1) those assuming elastic reflection of electrons from the infinitely conducting radiating source and then using a model analysis and (2) those assuming a known source current and charge distribution. This section is concerned with the second approach. The preceding comments on the first approach are nevertheless pertinent since previous analyses using the second approach seem to have used, without explanation, equations that rely for their validity either on an assumption of elastic reflection or on some other unexplained mechanism for complete separation of charge and source electrons.

M. H. Cohen [14] was apparently the first to obtain wave equations for the perturbed electron density using the second approach which showed strong excitation by source electrons.

Others have been Hessel and Shmoys [17], Chen [15], and Wait [16]. In this type of analysis the basic equations for the homogeneous compressible plasma are assumed to be (taking $u_0 \equiv 0$)

$$\nabla \times \vec{E} = -\mu_0 \frac{\partial \vec{H}}{\partial t} \tag{274}$$

$$\nabla \times \vec{H} = \vec{J}^s - en_0\vec{V} + \epsilon_0 \frac{\partial \vec{E}}{\partial t} \tag{275}$$

$$n_0 \nabla \cdot \vec{V} + \frac{\partial n}{\partial t} = Q \tag{276}$$

$$n_0 m\left(\frac{\partial V}{\partial t}\right) = -n_0 e\vec{E} - mv_0^2 \nabla n \tag{277}$$

$$\nabla \cdot \vec{J}^s + \frac{\partial p^s}{\partial t} = eQ \tag{278}$$

Obviously the third and fifth equations are plasma and source components of the more basic equation

$$\nabla \cdot (\vec{J}^s + \rho_0 \vec{V}) + \frac{\partial}{\partial t}\left(\rho^s + \rho_1\right) = 0 \tag{279}$$

where $\rho_0 = -en_0$, $\rho = -en$, and e is the magnitude of the electron charge ($e = |e|$).

Unfortunately, these equations are not as "basic" as implied above. Although presented in essentially this form by Cohen (though his applied force term has been dropped), the term "Q" has not been retained by subsequent authors and was dropped by Cohen after assuming elastic reflection. Cohen calls Q, "a fluid flux source"; it is employed here in a larger sense to include one of two things: either charge interchange between source and plasma, or the existence of a surface charge existing outside the antenna. To obtain the forms presented by Chen or Wait, new variables can be defined:

$$n_{1Q} = n - Q \tag{280}$$

$$\rho_Q^s = \rho^s - eQ \tag{281}$$

These substitutions give the modified equations

$$n_0 \nabla \cdot \vec{V} + \frac{\partial n_{1Q}}{\partial t} = 0 \tag{282}$$

$$\nabla \cdot \vec{J}^s + \frac{\partial \rho_Q}{\partial t} = 0 \tag{283}$$

In order to shorten this presentation, the reader is referred to Cohen [14]; his equation 8.9 shows that the solution of the complete set of equations (retaining Q) is

$$n_1 = \frac{1}{4\pi}\iiint\left[\frac{\rho^s}{eD_\rho^2} - \frac{i\omega Q}{v_0^2}\right]\frac{e^{ik_p r}}{r}dv \tag{284}$$

where

$$D_p = \frac{v_0}{\omega_p} \tag{285}$$

The derivations of Chen [15] or Wait [16] can be similarly modified to obtain this result. The previous analyses have assumed various forms for $\vec{J}^s$ and have been able to integrate (284) after using (278) when Q = 0.

This step should be employed with the realization that Q = 0 is equivalent to $\hat{n}\cdot\vec{v} = 0$ and as Cohen points out: "We have assumed that the condition $\hat{n}\cdot\vec{v} = 0$ is not correct, but it may be an adequate approximation in some circumstances [14]."

It is of interest to investigate Q for a cold plasma since for small thermal velocities this value of Q should be a good approximation. Using formulas similar to Chen's [16] for the divergence of the electric field: (from (275), (276), (278)),

$$\nabla\cdot\vec{E} = \frac{\rho^s + \rho_1}{\epsilon_0} \tag{286}$$

(from (276), (277), and (278)),

$$\nabla\cdot\vec{E} = \frac{1}{\epsilon_0}\left\{\frac{v_0^2\nabla^2\rho_1 + \rho_1 - j\omega eQ}{\omega_p^2}\right\} \tag{287}$$

In Chen's discussion of the simplification of similar equations when $v_0^2 \to 0$, he retained ρ_1. In the present case ρ_1 is associated only with regions external to the source and is zero, since the EA wave cannot propagate in a cold plasma; thus from (286) and (287)

$$Q = \frac{-\omega_p^2}{j\omega e}\rho^s \tag{288}$$

This result could of course also be obtained from equation (284), which is in fact obtainable from (286) and (287).

Thus it is seen that for a cold plasma, a fluid flux source, in Cohen's nomenclature (or in the present method of looking at the problem; a "charge interchange" or "surface charge"), ex-

ists which is proportional to both the external plasma density and the source surface charge density. The possibility that such a "source" exists for the warm plasma should not be discarded a priori simply because "elastic reflection may be an adequate approximation in some circumstances [14]."

Chen claims that the charge Q given in (288) is the limiting value of that radiated as an electroacoustic wave for warm plasmas. This does not coincide with Cohen's statement about the equivalence of letting $Q = 0$ and using elastic reflection, nor does it allow for the existence of charge interchange with a warm plasma.

The conclusion to be derived from this section is not that there is no excitation of the electroacoustic wave, but only that it is possible to modify existing analyses to account for a much smaller excitation. In the light of the inhomogeneous medium results it now seems impossible to obtain an accurate prediction without (1) knowledge of the proper boundary conditions, and (2) inclusion of the inhomogeneous medium effects.

REFERENCES

1. R. W. P. King, The Theory of Linear Antennas, Harvard University, Cambridge, Mass., 1956.
2. S. A. Schelkunoff, Advanced Antenna Theory, John Wiley, 1952, pp. 39-54.
3. J. A. Chu and L. J. Stratton, "Steady-State Solutions of Electromagnetic Field Problems, II: Forced Oscillations of a Conducting Sphere," J. Appl. Phys., Vol. 12, No. 2, March 1941, pp. 236-240.
4. R. W. P. King, C. W. Harrison, Jr., and D. H. Denton, Jr., "The Electrically Short Antenna as a Probe for Measuring Free Electron Densities and Collision Frequencies in an Ionized Region," J. Res. N. Bu. Sd., Sec. D., Vol. 65, No. 4, July-August 1961, pp. 371-384.
5. R. W. P. King and C. W. Harrison, Jr., "Half-Wave Cylindrical Antenna in a Dissipative Medium: Current and Impedance," J. Res. N. Bu. Sd., Sec. D, Vol. 64, No. 4, July-August 1960, pp. 365-380.
6. R. W. P. King and C. W. Harrison, Jr., "Dipoles in Dissipative Medium," Symposium on Electromagnetic Waves, University of Wisconsin, Madison, 1962.
7. G. Deschamps, "Impedance of an Antenna in a Conducting Medium," IRE, Trans. Antennas Propagation, Vol. AP-10, No. 5, September 1962, pp. 648-650.
8. C. T. Tai, "Antennas in Lossy Media," J. Res. N. Bu. Sd., Sec. D, Vol. 68, No. 4, April 1964, pp. 466-468.
9. J. R. Wait, "Antennas in Plasma," Antenna Theory, ed. by R. E. Collin and F. J. Zucker, to be published by McGraw-Hill.
10. K. Balmain, "The Impedance of a Short Dipole Antenna in a Magnetoplasma," Ph.D. thesis, University of Illinois, May 1963.
11. H. Weil and D. Walsh, "Radiation Resistance of an Electric Dipole in a Magnetoionic Medium," IEEE, Trans. Antennas Propagation, Vol. AP-12, No. 3, May 1964, pp. 297-304.
12. J. E. Jackson and J. A. Kane, The Simultaneous Measurement of Ionospheric Electron Densities by CW Propagation and RF Impedance Probe Techniques, NASA TN D-1098, Washington, D. C., January 1962.
13. H. A. Whale, The Impedance of an Electrically Short Antenna in the Ionosphere, NASA TN D-1546, Goddard Space Flight Center, Greenbelt, Md., January 1963.
14. M. H. Cohen, "Radiation in a Plasma, I: Cerenkov Effect," Phys. Rev., Vol. 123, No. 3, August 1961, pp. 711-721; "II: Equivalent Sources," Vol. 126, No. 2, April 1962, pp. 389-397; "III: Metal Boundaries," Vol. 126, No. 2, April 1962, pp. 398-404.
15. K-M Chen, Interaction of a Radiating Source with a Plasma, Report No. 4563-39-T, Institute of Science and Technology, The University of Michigan, Ann Arbor, July 1963. Also published in Proc. IEEE, London, Vol. 111, No. 10, October 1964, pp. 1668-1678.
16. J. R. Wait, "Radiation from Sources Immersed in Compressible Plasma Media," Can. J. Phys., Vol. 42, No. 9, September 1964, pp. 1760-1780.
17. A. Hessel and J. Shmoys, "Excitation of Plasma Waves by a Dipole in a Homogeneous Isotropic Plasma," Proc. of the Symposiumon Electromagnetics and Fluid Dynamics of Gaseous Plasma, April 1961, Vol. XI, MRI Symposia Series, Polytechnic Institute of Brooklyn, 1961, pp. 173-184.

18. J. R. Wait, "Theory of a Slotted-Sphere Antenna Immersed in a Compressible Plasma," J. Res. N. Bu. Sd., Vol. D, No. 10, October 1964, pp. 1127-1143.

19. G. Field, "Radiation by Plasma Oscillations," Astrophys. J., Vol. 124, No. 3, 1956, pp. 555-570.

20. V. L. Ginzburg, Propagation of Electromagnetic Waves in Plasmas, Gordon and Breach, 1961, Ch. IV.

21. G. Hok, "Electrokinetic and Electromagnetic Noise Waves in Electronic Waveguides," Proc. of the Symposium on Electronic Waveguides, Vol. III, MRI Symposia Series, Polytechnic Institute of Brooklyn, April 1958, pp. 255-268.

22. J. F. Denisse and J. L. Delcroix, Théories des Ondes dans les Plasmas, Dunod, Paris, 1951, Ch. 1.

23. L. Oster, "Linearized Theory of Plasma Oscillations," Rev. Mod. Phys., Vol. 32, No. 1, January 1960, pp. 141-168.

24. J. D. Krause, Antennas, McGraw-Hill, 1950, pp. 272-276.

25. C. T. Tai, "The Electromagnetic Theory of the Spherical Luneberg Lens," Report No. 667-17, Ohio State University, Columbus, August 1956.

26. I. Langmuir and L. Tonks, "A General Theory of the Plasma of an Arc," Phys. Rev., Vol. 34, No. 6, September 1929, pp. 876-924.

27. H. M. Mott-Smith and I. Langmuir, "The Theory of Collectors in Gaseous Discharges," Phys. Rev., Vol. 28, October 1926, pp. 727-763.

28. D. Bohm, E. H. S. Burshop and H. S. W. Massey, "The Use of Probes for Plasma Exploration in Strong Magnetic Fields," Characteristics of Electrical Discharges in Magnetic Fields, ed. by A. Guthrie, McGraw-Hill, 1949.

29. J. E. Allen, R. L. F. Boyd, and P. Reynolds, "The Collection of Positive Ions by a Probe Immersed in a Plasma," Proc. Phys. Soc. (London), Vol. 70, No. 447B, March 1957, Pt. 3, pp. 297-304.

30. I. B. Bernstein and I. N. Rabinowitz, "Theory of Electrostatic Probes in a Low-Density Plasma," Phys. Fluids, Vol. 2, No. 2, March-April 1959, pp. 112-121.

31. J. Laframboise, "Theory of Electrostatic Probes in a Collisionless Plasma at Rest," Fourth International Symposium on Rarified Gases, Toronto, 1964.

32. S. H. Lam, "Unified Theory for the Langmuir Probe in a Collisionless Plasma," Phys. Fluids, Vol. 8, No. 1, January 1965, pp. 73-87.

33. S. A. Self, "Exact Solution of the Collisionless Plasma-Sheath Equation," Phys. Fluids, Vol. 6, No. 12, December 1963, pp. 1762-1768.

34. S. A. Self, "Asymptotic Plasma and Sheath Representations for Low-Pressure Discharges," J. Appl. Phys., Vol. 36, No. 2, February 1965, pp. 456-459.

35. A. Caruso and A. Cavaliere, "The Structure of the Collisionless Plasma-Sheath Transition," Il Nuovo Cimento, Vol. XXVI, No. 6, December 1962, pp. 1389-1404.

36. J. V. Parker, "Theory of Plasma Wave Resonances in a Hot Nonuniform Plasma," Tech. Rept. No. 23, California Institute of Technology, Pasadena, June 1964.

37. J. C. Nickel, "Experimental Study of Plasma Wave Resonances in a Hot Nonuniform Plasma Column," Tech. Rept. No. 22, California Institute of Technology, Pasadena, May 1964.

38. J. C. Nickel, J. V. Parker, and R. W. Gould, "Resonance Oscillations in a Hot Nonuniform Plasma Column," Phys. Rev. Letters, Vol. 11, No. 5, September 1963, pp. 183-185.

39. L. Spitzer, Physics of Fully Ionized Gases, Interscience Publications, 1956, p. 18.

40. J. G. Fikioris, "Theory of Radially Stratified Media, Part I: The Biconical Antenna in a Radially Stratified Medium," Tech. Rept. No. 390, Harvard University Cruft Laboratories, Cambridge, January 1963.

41. C. T. Tai, "Some Wave Functions and Potential Functions Pertaining to Spherically Stratified Media," J. Res. N. Bu. Sd., Vol. 670, March-April 1963, pp. 199-202.

42. A. Yildiz, "Scattering of Plane Plasma Waves from a Plasma Sphere," Il Nuovo Cimento, Vol. XXX, No. 5, December 1963, pp. 1182-1207.

43. J. A. Stratton and L. J. Chu, "Steady-State Solutions of Electromagnetic Field Problems, Part I: Forced Oscillations of a Cylindrical Conductor; Part III: Forced Oscillations of a Prolate Spheroid," J. Appl. Phys., Vol. 12, No. 3, March 1941, pp. 230-235, 241-248.

44. W. E. Milne, The Numerical Solution of Differential Equations, John Wiley, 1953, Ch. II.

45. L. Collatz, The Numerical Treatment of Differential Equations, Springer, 1959, Ch. III.

46. H. Kober, Dictionary of Conformal Representations, Dover, 1957, pp. 3-8.

47. J. A. Stratton, Electromagnetic Theory, McGraw-Hill, 1941, p. 604.

48. Handbook of Mathematical Functions, ed. by M. Abramowitz and I. Stegen, National Bureau of Standards, Appl. Math. Series 55, June 1964, Ch. 10.

49. G. N. Watson, A Treatise on the Theory of Bessel Functions, Cambridge University, 1948, pp. 746-747.

50. D. A. Tidman and J. M. Boyd, "Radiation by Plasma Oscillations Incident on a Density Discontinuity," Phys. Fluids, Vol. 5, No. 2, February 1962, pp. 213-218.

51. J. V. Parker, J. C. Nickel,and R. W. Gould, "Resonance Oscillations in a Hot Nonuniform Plasma," Phys. Fluids, Vol. 7, September 1964, pp. 1489-1500.

52. L. Landau, "On the Vibrations of the Electronic Plasma," J. Phys., Vol. 10, No. 1, 1946, pp. 25-34.

53. G. Hok, "Noise Propagation in a Nonuniform Electron Gas," Electron Physics Laboratory Report 0500-3-T, The University of Michigan, Ann Arbor, March 1963.

54. A. H. Kritz and D. Mintzer, "Propagation of Plasma Waves Across a Density Discontinuity," Phys. Rev., Vol. 117, No. 2, January 1960, pp. 382-386.

55. S. K. Mitra, The Upper Atmosphere, The Asiatic Society, Calcutta, Vol. V, Monograph Series, 1952, pp. 259-265.

56. J. A. Fejer, "The Interaction of an Antenna with a Hot Plasma and the Theory of Resonance Probes," presented at the Conference on Non-Linear Processes in the Ionosphere, Boulder, Colorado, 16-17 December 1963.

57. S. R. Seshadri, "Radiation from an Electromagnetic Source in a Half-Space of Compressible Plasma - Surface Waves," Tech. Rept. No. 396, Harvard University Cruft Laboratories, Cambridge, March 1963.

58. D. A. Tidman, "Radio Emission by Plasma Oscillations in Nonuniform Plasmas," Phys. Rev., Vol. 117, No. 2, January 1960, pp. 366-374.

59. D. A. Tidman and G. H. Weiss, "Radio Emission by Plasma Oscillation in Non-uniform Plasma," Phys. Fluids, Vol. 4, No. 6, June 1961, pp. 703-710.

60. W. C. Hahn, "Small Signal Theory of Velocity Modulated Electron Beams," Gen. Elec. Rev., Vol. 42, No. 6, June 1959, pp. 258-270.

DISTRIBUTION LIST

Copy No.	Addressee
1-3 (1 repro)	Air Force Avionics Laboratory Wright-Patterson Air Force Base, Ohio 45433
(1-2) (repro)	ATTN: AVNT/H. F. Yoder
(3)	ATTN: AVWE (Mr. Wade Hunt)
4-5	Research and Technology Division Wright-Patterson Air Force Base, Ohio 45433
(4)	ATTN: SEPI
(5)	ATTN: SEPIR
6	Headquarters, USAF Washington, D. C. ATTN: SAFRD
7	Director, Air University Library Maxwell Air Force Base, Alabama 36112
8	U. S. Army Electronics Research and Development Laboratory Fort Monmouth, New Jersey 07703 ATTN: AMSEL-RD-SRE/Mr. S. J. Grossman
9	Chief, Bureau of Naval Weapons Department of the Navy, Washington, D. C. 20360 ATTN: Electronics Division, RAAV
10	Director, Naval Research Laboratory Washington, D. C. 20390 ATTN: Code 2021
11	Headquarters, USAF (AFXSA1) Air Battle Analysis Center Deputy Director of Plans for War Plans Directorate of Plans, DCS/P&O Washington, D. C. 20330
12	Headquarters, USAF Director of Research and Technology Washington, D. C. 20330 ATTN: AFRSTB/Mr. D. R. McKanna
13	Secretary, Committee on Electronics Office of Assistant Secretary of Defense Department of Defense, Washington, D. C. 20301
14	Institute for Defense Analyses 1666 Connecticut Avenue Washington, D. C. ATTN: Dr. Stanley Marder
15	U. S. Army Engineers, GIMRADA Fort Belvoir, Virginia 22060 ATTN: L. F. Ayers
16	Aerospace Corporation San Bernadino, California ATTN: E. N. Shomal, Librarian
17	Ohio State University Research Foundation 1314 Kinnear Road Columbus, Ohio 43210 ATTN: R. L. Cosgriff
18	Headquarters Research and Technology Division Bolling Air Force Base Washington, D. C. 20332 ATTN: RTTR
19	Rome Air Development Center Griffiss Air Force Base, New York 13442 ATTN: Documents Library/EMALD
20	SAFSP (SP-8C) Air Force Unit Post Office Los Angeles, California 90045 ATTN: Major Redwine
21	Conductron Corporation 343 South Main Street Ann Arbor, Michigan 48108 ATTN: Dr. L. J. Cutrona
22	Goodyear Aerospace Corporation Arizona Division Litchfield Park, Arizona 85340 ATTN: Mr. L. R. Blair
23	The Johns Hopkins University, Carlyle Barton Laboratory Charles & 34th Street Baltimore, Maryland 21218 ATTN: Mr. John M. Kopper
24	Massachusetts Institute of Technology Electronics Systems Laboratory Cambridge, Massachusetts 02139 ATTN: Mr. L. Swain, Jr.
25	Radio Corporation of America Defense Electronics Products Burlington, Massachusetts 01803 ATTN: Dr. W. C. Curtis
26	RAND Corporation 1700 Main Street Santa Monica, California 90406 ATTN: Dr. H. H. Bailey
27	Commanding Officer, U. S. Naval Ordnance Laboratory Corona, California 91720
28	Scientific and Technical Information Facility P. O. Box 5700 Bethesda, Maryland 20014 ATTN: NASA Representative (SAK/DL)
29	Aerospace Corporation El Segundo, California 90245 ATTN: Mr. S. Evans, Jr.
30	Airborne Instruments Laboratory Walt Whitman Road Melville, Long Island, New York 11749 ATTN: Mr. C. H. Gager
31	Hughes Aircraft Company Aerospace Group Culver City, California 90232 ATTN: M. D. Adcock
32	Westinghouse Electric Corporation Aerospace Division P. O. Box 746 Baltimore, Maryland 21203 ATTN: W. D. Fegeley
33	Raytheon Company Space and Information Systems Division Boston Post Road Sudbury, Massachusetts 01776 ATTN: Mr. Kenneth Kinnard
34	Aerospace Corporation P. O. Box 95085 Los Angeles, California 90045 ATTN: D. A. Lacer

Copy No.	Addressee
35	Motorola, Incorporated Military Electronics Division 8201 E. McDowell Road Scottsdale, Arizona 85257 ATTN: Mr. Carl Helber
36	National Aeronautics and Space Administration Manned Spacecraft Carrier, Electrical Systems Branch Houston, Texas 77058
37	Air Force Cambridge Research Laboratories Office of Aerospace Research Technical Services Division L.G. Hanscom Field, Bedford, Massachusetts 01731 ATTN: Research Library Branch, CRXL Stop #29
38	Headquarters, ESD L. G. Hanscom Field, Bedford, Massachusetts 01731
39	Lockheed Missiles and Space Division 3251 Hanover Street Palo Alto, California 94304
40	Chief, Bureau of Ships Department of the Navy, Washington, D. C. 20360 ATTN: Code 816
41-59	Defense Documentation Center Cameron Station Alexandria, Virginia 22314 ATTN: TISIA
60	Headquarters, U. S. Army Liaison Group Project MICHIGAN The University of Michigan P. O. Box 618 Ann Arbor, Michigan

UNCLASSIFIED

Security Classification

DOCUMENT CONTROL DATA - R&D

(Security classification of title, body of abstract and indexing annotation must be entered when the overall report is classified)

1. ORIGINATING ACTIVITY *(Corporate author)*
Willow Run Laboratories, Institute of Science and Technology, The University of Michigan, Ann Arbor, Michigan

2a. REPORT SECURITY CLASSIFICATION
Unclassified

2b. GROUP

3. REPORT TITLE
A STUDY OF AN INHOMOGENEOUSLY SHEATHED SPHERICAL-DIPOLE ANTENNA IN A COMPRESSIBLE PLASMA

4. DESCRIPTIVE NOTES *(Type of report and inclusive dates)*

5. AUTHOR(S) *(Last name, first name, initial)*
Larson, Ronal W.

6. REPORT DATE	7a. TOTAL NO. OF PAGES	7b. NO. OF REFS
September 1966	xv + 134	

8a. CONTRACT OR GRANT NO.	9a. ORIGINATOR'S REPORT NUMBER(S)
AF (33)615-1452	7000-25-T
b. PROJECT NO.	
c.	9b. OTHER REPORT NO(S) *(Any other numbers that may be assigned this report)*
d.	

10. AVAILABILITY/LIMITATION NOTICES
Qualified requesters may obtain copies of this document from DDC, Cameron Station, Alexandria, Virginia 22314. This document is subject to special export controls and each transmittal to foreign governments or foreign nationals may be made only with prior approval of AFAL(AVPT), WPAFB, Ohio.

11. SUPPLEMENTARY NOTES	12. SPONSORING MILITARY ACTIVITY
	Air Force Avionics Laboratory Research and Technology Division, AF Systems Command, Wright-Patterson Air Force Base, Ohio

13. ABSTRACT

This study investigated the terminating admittance and spatial field variations of a symmetrically excited spherical dipole in an inhomogeneous, compressible plasma using the macroscopic approach. Four coupled, first order, ordinary differential equations were obtained for each mode by employing modal decomposition. Numerical integration was performed on a digital computer with a sheath model in which the static electron density varied as the distance from the outer sheath edge.

Admittance plots are presented as a function of the sheath potential distribution, plasma frequency, electron temperature, radiator size, and for several alternative radiator boundary conditions: elastic electron reflection, zero perturbed electron density, and a bilinear admittance relation. The main effect of plasma compressibility was found to be an additional resonance caused by cancellation of reactive electromagnetic and electroacoustic energies. This manifests itself in a Smith Chart presentation as a loop or multiple loops when the plasma frequency, operating frequency, or electron thermal velocity are varied. The sheath was found to diminish the effects found with a homogeneous plasma and caused the susceptance to be increased significantly; each of the alternative boundary conditions gave similar results.

It is concluded that the sheath has been unjustifiably neglected in previous analyses and that the plasma compressibility has therefore been overemphasized. It is suggested that future experimental evidence of excitation of an electroacoustic wave be obtained with a moveable radial surface probe as well as by measurements of the admittance.

DD FORM 1 JAN 64 1473

UNCLASSIFIED

Security Classification

14. KEY WORDS	LINK A		LINK B		LINK C	
	ROLE	WT	ROLE	WT	ROLE	WT
Compressible plasma Antennas Spherical dipole Electroacoustic wave Sheath Inhomogeneity						

INSTRUCTIONS

1. ORIGINATING ACTIVITY: Enter the name and address of the contractor, subcontractor, grantee, Department of Defense activity or other organization *(corporate author)* issuing the report.

2*a*. REPORT SECURITY CLASSIFICATION: Enter the overall security classification of the report. Indicate whether "Restricted Data" is included. Marking is to be in accordance with appropriate security regulations.

2*b*. GROUP: Automatic downgrading is specified in DoD Directive 5200.10 and Armed Forces Industrial Manual. Enter the group number. Also, when applicable, show that optional markings have been used for Group 3 and Group 4 as authorized.

3. REPORT TITLE: Enter the complete report title in all capital letters. Titles in all cases should be unclassified. If a meaningful title cannot be selected without classification, show title classification in all capitals in parenthesis immediately following the title.

4. DESCRIPTIVE NOTES: If appropriate, enter the type of report, e.g., interim, progress, summary, annual, or final. Give the inclusive dates when a specific reporting period is covered.

5. AUTHOR(S): Enter the name(s) of author(s) as shown on or in the report. Enter last name, first name, middle initial. If military, show rank and branch of service. The name of the principal author is an absolute minimum requirement.

6. REPORT DATE: Enter the date of the report as day, month, year, or month, year. If more than one date appears on the report, use date of publication.

7*a*. TOTAL NUMBER OF PAGES: The total page count should follow normal pagination procedures, i.e., enter the number of pages containing information.

7*b*. NUMBER OF REFERENCES: Enter the total number of references cited in the report.

8*a*. CONTRACT OR GRANT NUMBER: If appropriate, enter the applicable number of the contract or grant under which the report was written.

8*b*, 8*c*, & 8*d*. PROJECT NUMBER: Enter the appropriate military department identification, such as project number, subproject number, system numbers, task number, etc.

9*a*. ORIGINATOR'S REPORT NUMBER(S): Enter the official report number by which the document will be identified and controlled by the originating activity. This number must be unique to this report.

9*b*. OTHER REPORT NUMBER(S): If the report has been assigned any other report numbers *(either by the originator or by the sponsor)*, also enter this number(s).

10. AVAILABILITY/LIMITATION NOTICES: Enter any limitations on further dissemination of the report, other than those imposed by security classification, using standard statements such as:

(1) "Qualified requesters may obtain copies of this report from DDC."

(2) "Foreign announcement and dissemination of this report by DDC is not authorized."

(3) "U. S. Government agencies may obtain copies of this report directly from DDC. Other qualified DDC users shall request through

_____."

(4) "U. S. military agencies may obtain copies of this report directly from DDC. Other qualified users shall request through

_____."

(5) "All distribution of this report is controlled. Qualified DDC users shall request through

_____."

If the report has been furnished to the Office of Technical Services, Department of Commerce, for sale to the public, indicate this fact and enter the price, if known.

11. SUPPLEMENTARY NOTES: Use for additional explanatory notes.

12. SPONSORING MILITARY ACTIVITY: Enter the name of the departmental project office or laboratory sponsoring *(paying for)* the research and development. Include address.

13. ABSTRACT: Enter an abstract giving a brief and factual summary of the document indicative of the report, even though it may also appear elsewhere in the body of the technical report. If additional space is required, a continuation sheet shall be attached.

It is highly desirable that the abstract of classified reports be unclassified. Each paragraph of the abstract shall end with an indication of the military security classification of the information in the paragraph, represented as *(TS)*, *(S)*, *(C)*, or *(U)*.

There is no limitation on the length of the abstract. However, the suggested length is from 150 to 225 words.

14. KEY WORDS: Key words are technically meaningful terms or short phrases that characterize a report and may be used as index entries for cataloging the report. Key words must be selected so that no security classification is required. Identifiers, such as equipment model designation, trade name, military project code name, geographic location, may be used as key words but will be followed by an indication of technical context. The assignment of links, rules, and weights is optional.